DECOVALEX-2023 Task F Specification Revision 8

Spent Fuel and Waste Disposition

Prepared for
US Department of Energy
Spent Fuel and Waste Science and Technology

Tara LaForce, Rick Jayne,
Rosie Leone, Emily Stein
Sandia National Laboratories

Son Nguyen
Canadian Nuclear Safety Commission

May 15, 2022
SAND2022-xxxx O

DISCLAIMER

This information was prepared as an account of work sponsored by an agency of the U.S. Government. Neither the U.S. Government nor any agency thereof, nor any of their employees, makes any warranty, expressed or implied, or assumes any legal liability or responsibility for the accuracy, completeness, or usefulness, of any information, apparatus, product, or process disclosed, or represents that its use would not infringe privately owned rights. References herein to any specific commercial product, process, or service by trade name, trade mark, manufacturer, or otherwise, does not necessarily constitute or imply its endorsement, recommendation, or favoring by the U.S. Government or any agency thereof. The views and opinions of authors expressed herein do not necessarily state or reflect those of the U.S. Government or any agency thereof.

Sandia National Laboratories is a multimission laboratory managed and operated by National Technology and Engineering Solutions of Sandia LLC, a wholly owned subsidiary of Honeywell International Inc. for the U.S. Department of Energy's National Nuclear Security Administration under contract DE-NA0003525.

Sandia National Laboratories

SUMMARY

This report is the revised (Revision 8) Task F specification for DECOVALEX-2023. Task F is a comparison of the models and methods used in deep geologic repository performance assessment. The task proposes to develop a reference case for a mined repository in a fractured crystalline host rock and a reference case for a mined repository in a salt formation. Teams may choose to participate in the comparison for either or both of the reference cases. For each reference case, a common set of conceptual models and parameters describing features, events, and processes that impact performance will be given, and teams will be responsible for determining how best to implement and couple the models. The comparison will be conducted in stages, beginning with a comparison of key outputs of individual process models, followed by a comparison of a single deterministic simulation of the full reference case, and moving on to uncertainty propagation and uncertainty and sensitivity analysis. This report provides background information, a summary of the proposed reference cases, and a staged plan for the analysis.

Report Version Number	Date	
SAND2020-4598 O (rev 0)	April 29 2020	Version for April 2020 kickoff meeting
SAND2020-8494 O (rev 1)	August 13 2020	Benchmark 6.3.3 and appendix updated
SAND2020-12645 O (rev 2)	November 11 2020	Added model domain to benchmark 6.3.3 Added four-fracture benchmark 6.3.4
SAND2021-01910 O (rev 3)	January 7 2021	Updated pressure, aperture, and permeability of four-fracture benchmark 6.3.4 Added benchmark 6.3.5
SAND2021-3155 O (rev 4)	March 15, 2021	Updated 4 fracture plus stochastic fracture parameters
SAND2021-6658 O (rev 5)	June 2, 2021	Added revised 4 fracture plus stochastic fracture 6.3.6
SAND2021-11892 O (rev 6)	September 24, 2021	Revised schedule (Section 2.1) Defined initial salt reference case (Section 4) Added 2D transport benchmark 9.3.1
SAND2021-13423 O (rev 7)	October 23, 2021	Defined crystalline reference case with tracer source term (Section 3)
SAND2022-xxxx O (rev 8)	May 15, 2022	Crystalline: corrected expression for P32, corrected tracer source term text, added output for comparison (Section 3) Salt: Updated reference case shaft properties and tracers for transport (Section 4)

ACKNOWLEDGEMENTS

Thanks to DECOVALEX organizers Jens Birkholzer and Alex Bond for proposing Task F, and for their guidance in defining its boundaries.

Thanks to the members of the participating teams for their many contributions to the reference cases.

Thanks to Sandia National Laboratories researchers Peter Swift, Paul Mariner, Rick Jayne, Tara LaForce, Michael Nole, and Kris Kuhlman for their input to and reviews of the draft, and to Rick for compiling information for the salt reference case.

Thanks to Tanja Frank of GRS for providing shaft properties for the salt case.

Thanks to the leadership team at the U. S. Department of Energy, Office of Nuclear Energy, Spent Fuel and Waste Science and Technology Campaign, Prasad Nair, Jorge Monroe-Rammsy, and Tim Gunter, for their support of this project.

CONTENTS

ACRONYMS

1-D	1-dimensional
2-D	2-dimensional
3-D	3-dimensional
BFZ	brittle fracture zone
BWR	boiling water reactor
DECOVALEX	DEvelopment of COupled models and their VALidation against Experiments
DOE	Department of Energy (US)
DRZ	disturbed rock zone
FEPs	features, events, and processes
HCD	hydraulic conductor domain
HRD	hydraulic rock mass domain
MTU	metric tons uranium
NWMO	Nuclear Waste Management Organization (Canada)
OCRWM	Office of Civilian Radioactive Waste Management (US)
OoR	out of reactor
PA	performance assessment
PWR	pressurized water reactor
SA	sensitivity analysis
SKB	Svensk Kärnbränslehantering AB (Sweden)
SNF	spent nuclear fuel
THM	thermal-hydraulic-mechanical
TPC	Taiwan Power Company (Taiwan)
UQ	uncertainty quantification
US	United States

VARIABLES AND THEIR UNITS

b	half fracture aperture (m)
c	concentration (mol/L)
D	hydrodynamic dispersion coefficient (m^2/s)
D^*	molecular diffusion coefficient in water (m^2/s)
F_r	flow-related transport resistance in the fractured rock (y/m)
J	solute flux ($mol/m^2/s$)
k	permeability (m^2)
K_d	linear distribution coefficient (m^3/kg)
P	pressure (Pa)
P_{32}	fracture intensity as fracture area per unit volume of rock (m^2/m^3)
q	specific discharge (also called Darcy velocity) (m/s or m/y, as appropriate)
R	retardation coefficient (-)
$t_{1/2}$	halflife (s or y, as appropriate)
t_r	travel time to the biosphere in the fractured rock (y)
v	average linear porewater velocity (m/s, m/d, or m/y, as appropriate)
α_L	longitudinal dispersivity (m)
ϕ	porosity (-)
λ	decay constant (1/s)
μ	viscosity (Pa-s)
ρ	density (kg/m^3)
ρ_b	bulk density (kg/m^3)
ρ_s	solid grain density (kg/m^3)
τ	tortuosity (-)

DECOVALEX-2023 TASK F SPECIFICATION

This task specification is intended for the participants in DECOVALEX-2023 Task F (Performance Assessment).

1. Introduction

The DECOVALEX program is in general interested in coupled processes (e.g., thermal, hydrological, mechanical, and chemical) relevant to deep geologic disposal of nuclear waste. Task F of DECOVALEX-2023 involves comparison of the models and methods used in post-closure performance assessment of deep geologic repositories. A generic reference case describing a repository for commercial spent nuclear fuel (SNF) in a fractured crystalline host rock is proposed as the primary system for comparison. A second generic reference case describing a repository for commercial SNF in a salt formation (bedded or domal) will be developed given sufficient interest and resources. Although a direct comparison cannot be made between simulations of a crystalline repository and simulations of a salt repository, it is expected that lessons learned regarding, for instance, methods of coupling process models, propagating uncertainty, or conducting sensitivity analysis will be transferable between concepts.

The primary objectives of Task F are to build confidence in the models, methods, and software used for performance assessment (PA) of deep geologic repositories, and/or to bring to the fore additional research and development needed to improve PA methodologies. The objectives will be accomplished through a staged comparison of the models and methods used by participating teams in their PA frameworks, including: (1) coupled-process submodels (e.g., waste package corrosion, spent fuel dissolution, radionuclide transport) comprising the full PA model; (2) deterministic simulation(s) of the entire PA model for defined reference scenario(s); (3) probabilistic simulations of the entire PA model; and (4) uncertainty quantification (UQ) and sensitivity analysis (SA) methods/results for probabilistic simulations of defined reference scenario(s).

1.1 Performance Assessment

Performance assessment is a tool of decision management that provides information from quantitative evaluations of the behavior of a complex system to the decision makers. PA involves evaluating the level of confidence (taking into account identified uncertainties) in the estimated performance of the system, and seeks to provide reasonable assurance that the repository system will meet applicable safety standards Throughout the lifetime of a repository program, performance assessment is used in an iterative fashion to support site selection, site characterization, and repository design, and to inform data collection and model development.

At any iteration, the first steps of the performance assessment process are to establish performance measures and to develop conceptual models of the repository system from knowledge of the natural and engineered system components (Figure 1-1). Development of computational models may go hand-in-hand with development of conceptual models. Ultimately one or more computational models appropriate for forward simulation of the problem and calculation of performance measures is developed. Then, performance measures are calculated, uncertainty and sensitivity analysis performed, and results synthesized.

1.2 Task F

The stages of Task F will follow a similar process (Figure 1-2). As a group, participating teams will agree on the characteristics of the natural and engineered systems, performance measures, and conceptual models describing processes affecting radionuclide mobilization and transport in the repository system (indicated in blue). Each team will then develop its own forward model(s), calculate the performance measures, and perform uncertainty and sensitivity analysis. At each of the independent stages (indicated in green), a comparison of results will be made.

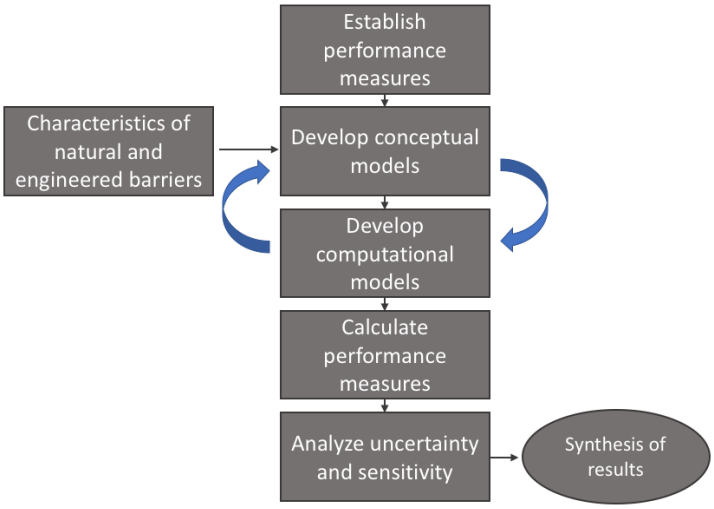

Figure 1-1. The performance assessment process (modified from OCRWM 1990).

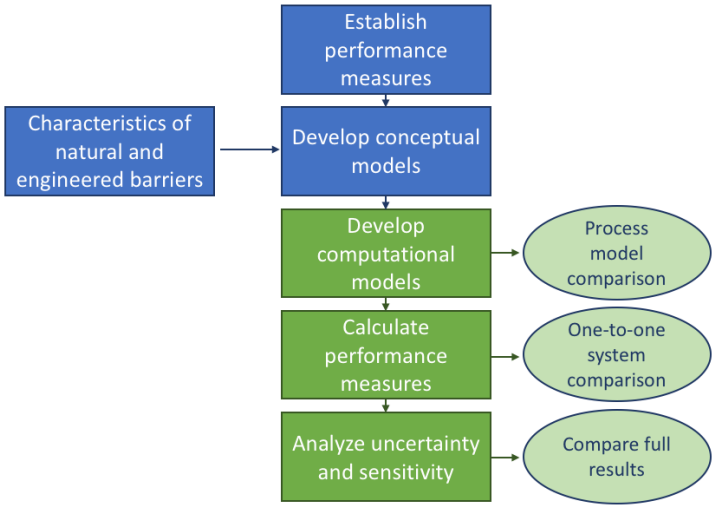

Figure 1-2. Task F work flow. Items in blue rectangles will be given by the task lead or developed as a group. Items in green rectangles will be completed by individual teams. Comparisons to be performed are in ovals.

1.2.1 Characteristics of the Natural and Engineered Barrier Systems

Forward modeling requires information characterizing the repository system and its subsystems. For each of the generic reference cases, we assume all necessary information is available. Key features, events, and processes (FEPs) and associated uncertainties have been identified and adequately characterized.

1.2.2 Performance Measures

Task F will focus on performance measures indicative of the ability of the repository system to isolate radionuclides from the biosphere through containment and retardation. Performance measures will include those related to the overall performance of the repository system, such as radionuclide

concentrations in groundwater some distance from the repository, and those related to the performance of individual components of the engineered or natural system, such as canister thickness, radionuclide flux from one component of the system to another, and path length.

1.2.3 Conceptual Models

Conceptual models describe the key FEPs affecting performance measures. Task F requires that participating teams work from a common understanding of, for instance, regional hydrogeologic conditions, waste canister failure mechanisms, and processes affecting radionuclide transport in the repository and in the host rock.

Conceptual models of interest may also include scenarios for evolution of the repository system that consider the effects of climate cycles or future tectonic events.

1.2.4 Computational Models

Each team will be responsible for choosing specific computational models to simulate the key FEPs. For example, teams may choose to simulate flow in fractures using a discrete fracture network (DFN) or an equivalent continuous porous medium (ECPM), and to simulate radionuclide transport using the advection/dispersion equation or particle tracking. Generally speaking, a team may choose to include or neglect a particular process or feedback between processes, to use a more or less mechanistic model, and to couple processes more or less tightly.

1.2.5 Quantitative Analysis of Performance Measures

Performance measures resulting from deterministic simulations of the reference case scenario(s) as well as distributions of performance measures resulting from propagation of uncertainty will be compared.

1.2.6 Uncertainty and Sensitivity Analysis

Performance assessment is subject to a variety of uncertainties, which may be categorized in different ways by different programs. Scenario uncertainty relates to uncertainty about FEPs that may affect the future evolution of the repository system. Conceptual or model uncertainty relates to uncertainties regarding understanding and representation (or omission) of processes affecting performance. Uncertainties regarding how well parameter values are known, occurrence of random events, and stochastic distribution of spatially heterogeneous properties may be lumped as data uncertainties or depending on the design of the analysis separated into epistemic (state of knowledge) uncertainties and aleatory (roll of the dice) uncertainties.

Uncertainty and sensitivity analysis in Task F will directly address uncertainties through quantification, sampling, and propagation of uncertain inputs through multiple realizations of the forward model(s).

2. Proposed Task Structure

DECOVALEX Tasks typically involve three model comparison components of increasing complexity, the first two of which are well-constrained by synthetic or experimental data and may involve identifying processes contributing to observed phenomenon, and developing and parameterizing models that explain the data:

- Benchmarks: Relatively simple cases, either synthetic or well-constrained experiments to act as a 'warm-up' for participants and to allow codes and process models to be compared.
- Test Cases: More complex modelling, often with detailed comparison against experimental data.
- Applications: Forward modelling that applies learning from Benchmarks and Test Cases to situations of direct interest for radioactive waste disposal, at larger spatial and/or temporal scales.

Task F is atypical in that it does not include a comparison to experimental data and does not seek to develop or parameterize models that explain data. Task F assumes that processes have been identified and models have been defined and parameterized. Through comparison of forward models of increasing complexity, Task F seeks to understand the uncertainty introduced by modeling choices (model fidelity, alternate models, methods of coupling) and uncertain model inputs:

- Benchmarks and Process Models: Comparison of codes and process model implementations on relatively simple problems that address a subset of the features and/or processes included in the full reference case simulation. These comparisons will develop a common understanding among participants and identify differences in model behaviour that may propagate through the more complex analyses. Uncertainty propagation may be included at this stage to test methods, but will be limited by the simplicity of the test problems.
- Deterministic Reference Case: Comparison of a full reference case simulation that addresses coupling between processes and results in multiple performance measures. These comparisons will identify differences in model behaviour that appear to arise from methods of coupling, omission of FEPs, or models of differing fidelity.
- Uncertainty Propagation: Comparison of uncertainty in performance measures resulting from propagation of uncertainty through the reference case simulation, and comparison of sensitivity of performance measures to uncertain model inputs.
- Sensitivity Analysis: Interested teams may also compare the utility of different sensitivity analysis methods, such as correlation, regression, or variance-based decomposition; and the use of metamodels and/or data transformations.

2.1 Outline Structure

The following outline structure is proposed:

- Step 0C: Review the DECOVALEX-2023 crystalline reference case proposal. Agree on key FEPs. Finalize details of conceptual model specification and parameterization for one scenario.
- Step 1C: Identify individual process models for benchmark comparisons and make the comparisons. Benchmarks will include simulation of advection/diffusion/dispersion; fracture flow and transport; radioactive decay and ingrowth; rate-controlled wasteform degradation and release of radionuclides. Others will be developed as needed throughout the course of the comparison.

- Step 2C: Crystalline reference case deterministic simulation. (May include multiple realizations of the fracture network.)
- Step 3C: Identify uncertain inputs and appropriate probability distributions for the crystalline reference case. Compare mean, median, and other quantitative metrics of uncertainty for performance measures. Calculate prescribed measure of sensitivity such as partial correlation coefficients and standardized regression coefficients, and compare them.
- Step 4C (optional): Interested teams may apply sensitivity analysis methods of their choice to the crystalline reference case for a comparison of sensitivity analysis methods.
- Step 0S: Develop a DECOVALEX-2023 salt reference case. Agree on key FEPs. Finalize details of conceptual model specification and parameterization.
- Step 1S: Identify individual process models for benchmark comparisons and make the comparisons. Benchmarks may include simulation of salt creep; crushed salt reconsolidation; advection/diffusion/dispersion; thermal conduction; radioactive decay and ingrowth; rate-controlled wasteform degradation and release of radionuclides; and other processes identified in the course of building the reference case.
- Step 2S: Salt reference case deterministic simulation.
- Step 3S: Identify uncertain inputs and appropriate probability distributions for the salt reference case. Compare mean, median, and other quantitative metrics of uncertainty for performance measures. Calculate prescribed measure of sensitivity such as partial correlation coefficients and standardized regression coefficients, and compare them.
- Step 4S (optional): Interested teams may apply sensitivity analysis methods of their choice to the salt reference case for a comparison of sensitivity analysis methods.

Table 2-1. Revised schedule of Task F steps. Green indicates crystalline. Orange indicates salt.

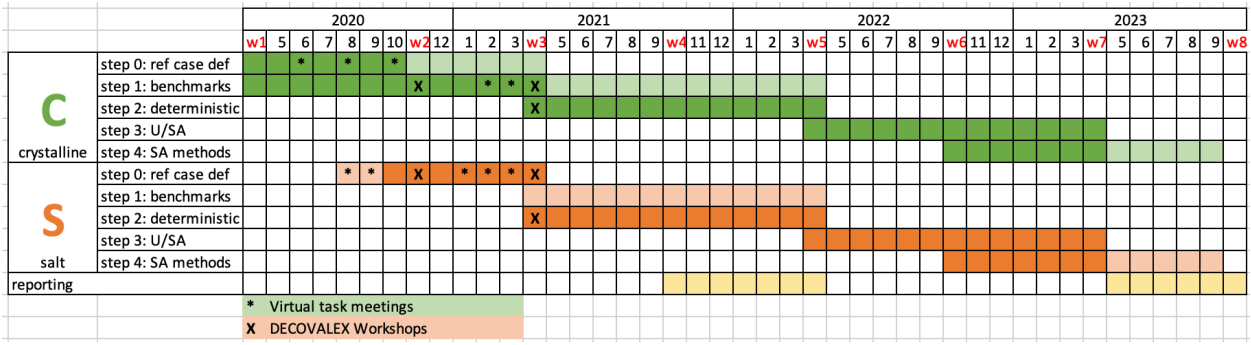

2.2 Possible Interfaces with Other DECOVALEX-2023 Tasks

Depending on the interest of participants, Task F may benefit from alignment with other DECOVALEX-2023 tasks.

The crystalline reference case offers an opportunity to consider the influence of stress state on fracture transmissivity and/or fracture slip, and may benefit from alignment with Task G (Safety Implications of Fluid Flow, Shear, Thermal and Reaction Processes within Crystalline Rock Fracture Networks (SAFENET)).

Crystalline reference participants could also consider simulating H_2 generation associated with iron corrosion, and possible alignment with Task B (Modelling Advection of Gas in Clays (MAGIC)).

The salt reference case may benefit from alignment with Task E (Brine Availability Test in Salt (BATS)).

3. Crystalline Reference Case

This section proposes a generic reference case for a mined repository in fractured crystalline rock. Step 0 of Task F will be for participating teams to agree on a common description of the features, events, and processes (FEPs) to consider in the reference case, and to quantitatively characterize and parameterize associated materials and models using values from the literature.

The following description of the reference case (Revision 7 of the Task Specification) is intended for simulations of steady state flow and transient transport given generic tracer source terms in the repository. Further decisions regarding key FEPs affecting evolution of the engineered and natural systems and scenarios of interest will guide further development of the reference case.

The reference case is described in terms of the geologic setting (Section 3.1), emplacement concept (Section 3.2), inventory (Section 3.3), repository layout (Section 3.4), engineered barrier system (Section 3.5), and natural barrier system (Section 3.7). Tracer source terms for the initial simulations and model outputs for comparison are in Section 3.7.3 and Section 3.9, respectively. Given a common description of the reference case components, each team is responsible for deciding how to represent the components in their performance assessment model. Such decisions may include, for example, simplifying the geometry of a feature, representing each component of the repository versus lumping components of the repository, or treating the fractured rock as a discrete fracture network versus treating it as a continuous porous medium.

In the crystalline reference case, uncertainty is introduced in the first iteration of the reference case due to the uncertain distribution of fractures with length less than 1 km. Given the stochastic distributions in Section 3.7.2, teams should generate 10 realizations of the fractured rock and run 10 realizations of their performance assessment model. Ten realizations of the discrete fracture network (DFN) will be provided for teams that lack the capability to generate fractured rock realizations. It is recommended that teams using the provided DFNs make independent choices about upscaling, if they choose to represent the rock as a continuous porous medium.

3.1 Geologic Setting

The reference case repository is located beneath a gently sloping hill in a domain 5 km in length, 2 km in width, and 1 km in depth. The repository is located in the west (left) side of the domain and the area of lowest elevation is located in the east (right) side of the domain. Conceptually, the area of lowest elevation represents the location where water would collect at the surface forming a feature such as a lake or wetland.

Surface elevation decreases 20 m over a distance of 2 km; it is assumed that the hydraulic pressure at the top surface of the domain mimics the topography (Figure 3-1). The surface elevation (z, in meters) is described as a function of distance (x, in meters):

$$[z = 1020]_{0 \le x < 1700}$$

$$[z = \sin(r) + 1010]_{1700 \le x \le 3700}$$

$$[z = 1000]_{3700 < x \le 5000}$$

where $r(x = 1700) = \pi/2$ and $r(x = 3700) = 3\pi/2$. Hydraulic pressure is calculated from a reference pressure of 101,325 Pa at z = 1000 m, assuming a water density of 1000 kg/m^3 or using the equation of state available in a team's flow simulator. No flow boundary conditions are imposed at all other faces of the domain.

The cross section in Figure 3-1 shows three different depth zones in which fracture intensity and fracture transmissivity decrease with depth; depth zones are described in more detail in Section 3.7.

In such a setting, salinity could be expected to increase with depth, and a layer of sedimentary overburden could be expected. However, for the purposes of simplifying the reference case, variation in salinity and existence of overburden are neglected.

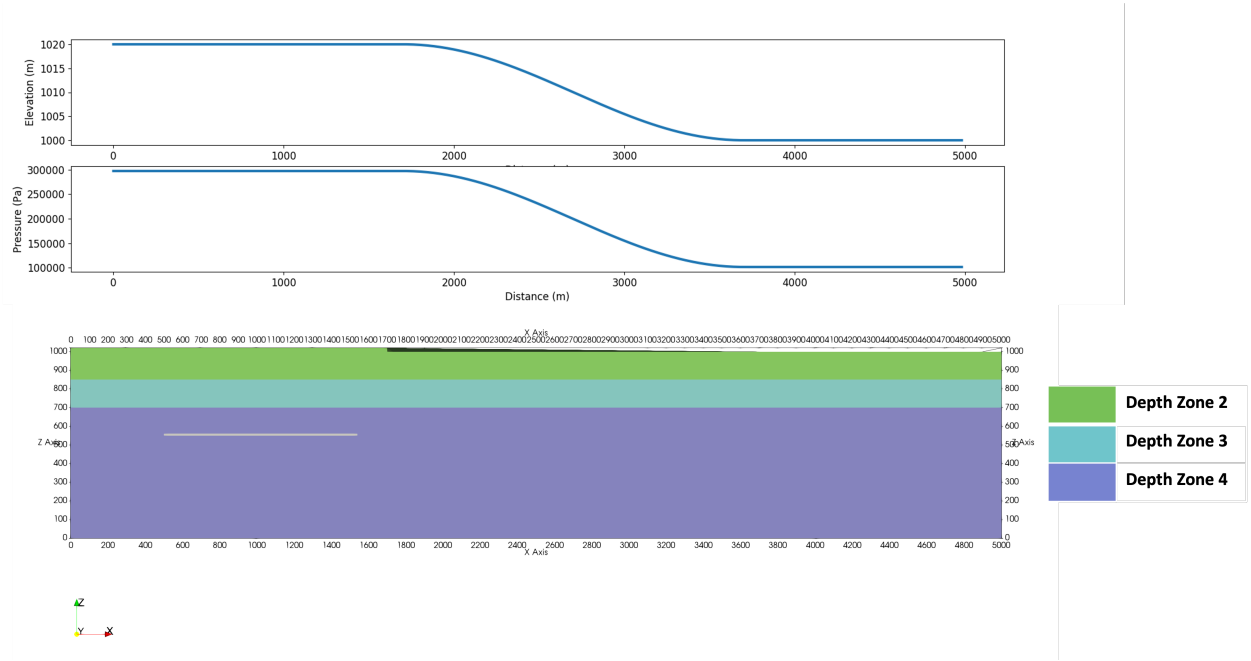

Figure 3-1 Elevation profile and corresponding pressure boundary condition (top) and depth zones in the domain (bottom).

3.2 Emplacement Concept

The generic reference case uses the KBS-3V emplacement concept developed for the Swedish and Finnish repository programs (Pettersson and Lönnerberg 2008), and adopted by several countries as the reference design for a generic reference case or in the preliminary stages of site investigation (TPC 2017; Choi et al. 2013; NWMO 2012). The KBS-3V concept is developed for a repository mined at a depth of approximately 500 m in sparsely fractured crystalline rock. Copper canisters each containing a nominal inventory of 4 pressurized water reactor (PWR) assemblies are emplaced within rings of compacted bentonite in vertical deposition holes beneath the floor of a deposition tunnel, and tunnels are backfilled.

The repository system isolates radionuclides from the biosphere primarily through containment, and secondarily through retardation. The depth of burial together with the hydraulic, chemical, and mechanical environment at depth protects the canisters from failure due to corrosion or mechanical loading. The canister itself is designed to withstand mechanical loading and resist corrosion under geochemical conditions at depth. The bentonite buffer additionally protects the canister by slowing transport of corrodents, absorbing shear motion, and preventing direct contact of the canister with the host rock. In the case of canister failure and depending on failure mechanism, the low permeability and high adsorption capacity of the bentonite retards radionuclide transport. Adsorption and matrix diffusion along fracture flow paths also retard radionuclide transport.

3.3 Inventory

The waste inventory is 4350 metric tons uranium (MTU) in the form of PWR SNF. Assuming each PWR assembly contains 0.435 MTU, 2500 4-PWR canisters are required to dispose of the inventory. The waste inventory is deliberately small in order to reduce the computational burden of simulations.

Characterization: Initial radionuclide inventory is calculated assuming an initial enrichment of 4.73 wt% U-235, 60 GWd/MTU burnup, 50 years out of reactor (OoR) (Carter et al. 2013). Assuming 60 GWd/MTU burnup will provide a conservative upper-bound on heat generation, if future iterations of the reference case considered heat.

Processes to consider in this iteration of the reference case:

- Initial reference case simulations do not consider the radionuclide inventory; instead only tracer transport is considered (Section 3.7.3).

3.4 Repository Layout

The repository, located at a depth of approximately 450 m, comprises 50 deposition drifts branching off two parallel access tunnels (Figure 3-2). The deposition drifts are spaced 40 m center-to-center; 50 deposition holes within each tunnel are spaced 6 m center-to-center. This spacing ensures that peak buffer temperatures do not exceed 100º C (Pettersson and Lönnerberg 2008). The deposition drifts are 306 m in length so that the deposition tunnel extends 6 m beyond the center of the last deposition hole at both ends. There are 50 individual deposition drifts which results in a total of 2500 deposition boreholes.

The geometry of the deposition holes is given together with the description of the buffer in Section 3.5.3. The geometry of the access tunnels and deposition drifts is given together with the description of the backfill in Section 3.5.4.

The dimensions of the repository are 1040 m from east to west and 662 m from north to south. With the left, front, bottom corner of the domain defined as (0, 0, 0) in (x, y, z), the reference points locating the repository in the domain are:

- The west face of the short tunnel connecting the two central tunnels is at x = 500 m.
- The midline of the repository in the y direction is at y = 1000.
- The floor of the drifts and tunnels is at z = 550 m (470 m below a surface elevation of 1020 m, or 450 m below a surface elevation of 1000 m).

For simplicity, the shafts and a ramp that would connect the repository to the surface are neglected.

The repository is located in the domain such that all parts of the repository are greater than 100 m from the deterministic fracture zones described in Section 3.7.1. A 100-m offset distance of deposition holes from major deformation zones that have the potential to experience large displacements in the case of a seismic event or to provide a highly transmissive transport path to the biosphere will be enforced throughout further development of the reference case.

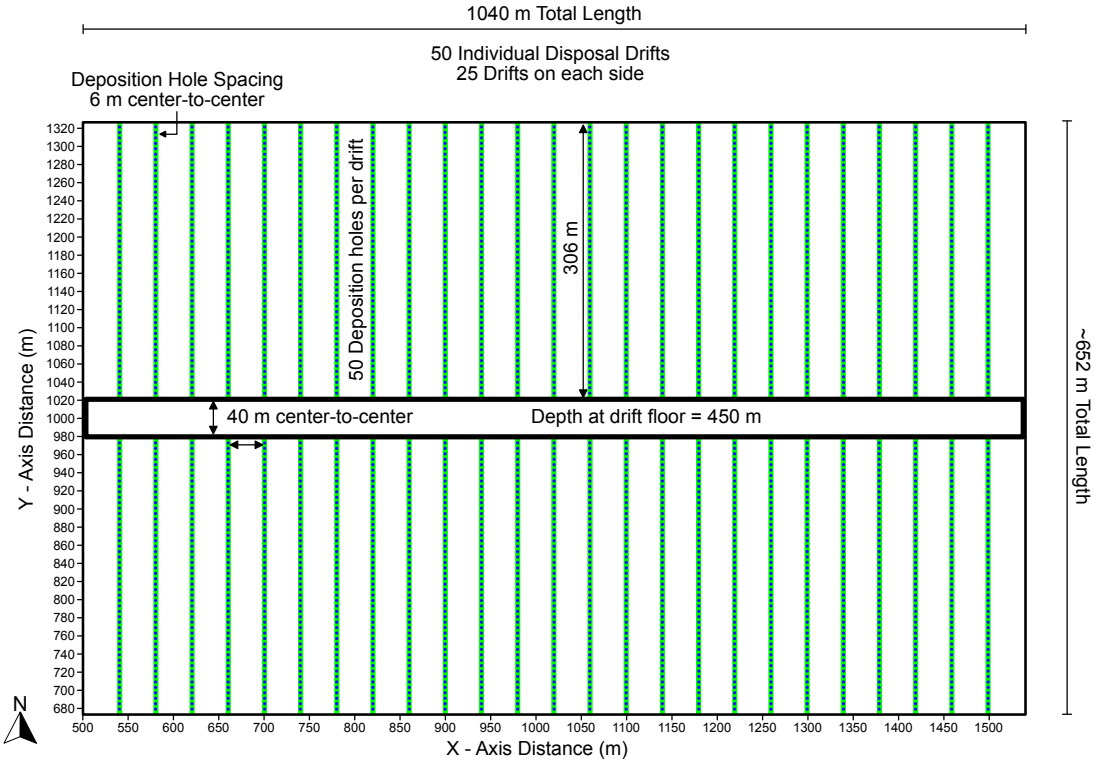

Figure 3-2. Repository layout for the crystalline reference case. (Black outline around the repository is not a tunnel.)

3.5 Engineered Barrier System

3.5.1 Wasteform

Fuel rods are comprised of UO_2 pellets in Zircaloy cladding tubes. No performance credit is taken for the cladding. Upon inundation of a breached canister, radionuclides are released from the UO_2 fuel in two fractions. A fraction of the fission products (accumulated in void spaces within the fuel rods) is released instantly. All other radionuclides are released by rate-controlled congruent dissolution of the UO_2 wasteform.

Characterization: UO_2 dissolution is modeled assuming a fractional rate appropriate for the geochemical environment (Werme et al. 2004, Section 3.7).

Safety function: Rate-controlled dissolution retards radionuclide release.

Processes to consider in this iteration of the reference case:

- Initial reference case simulations do not consider the UO_2 wasteform; instead only tracer transport is considered (Section 3.7.3).

3.5.2 Waste Package

The waste package for the KBS-3V emplacement concept is a copper canister with cast iron insert (Figure 3-3). The copper shell and cast iron insert are described in the following sections. The canister dimensions are 4905 mm in length and 1050 mm in diameter (Figure 3-4).

Figure 3-3. Exploded view of the canister components (from left: copper base, copper tube, insert, steel lid for insert and copper lid) (from SKB 2011, TR-11-10).

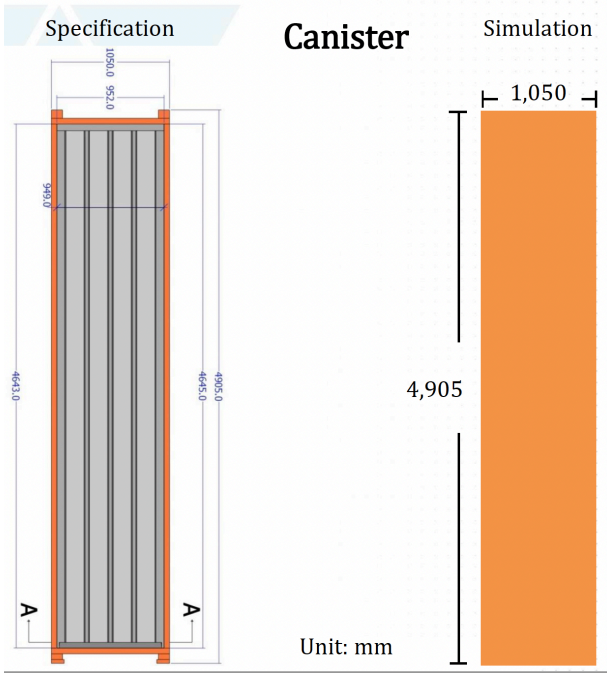

Figure 3-4. Canister dimensions in engineering specification (left) and for use in the reference case (right) (from Chang et al. 2021).

3.5.2.1 Canister Insert

The canister insert for the KBS-3V concept comes in two designs, one for 12 BWR (boiling water reactor) fuel assemblies and one for 4 PWR fuel assemblies (Figure 3-5). The reference case assumes 4 PWR fuel assemblies. Both insert designs consist of nodular cast iron with a steel tube cassette for each fuel element.

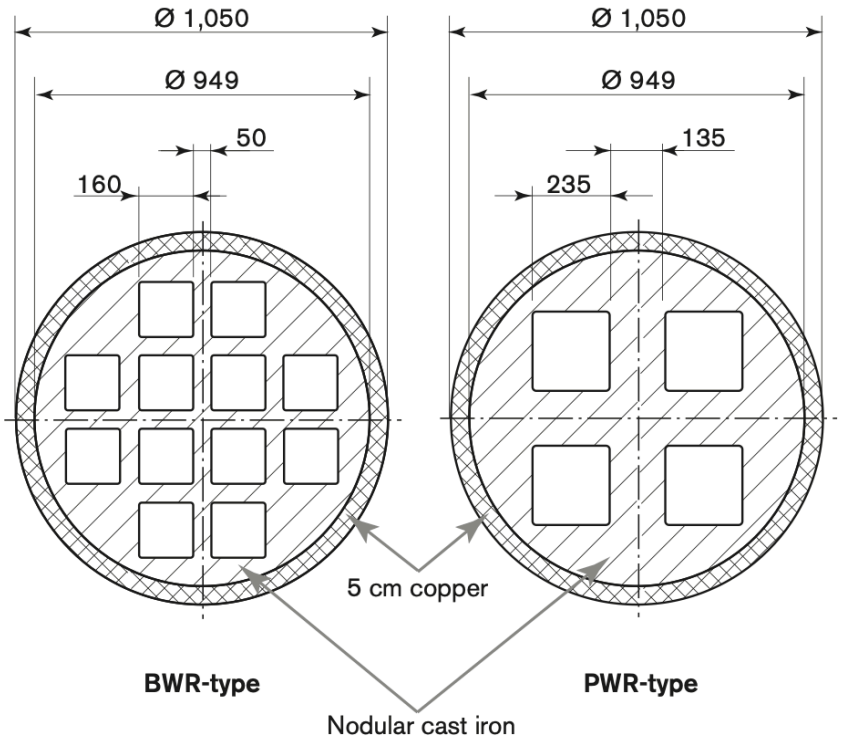

Figure 3-5. Cross section of insert designs of the BWR and PWR type inserts for the KBS-3V concept (from SKB 2011).

Characterization: Teams are responsible for choosing canister properties consistent with their approach to constructing a performance assessment model. For example, if a porous medium flow and transport model is used, it may be necessary to assign permeability and porosity to the canister. If future iterations of the reference case require specific properties to be specified, the properties of the cast iron insert will be taken from SKB (2010a), Section 3.1.

Safety function: Mechanical strength resists isostatic loading and shear stress to contain radionuclides.

Processes to consider in this iteration of the reference case:

- Initial tracer transport simulations assume canisters provide no containment function. Therefore, no processes are considered.

3.5.2.2 Canister Shell

The canister shell goes on the outside of the canister insert and consists of 5-cm thick copper (Figure 3-5).

Characterization: Teams are responsible for choosing canister properties consistent with their approach to constructing a performance assessment model. For example, if a porous medium flow and transport model is used, it may be necessary to assign permeability and porosity to the canister. If future iterations of the reference case require specific properties to be specified, the properties of the copper shell will be taken from SKB (2010a), Section 3.2.

Safety function: The copper canister contains radionuclides by resisting corrosion in repository geochemical conditions. Because it is ductile, it resists shear failure.

Processes to consider in this iteration of the reference case:

- Initial tracer transport simulations assume canisters provide no containment function. Therefore, no processes are considered.

3.5.3 Buffer

Figure 3-6 shows the geometry of the canister and bentonite buffer in the deposition hole, which is 8155 mm in length and 1750 mm in diameter. Each canister is surrounded by blocks of compacted bentonite. The buffer consists of one solid bottom block, six ring-shaped blocks around the canister and three solid blocks on top of the canister. Gaps between bentonite blocks and the wall of the deposition hole are filled with bentonite pellets. Although Figure 3-6 indicates that the bulk density of the buffer would vary along the length of the deposition hole, the reference case does not take into account this variation.

The main function of the buffer is to restrict water flow around the canister. This is achieved by a low hydraulic conductivity, which makes diffusion the dominant transport mechanism, and a swelling pressure, which makes the buffer self-sealing. The buffer should also keep the canister in position in the deposition hole, dampen rock shear movements and maintain its properties for the timescale of the assessment.

A number of processes affecting canister integrity and radionuclide transport occur in the bentonite. Hydraulic, mechanical, and chemical processes including inflow, erosion, and reactive transport of solutes may be considered as the reference case progresses.

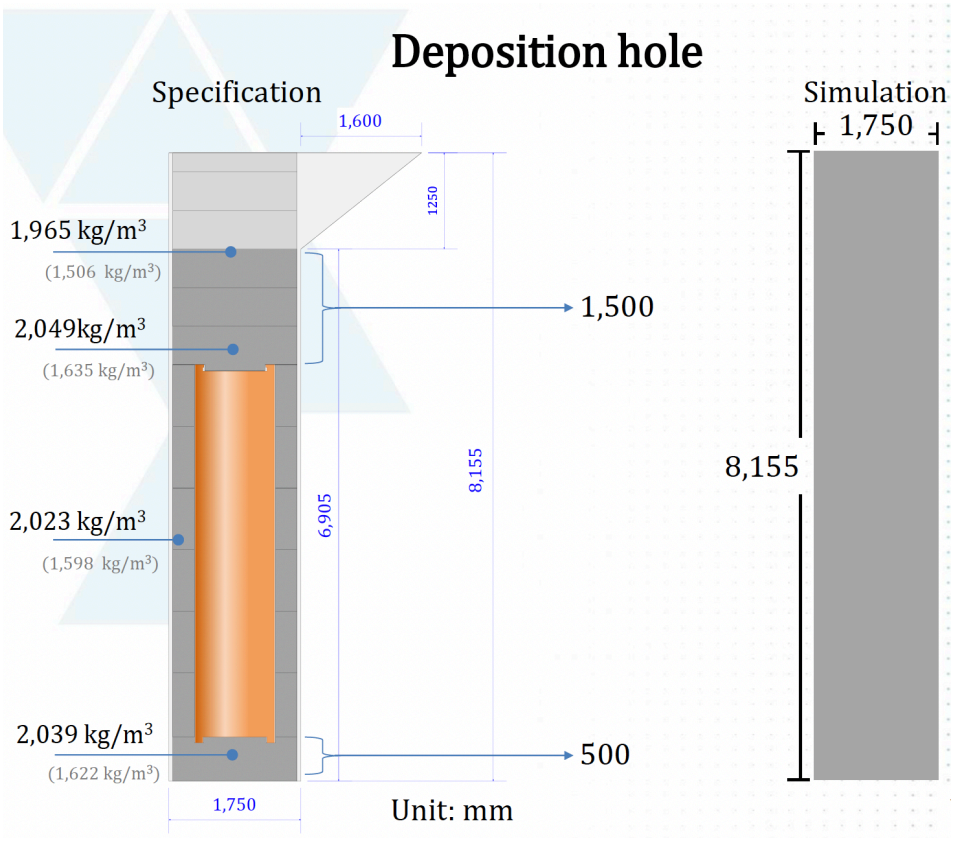

Figure 3-6. Deposition hole dimensions in engineering specification (left) and for use in the reference case (right) (from Chang et al. 2021). The thickness of the buffer around the canister is 35 cm.

Characterization: Hydraulic properties of the bentonite buffer are given in Table 3-1.

Safety function: Bentonite buffer provides the hydraulic, mechanical, and chemical conditions that support canister integrity. The low permeability and high adsorption capacity of bentonite retard radionuclide transport.

Processes to consider in this iteration of the reference case:

- Advection and diffusion of tracer. Diffusive transport dominates in intact buffer.

Table 3-1 Material properties of buffer.

Parameter	Value	Reference
Permeability (m^2)	6×10^{-21}	SKB TR-10-44 (Table 12-3)
Porosity (unitless)	0.44	SKB TR-10-15 (Appendix B) SKB TR-10-50 (Table 3-2)
Effective Diffusivity* (m^2/s)	1.4×10^{-10}	SKB TR-10-52 (Equation 5-4)
*Effective diffusivity, $D_e = D_m \phi \tau$, where D_m, the molecular diffusion coefficient in free water, = 1.0E-09 m^2/s, ϕ is porosity and τ is tortuosity (a number < 1).		

3.5.4 Backfill

Figure 3-7 shows the geometry of the access (main) tunnels and deposition tunnels. The reference case assumes nominal rectangular cross sections. The access tunnels are nominally 10 m in width and 7 m in height. The deposition drifts are nominally 4.2 m in width and 4.8 m in height. Deposition tunnels are backfilled with compacted bentonite blocks and bentonite pellets. For simplicity, the reference case will assume that access tunnels are backfilled with the same.

Although the processes that can occur in the backfill are similar to those that occur in the buffer, they are of less interest in the reference case because the backfill exerts less influence on canister integrity and radionuclide transport. For this reason the reference case will not consider processes such as erosion or settling that may affect the performance of the backfill.

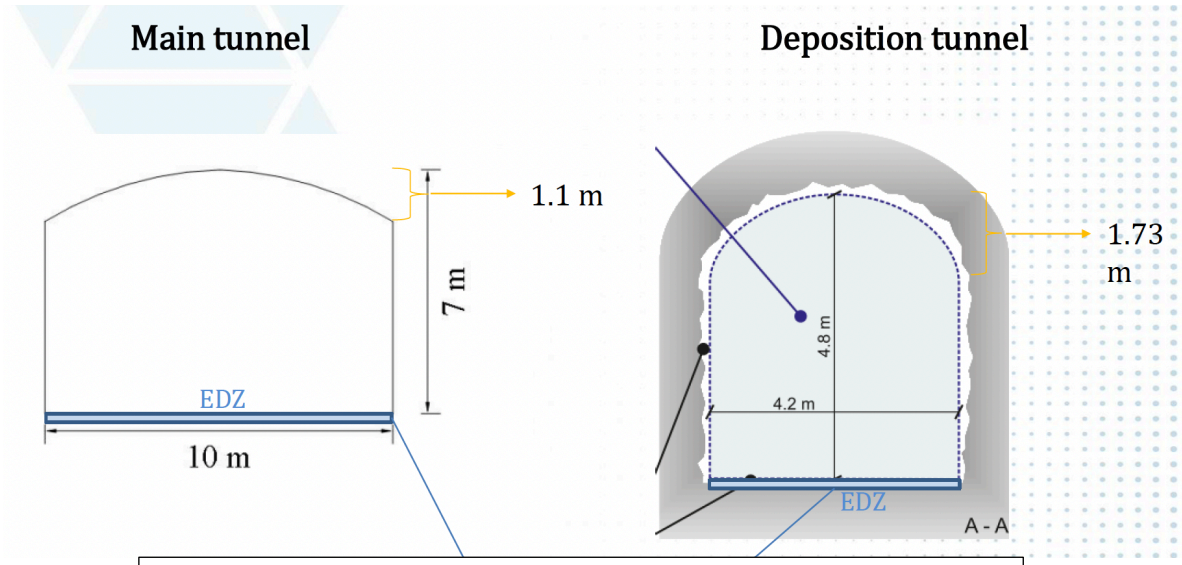

Figure 3-7. Cross section of the access tunnel (right) and deposition tunnel (left) with nominal dimensions indicated (Chang et al. 2021 after SKB TR-10-16 (pg. 28) and SKB R-09-59 (pg. 36)).

Characterization: Hydraulic properties of the bentonite backfill are given in Table 3-2.

Safety function: The backfill provides the hydraulic, mechanical, and chemical, conditions that help maintain canister and buffer emplacement in the deposition holes. The low permeability and high adsorption capacity of bentonite retard radionuclide transport.

Processes to consider in this iteration of the reference case:

- Advection and diffusion of tracer. Diffusive transport dominates in intact backfill.

Table 3-2 Material properties of the backfill.

Parameter	Value	Reference
Permeability (m^2)	1.5×10^{-20}	SKB TR-10-44 (Table 12-3)
Porosity (unitless)	0.46	SKB TR-10-50 (Table 3-2)
Effective Diffusivity* (m^2/s)	1.6×10^{-10}	SKB TR-10-52 (Equation 5-4)
*Effective diffusivity, $D_e = D_m \phi \tau$, where D_m, the molecular diffusion coefficient in free water, = 1.0E-09 m^2/s, ϕ is porosity and τ is tortuosity (a number < 1).		

3.5.5 Plugs in Deposition Tunnels

Plugs constructed with low-pH concrete will keep the backfill in the deposition tunnels in place until the main tunnel is backfilled (SKB 2010c, Section 2.5). Plugs perform no post-closure safety function. Although dissolution of cement will locally affect groundwater chemistry, the plugs are distant from deposition holes, and the reference case neglects them.

3.5.6 Grout

During excavation, fractures with high inflow rates are grouted with low-pH shotcrete to minimize inflow to the excavation. Grout affects inflow into the repository during excavation, and therefore may be considered in establishing initial conditions for post-closure groundwater flow simulations. It performs no post-closure safety function and is not expected to be durable; dissolution will locally affect groundwater chemistry. Other than possible consideration in establishing post-closure initial conditions, the reference case does not consider the hydraulic or chemical effects of grout on flow and transport.

3.6 Excavation Damage Zone (EDZ)

3.6.1 Tunnel EDZ

The EDZ is the portion of the tunnel wall whose properties are changed due to excavation or changes in stress field associated with excavation. The EDZ forms a potential path for radionuclide transport, because its permeability and to a lesser extent porosity are higher than in the intact host rock. It does not perform a post-closure safety function, and has no associated performance measure. Initial reference case simulations neglect the EDZ.

3.6.2 Deposition Hole EDZ

Thermal spalling may occur in the deposition holes, increasing the permeability of the host rock and mass transfer rates between the deposition hole and the fractures. It does not perform a post-closure safety function, and has no associated performance measure. Initial reference case simulations neglect thermal spalling.

3.7 Natural Barrier System

The crystalline host rock is characterized by occurrence of large-scale, highly-fractured brittle deformation zones and intervening masses of competent rock containing sparse networks of connected fractures. Following the example of SKB (e.g., Joyce et al. 2010), the former are named Hydraulic Conductor Domains (HCD) and the latter are named Hydraulic Rock Mass Domains (HRD).

The fractures within the HRD are subdivided up into three different depth zones, representing vertical variations within the subsurface. Each depth zone contains three different families, representing variations in orientation (strike and dip, or equivalently, trend and plunge) and hydraulic properties.

Conceptually, present day properties such as transmissivity of individual fractures exhibit a dependence on the present day stress field. As a result, there is a greater density of fractures, larger proportion of subhorizontal fractures, and higher fracture transmissivity at shallower depths, and lower density of fractures, lower proportion of subhorizontal fractures, and lower fracture transmissivity at greater depths.

HCD and HRD are described in more detail below.

Safety function: The crystalline host rock and depth of the repository within it provide hydraulic, mechanical, and chemical conditions that protect the waste canisters. Matrix diffusion and adsorption retard radionuclide transport.

Processes to consider in this iteration of the reference case:

- Steady-state flow in open, connected fractures and fracture zones.
- Advection and diffusion of tracer. Advection dominates in fractures.
- Initial simulations will not include fracture-matrix diffusion. However, we will seek to add this process in the near future.

3.7.1 Hydraulic Conductor Domains (Deterministic Features)

Hydraulic Conductor Domains (HCD) are defined as local to regional-scale deformation zones with widths of meters and lengths greater than a kilometer that contain a high density of transmissive fractures. HCDs are observable on surface outcrops, as surface lineaments, and as highly fractured intervals in boreholes. Their locations, dimensions, and orientation are constrained by these observations, so that they are included as deterministic features in hydrogeological models and in flow and transport simulations.

Characterization: The reference case employs a representative set of deterministic deformation zones whose spacing and orientations are derived from observations of Brittle Fracture Zones (BFZ) at Olkiluoto (Hartley et al. 2018, Table 3-3, 3-28, 3-29). In the reference case, the deterministic deformation zones, or HCDs, are represented as singular, planar features – essentially large deterministic fractures. The aperture and transmissivity of the deterministic fractures are defined as outlined in Section 3.7.2 using the cubic law and the correlated relationship between fracture transmissivity and fracture radius, where the dimensionless coefficients a and b are taken from the EW fractures in Depth Zone 3 (Table 3-4). The deterministic fractures are defined by Table 3-3 and shown in Figure 3-8. These circular subhorizontal and subvertical features are spaced throughout the domain.

Table 3-3 Location and orientation of the deterministic fractures.

ID #	Radius (m)	Translation (x, y, z coordinates of fracture center, m)*	Unit Normal Vector (orientation)
1	3451.39	{-501.41,1823.58,-481.95}	{-0.67342,0.73387,-0.08904}
2	897.266	{-55.38,-452.20,284.20}	{-0.24506,-0.013604,-0.96941}
3	650.303	{2072.39,-676.33,372.32}	{-0.38242,0.09575,-0.91901}
4	2318.13	{-606.04,1176.42,-1042.55}	{-0.50116,-0.63138,-0.59177}
5	1595.92	{1769.15,241.45,124.63}	{-0.55597,0.78048,-0.28590}
6	1625.51	{2275.47,-849.96,-923.85}	{-0.59401,-0.80091,0.07533}
*The (x, y, z) coordinates of the fracture center are given relative to the position (0, 0, 0) at the center of the domain. Add (2500, 1000, 500) to place the fractures relative to the position (0, 0, 0) at the left, front, bottom corner of the domain.			

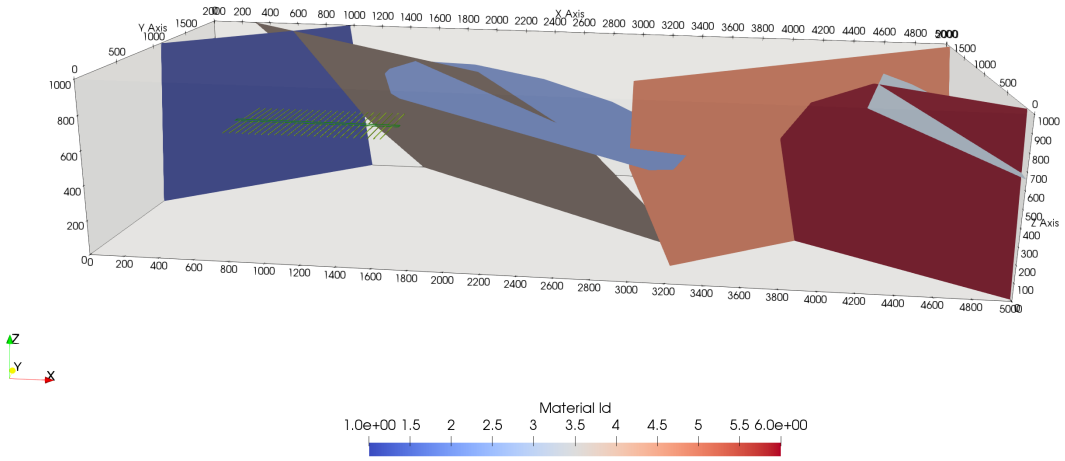

Figure 3-8 Deterministic fractures in the model domain.

3.7.2 Hydraulic Rock Mass Domains (Stochastic Discrete Fracture Networks)

Hydraulic Rock Mass Domains (HRD) outside the HCDs contain fractures and minor deformation zones with lengths ranging from less than 1 m up to 1 km that are not deterministically mapped. A subset of these features (generalized as discrete fractures) forms a connected network of open fractures through which groundwater can flow. Within each HRD and/or depth interval within an HRD, fractures are grouped into fracture families on the basis of orientation, and characterized by fracture intensity and probability distributions for size, orientation, and location. Stochastic realizations of discrete fracture networks (DFNs) for use in the hydrogeological model can be generated from these distributions. Alternatively, teams may choose to generate equivalent continuous porous media or other representations of the fractured rock from the stochastic characterization of the fracture network.

Characterization: The intensity of open fractures and probability distributions describing size, orientation, and location of open fractures in three depth zones (Figure 3-1) are taken from the Case A parameterization of the western central hydraulic unit (CHUW) at Olkiluoto, Depth Zones 2-4 (Hartley et al. 2013, Table D-4). With the bottom of the domain at z = 0, Depth Zone 2 extends from the top surface to z = 850 m; Depth Zone 3 extends from z = 850 m to z = 700 m; and Depth Zone 4 extends from z = 700 m to z = 0 m. The probability distributions characterizing the stochastic fracture network are described in the following sections and corresponding parameters for each fracture family are given in Table 3-4.

This particular Olkiluoto hydraulic unit is proposed for use in the reference case because it provides an opportunity to investigate the hydromechanical coupling between stress field and fracture transmissivity in later iterations of the reference case.

Table 3-4 Parameters for stochastic fractures

		Pole Orientation (Fisher Distribution)	Fracture Radius [m] (Power-law Distribution)	Intensity of open fractures	Transmissivity [m^2/s]

		Mean Trend φ [°]	Mean Plunge θ [°]	Concentration κ k		r_0 [m]	P_{32} [m^2/m^3]	a	b
CHUW dz2	E-W	176	4.4	9.4	2.58	0.04	0.21	8.0E-9	0.8
	N-S	270.4	0.2	8.3	2.52	0.04	0.25	1.5E-8	0.8
	SH	300.1	78.9	5.7	2.45	0.04	0.91	1.2E-8	0.8
CHUW dz3	E-W	176	4.4	9.4	2.50	0.04	0.11	2.2E-9	0.7
	N-S	270.4	0.2	8.3	2.65	0.04	0.13	6.0E-9	0.6
	SH	300.1	78.9	5.7	2.35	0.04	0.34	2.0E-9	1.2
CHUW dz4	E-W	176	4.4	9.4	2.40	0.04	0.07	7.0E-11	0.7
	N-S	270.4	0.2	8.3	2.40	0.04	0.08	8.0E-11	0.9
	SH	300.1	78.9	5.7	2.40	0.04	0.17	6.0E-11	1.0

3.7.2.1 Fracture Orientation and Location

Three fracture families, two subvertical and one subhorizontal are defined for each depth zone. The orientation of a fracture can be described by providing the orientation of a pole normal to the plane of the fracture (as in Hartley et al. 2013). For each fracture family, the probability distribution describing the orientation of poles is a Fisher distribution, an isotropic, directional distribution equivalent to a Gaussian distribution on a sphere (von Mises-Fisher distribution, accessed 23 October 2021). The Fisher distribution is parameterized by a mean direction (defined by mean trend (φ) and mean plunge(θ)) and a concentration parameter (κ). The larger κ, the more concentrated the poles on the surface of the sphere.

Although Hartley et al. (2013) gives a bivariate Bingham distribution for the subhorizontal (SH) families, the simpler Fisher distribution is used as a substitution in the reference case.

Fracture locations are uniformly distributed in 3-dimensional space, limited by the fracture intensity of each fracture family.

3.7.2.2 Fracture Radius and Intensity

The probability distribution of fracture radii (r, [m]) is a truncated power law distribution, with the form of (Follin et al. 2007):

$$f(r) = \frac{k r_0^k}{r^{k+1}}$$

where r_0 is the minimum radius and k is a constant, respectively.

Fracture intensity is expressed as fracture area per unit volume of rock (P_{32} [m^2/m^3]). The P_{32} values in Table 3-4 represent the intensity of open, flowing fractures, and were calibrated to borehole flow data assuming r_0 = 0.04 m and maximum radius (r_{max}) of 564 m (Hartley et al. 2013). P_{32} is related to the average number of fractures per unit volume of rock (n_0) by (Swiler et al. 2020):

$$P_{32} = n_0 \int_{r_0}^{r_{upper}} p(r)\pi r^2 dr = n_0 \int_{r_0}^{r_{upper}} \frac{k r_0^k}{r^{k+1}} \pi r^2 dr = \frac{n_0 \pi k r_0^k}{2-k} [r^{2-k}]_{r=r_0}^{r=r_{upper}}.$$

P_{32} over the range r_0 = 0.04 m to r_{max} = 564 m is equivalent to billions of fractures per km^3, the vast majority of which have radii < 1 m. To determine the P_{32} for a smaller range of radii (e.g., minimum radius, r_{min} = 30 m to r_{max} = 564 m), integrate the above over the range r_{min} to r_{max} (Swiler et al. 2020):

$$P_{32}[r_{min}, r_{max}] = \frac{\pi n_0 k r_0^k}{2-k}[r_{max}^{2-k} - r_{min}^{2-k}].$$

3.7.2.3 *Fracture Transmissivity, Aperture, and Permeability*

Fracture transmissivity (T [m^2/s]) is a function of fracture radius. The reference case uses the fully-correlated relationship defined in Follin et al. (2007):

$$\log T = \log a r^b$$

Where r is radius [m] and the coefficients a and b are dimensionless constants. Fracture aperture is calculated from the transmissivity using the cubic law (Bear et al. 1993):

$$aperture = \left(12T\frac{\mu}{\rho g}\right)^{\frac{1}{3}}$$

Where μ is viscosity of water [Pa s], ρ is density of water [kg/m^3], and g is the acceleration due to gravity [m/s^2]. Permeability (k [m^2], not to be confused with the exponent in the power law) is defined as,

$$k = \frac{aperture^2}{12}$$

The resulting stochastic fractures are shown in Figure 3-9.

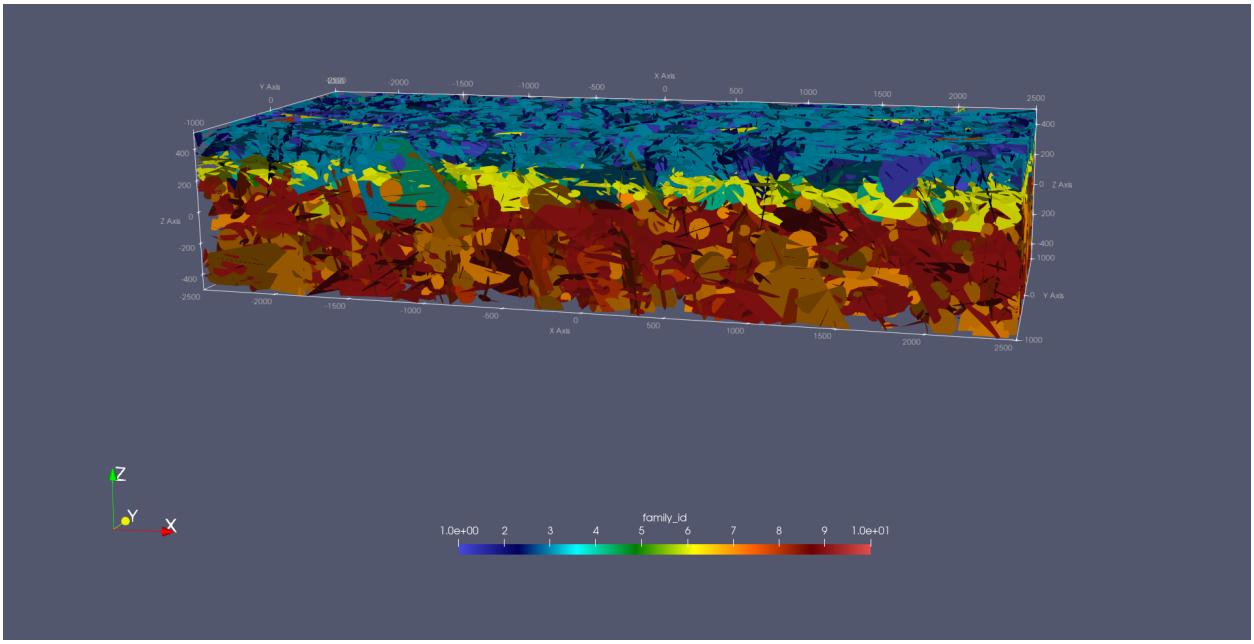

Figure 3-9 Stochastic fractures, colored by fracture family in each depth zone.

3.7.3 Fractured Rock Matrix

Future iterations of the reference case will consider fracture-matrix diffusion. At that time it will be necessary to characterize the matrix of the fractured rock. Additionally, teams choosing to use a porous

medium representation of the crystalline rock need parameters describing the rock matrix. Parameters for both purposes are given in Table 3-5.

Table 3-5. Material properties of the fractured rock matrix.

Parameter	Value	Reference
Permeability (m^2)	10^{-18}	Hartley et al. 2012 (Section 7.1)
Porosity (unitless)	0.0018	SKB TR-10-50 (Section 2.5)
Effective Diffusivity* (m^2/s)	$10^{-13.7}$	SKB TR-10-52 (Equation 2-2)
Distance available for diffusion in the matrix (m)	12.5	SKB TR-10-50 (Table 3.2)
*Effective diffusivity, $D_e = D_m \phi \tau$, where D_m, the molecular diffusion coefficient in free water, = 1.0E-09 m^2/s, ϕ is porosity and τ is tortuosity (a number < 1).		

3.8 Conservative Tracer Transport

In the first iteration of the reference case, teams will model steady state flow and conservative transport of two tracers (Table 3-6). Tracer 1 and Tracer 2 are modeled after ^{129}I. Both have an atomic weight of 128.9 g/mol. The total inventory of the two tracers in each waste package is 5.45 g (0.0423 moles), equivalent to $1/100^{th}$ of the expected inventory of ^{129}I in a waste package containing 4 pressurized water reactor assemblies. The inventory of Tracer 1 is 0.545 g (0.00423 moles), or 10% of the total; it is instantly released at the start of the transport simulation. The inventory of Tracer 2 is 4.90 g (0.038 moles), or 90% of the total; it is released at a fractional rate of 10^{-7}/year throughout the transport simulation. (Representative ^{129}I inventory is calculated from values in Table 4-1; instant release fraction and fractional rate of release are taken from Table 4-7 and Table 4-8, respectively.)

Teams should establish a steady state flow solution using a constant pressure (Dirichlet) boundary condition at the top surface of the domain (see Section 3.1) and no flow boundary conditions at all other faces of the domain. Then, start transport simulations from a steady-state flow solution and run to 100,000 years. Initially the domain is empty of tracer everywhere except in the waste packages. Tracer is allowed to advect out of the domain at the top surface; zero gradient boundary conditions should be applied to prevent diffusion out of the domain.

Table 3-6. Tracer inventories and release mechanisms for initial reference case simulations.

	Atomic weight	Inventory per waste package	Release mechanism
Tracer 1	128.9 g/mole	0.545 g	Instant
Tracer 2	128.9 g/mol	4.9 g	10^{-7}/year

3.9 Output Metrics for Comparison

Teams should generate 10 realizations of the fractured rock and run 10 realizations of their performance assessment model. (Ten realizations of the discrete fracture network (DFN) will be provided for teams that lack the capability to generate fractured rock realizations.)

Conceptually, the reference case will consider two pathways by which a person could ingest radionuclides. The first is by drinking water from a well located at the end of the highest consequence path between the repository and the surface of the hillslope (1700 m < x < 3700 m). The second is by drinking water from the hypothetical body of water resting on the area of lowest elevation (3700 m < x < 5000 m). The following outputs for comparison are designed with these two ingestion pathways in mind.

1. Find the location on the surface of the hillslope (1700 m < x < 3700 m) where the tracer mass flow is greatest. At this location,
    a. Plot mass flow (moles/year) of each tracer across the top surface of the domain as a function of time (years).
    b. Plot cumulative mass flow (moles) of each tracer across the top surface of the domain as a function of time (years).
2. Integrate over the area of lowest elevation (3700 m < x < 5000 m) to:
    a. Plot mass flow (moles/year) of each tracer across the top surface of the domain where 3700 < x < 5000 m (into the body of water) as a function of time (years).
    b. Plot cumulative mass flow (moles) of each tracer across the top surface of the domain where 3700 < x < 5000 m (into the body of water) as a function of time (years).

The first comparison, of tracer transport at a point location, is an attempt at locating and comparing fluxes at the highest consequence location for a well. Likely, this comparison will need to be refined to account for differences in grid discretization and other choices made by modeling teams.

We will also compare outputs that will assist in understanding system behavior and whether teams are achieving similar system behavior:

3. Record the steady state flow of water (kg/year) into and out of the top surface of the domain over the area where 0 m < x < 1700 m (top of hill).
4. Record the steady state flow of water (kg/year) into and out of the top surface of the domain over the area where 1700 m < x < 3700 m (hillslope).
5. Record the steady state flow of water (kg/year) into and out of the top surface of the domain over the area where 3700 m < x < 5000 m (area of lowest elevation).
6. Integrate over the area of the hillslope:
    a. Plot the mass flow (moles/year) of each tracer across the top surface of the domain over the area where 1700 < x < 3700 m (to the hillslope) as a function of time (years).
    b. Plot the cumulative mass flow (moles) of each tracer across the top surface of the domain over the area where 1700 < x < 3700 m (to the hillslope) as a function of time (years).
7. Find the location in the area of lowest elevation where the tracer mass flow is greatest. At this location:
    a. Plot mass flow (moles/year) of each tracer across the top surface of the domain as a function of time (years).
    b. Plot cumulative mass flow (moles) of each tracer across the top surface of the domain as a function of time (years).
8. Plot the inventory (moles) of each tracer in the repository as a function of time (years). The initial inventory of Tracer 1 in the repository is 2500×0.00423 moles; the initial inventory of Tracer 2 is 2500×0.038 moles. The inventory in the repository will decrease with time.

3.10 Scenarios that may be considered in future rounds of modeling

Three scenarios are proposed. All scenarios involve simulation of processes affecting flow and transport in fractures, and will require teams to make choices regarding, for instance, fracture size range, transmissivity functions, use of DFN and ECPM, use of particle tracking, and treatment of matrix diffusion.

3.10.1 Canister Failure by Corrosion under Temperate Climate Conditions

In this scenario, fracture inflow rates to one or more deposition holes are large enough to cause piping and erosion of bentonite, creating an advective pathway to the copper canister. Resulting transport rate of sulphide to the canister is sufficient to cause the copper to corrode through. This scenario provides an opportunity to investigate the coupling between fracture flow rates, bentonite erosion, solute transport, and corrosion.

3.10.2 Shear Failure of the Canister Due to Ground Motion

In this scenario, a seismic event occurs that is large enough to cause shear failure of one or more canisters. Bentonite buffer remains essentially intact, so that the dominant transport mechanism between canister and fractured host rock is diffusion. This scenario provides an opportunity to investigate the coupling between stress, slip on fractures, and canister shear failure (for geomechanics enthusiasts) and/or to investigate alternate models for radionuclide retardation in the bentonite including adsorption isotherms, ion exchange, and/or surface complexation (for geochemistry enthusiasts).

3.10.3 Glacial Loading

In this scenario, glacial loading causes pore pressures and the stress field to change. The changes in normal and shear stress on each fracture (and deterministic HCD) cause changes in transmissivity. For the ambitious, this scenario may provide an opportunity to explore coupling between changes in stress field and canister failure mechanisms. For the less ambitious, we could simply assume canister failure and investigate influence on flow and transport modeling.

4. Salt Reference Case

The salt reference scenario presented here will not focus on an undisturbed scenario for a salt repository. It has been shown through multiple performance assessments RESUS, KOMTESS, ISIBEL and VSG (Bollingfehr et al., 2008; Beuth et al., 2012; Bollingfehr et al., 2017; Bollingfehr et al., 2018; Bertrams et al., 2020) that there are no radiological consequences within 1,000,000 years for disposal in salt formations because of their very low permeability and moisture content. Additionally, the integrity of rock salt is given for at least 1,000,000 years for salt rock barriers greater than 200 m in thickness (which is the scenario presented here), which provides no pathway through permeable anhydrite, boudinage, or isolated salt blocks. As a result, here we present a disturbed scenario in which the shaft seals fail 1000 years after repository closure, allowing an influx of brine down the shafts and into the repository.

For this task a staged development of models is planned, building up to a full PA. This stepwise process is done to ensure the consistency between each team's modeling efforts as complexities are added. The planned staged development is:

1. Flow + radionuclide mobilization and transport (problem description will include variably saturated initial conditions)
2. + drift convergence (salt creep and backfill consolidation will be considered)
3. + heat flow and temperature-dependence of drift convergence
4. + model uncertainty in backfill consolidation model
5. (+ gas generation)

The description of the engineered and natural barrier systems will be updated as the exercise progresses so that necessary information is available at each stage of model development.

4.1 Geologic Setting

The salt reference case considers a mined repository for spent nuclear fuel (SNF) and vitrified high-level waste (HLW) in a salt dome. The generic geological cross section of a salt dome developed for the RESUS project (Bertrams et al. 2020) is simplified to 6 homogeneous geologic units for use in this reference case (Figure 4-1). It is assumed that the salt dome geometry shown in Figure 4-1 extends for 9 km perpendicular to the plane of the cross section. The ground surface is at about 50 m above mean sea level (amsl) and the top of the salt dome is roughly -150 m amsl. The base of the salt diapir is at about -3150 amsl and is underlain by basement rock, which extends to the base of the section at about -5500 amsl. The repository is mined at a depth of 850 m below the ground surface, such that the floor of the respository is at an elevation of -800 amsl.

The geometry of the salt dome cross section will be provided to teams as a geometry file. Teams are likely to develop model domains that are considerably shallower than the section shown here. Thus, properties of the basement unit should not be needed.

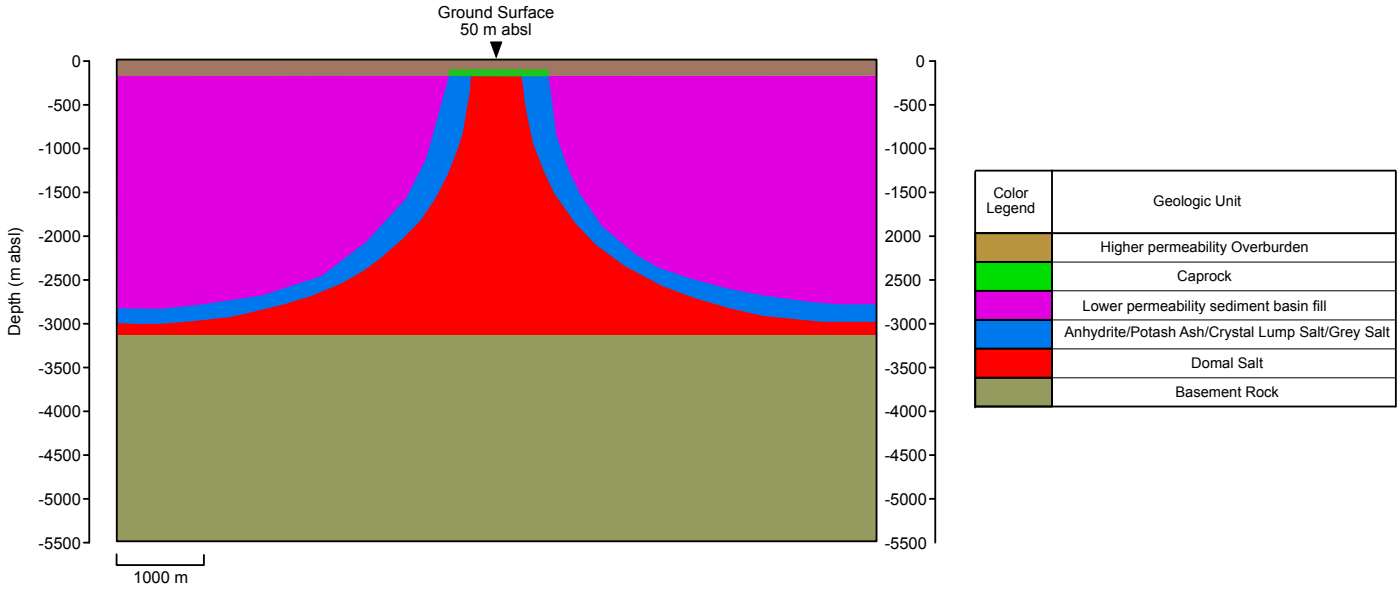

Figure 4-1. Geological cross-section with model units for the generic salt reference case. The model units are simplified from Bertrams et al. (2020). Hydrologic, mechanical, and thermal properties of the upper five units are given in Section 4.4.

4.2 Inventory

To reduce the computational burden of this comparison exercise, the salt reference case assumes fairly small inventories of SNF and HLW. For the same reason, the radionuclides included in transport simulations are limited to a small set of mobile, long-lived fission products (^{129}I and ^{235}Cs) and a single transuranic decay chain (^{241}Am -> ^{237}Np -> ^{233}U -> ^{229}Th), which includes ingrowth and decay of long-lived ^{237}Np.

Additional radionuclides may be added as model development progresses. With seal failure occurring 1000 years post-closure, shorter-lived radionuclides may be of interest. A comprehensive radionuclide screening has not yet been performed.

4.2.1 Spent Nuclear Fuel

The reference case assumes that the inventory of SNF consists entirely of pressurized water reactor (PWR) assemblies packaged in 500 POLLUX®-10 containers (described in Section 4.3.2), each of which contains (as the name suggests) 10 assemblies. Each assembly contains 0.435 metric tons heavy metal (MTHM) for a total of 2175 MTHM. To place this value in context, it is 3.1% of the 70,000 MTHM repository specified by the U.S. Nuclear Waste Policy Act and 20.7% of the total SNF inventory expected in Germany (Bertrams et al., 2020).

Following the example of previous reference cases developed in the U.S. program (e.g., Mariner et al. 2015; LaForce et al. 2020), the initial radionuclide inventory and heat of decay versus time for SNF is calculated assuming an initial enrichment of 4.73 wt% ^{235}U and 60 GWd/MTHM burn-up (Appendix C, Carter et al. 2013). A storage time of 100 years out of reactor (OoR) prior to emplacement in the repository is assumed. In the U.S., the average burn-up of SNF assuming decommissioning without replacing existing nuclear power plants is predicted to be 54 GWd/MTHM (Carter et al. 2013). Therefore, the assumption of 60 GWd/MTHM results in a conservatively high heat load.

Inventories of radionuclides at the time of emplacement (Table 4-1) are expressed as grams radionuclide per MTHM and grams radionuclide per grams total waste. The former ratio includes only the initial mass of heavy metal (i.e., ^{238}U) in the denominator; the latter ratio includes the total mass of the UO_2 ceramic wasteform in the denominator. Table 4-1 also provides the atomic weight and decay constant for each radionuclide (isotope).

The heat of decay versus time for a POLLUX®-10 container containing 10 PWR assemblies (Table 4-2 and Figure 4-2) is calculated from the complete radionuclide inventories provided by Carter et al. (2013, Appendix C). At the time of emplacement (100 y OoR), the power output per POLLUX®-10 container is about 2400 W.

Heat of decay versus time is provided for completeness. The first stage of model development (flow and transport) does not require implementation of a heat source term.

See Section 4.3.2 for characterization of the UO_2 wasteform and the POLLUX®-10 container.

Table 4-1. Inventory of selected radionuclides in PWR SNF at 100 y OoR.

Isotope	Inventory (g/MTIHM)[1]	Inventory (g/g waste)[2]	Atomic weight (g/mol)[3]	Approximate Decay Constant (1/s)[4]
^{241}Am	1.46E+03	1.01E-03	241.06	5.08E-11
^{243}Am	2.69E+02	1.87E-04	243.06	2.98E-12
^{238}Pu	2.84E+02	1.97E-04	238.05	2.56E-10
^{239}Pu	7.40E+03	5.14E-03	239.05	9.01E-13
^{240}Pu	4.11E+03	2.85E-03	240.05	3.34E-12
^{242}Pu	8.17E+02	5.67E-04	242.06	5.80E-14
^{237}Np	1.40E+03	9.72E-04	237.05	1.03E-14
^{233}U	4.33E-02	3.01E-08	233.04	1.38E-13
^{234}U	5.11E+02	3.55E-04	234.04	8.90E-14
^{236}U	6.27E+03	4.35E-03	236.05	9.20E-16
^{238}U	9.10E+05	6.32E-01	238.05	4.87E-18
^{229}Th	1.48E-05	1.03E-11	229.03	2.78E-12
^{230}Th	1.04E-01	7.22E-08	230.03	2.75E-13
^{226}Ra	3.99E-05	2.77E-11	226.03	1.37E-11
^{36}Cl	5.01E-01	3.48E-07	35.97	7.30E-14
^{99}Tc	1.28E+03	8.89E-04	98.91	1.04E-13
^{129}I	3.13E+02	2.17E-04	128.9	1.29E-15
^{135}Cs	7.72E+02	5.36E-04	134.91	9.55E-15

[1] from Carter et al. (2013, Table C-2)
[2] (g isotope/g waste) = (g isotope/MTIHM)/(g waste/MTIHM), where g waste = g all isotopes (1.44×10^6 g per initial MTHM)
[3] Weast and Astle (1981)
[4] Decay constants from ORIGEN (Croff, 1983)

Table 4-2. Predicted heat output per POLLUX-10 container as function of time.

Time (y)[a]	Heat (W)	Time (y)[a]	Heat (W)
0.0E+00	2.381E+03	4.5E+02	5.673E+02
1.0E+00	2.356E+03	5.0E+02	5.326E+02
2.0E+00	2.332E+03	6.0E+02	4.750E+02
3.0E+00	2.309E+03	7.0E+02	4.287E+02
4.0E+00	2.286E+03	8.0E+02	3.904E+02
5.0E+00	2.263E+03	9.0E+02	3.582E+02
6.0E+00	2.241E+03	1.0E+03	3.309E+02
7.0E+00	2.219E+03	1.2E+03	2.875E+02
8.0E+00	2.197E+03	1.4E+03	2.555E+02

9.0E+00	2.176E+03	1.6E+03	2.315E+02
1.0E+01	2.156E+03	1.8E+03	2.134E+02
2.0E+01	1.969E+03	2.0E+03	1.996E+02
3.0E+01	1.814E+03	2.5E+03	1.770E+02
4.0E+01	1.683E+03	3.0E+03	1.636E+02
5.0E+01	1.572E+03	3.5E+03	1.546E+02
6.0E+01	1.478E+03	4.0E+03	1.476E+02
7.0E+01	1.396E+03	4.5E+03	1.416E+02
8.0E+01	1.325E+03	5.0E+03	1.363E+02
9.0E+01	1.263E+03	6.0E+03	1.267E+02
1.0E+02	1.208E+03	7.0E+03	1.182E+02
1.2E+02	1.116E+03	8.0E+03	1.104E+02
1.4E+02	1.041E+03	9.0E+03	1.032E+02
1.6E+02	9.778E+02	1.0E+04	9.672E+01
1.8E+02	9.243E+02	1.5E+04	7.151E+01
2.0E+02	8.780E+02	2.0E+04	5.491E+01
2.5E+02	7.846E+02	2.5E+04	4.362E+01
3.0E+02	7.128E+02	3.0E+04	3.568E+01
3.5E+02	6.552E+02	3.5E+04	2.989E+01
4.0E+02	6.076E+02	4.0E+04	2.552E+01
4.5E+02	5.673E+02	4.5E+04	2.213E+01
5.0E+02	5.326E+02	5.0E+04	1.942E+01
6.0E+02	4.750E+02	6.0E+04	1.539E+01
7.0E+02	4.287E+02	7.0E+04	1.259E+01
8.0E+02	3.904E+02	8.0E+04	1.058E+01
9.0E+02	3.582E+02	9.0E+04	9.126E+00
1.0E+03	3.309E+02	1.0E+05	8.065E+00
1.2E+03	2.875E+02	2.0E+05	5.337E+00
1.4E+03	2.555E+02	3.0E+05	5.021E+00
1.6E+03	2.315E+02	4.0E+05	4.624E+00
1.8E+03	2.134E+02	5.0E+05	4.196E+00
2.0E+03	1.996E+02	6.0E+05	3.802E+00
2.5E+03	1.770E+02	7.0E+05	3.463E+00
3.0E+03	1.636E+02	8.0E+05	3.180E+00
3.5E+03	1.546E+02	9.0E+05	2.944E+00
4.0E+03	1.476E+02	1.0E+06	2.749E+00

[a] Time of emplacement (100 y OoR) is 0 y in this table.

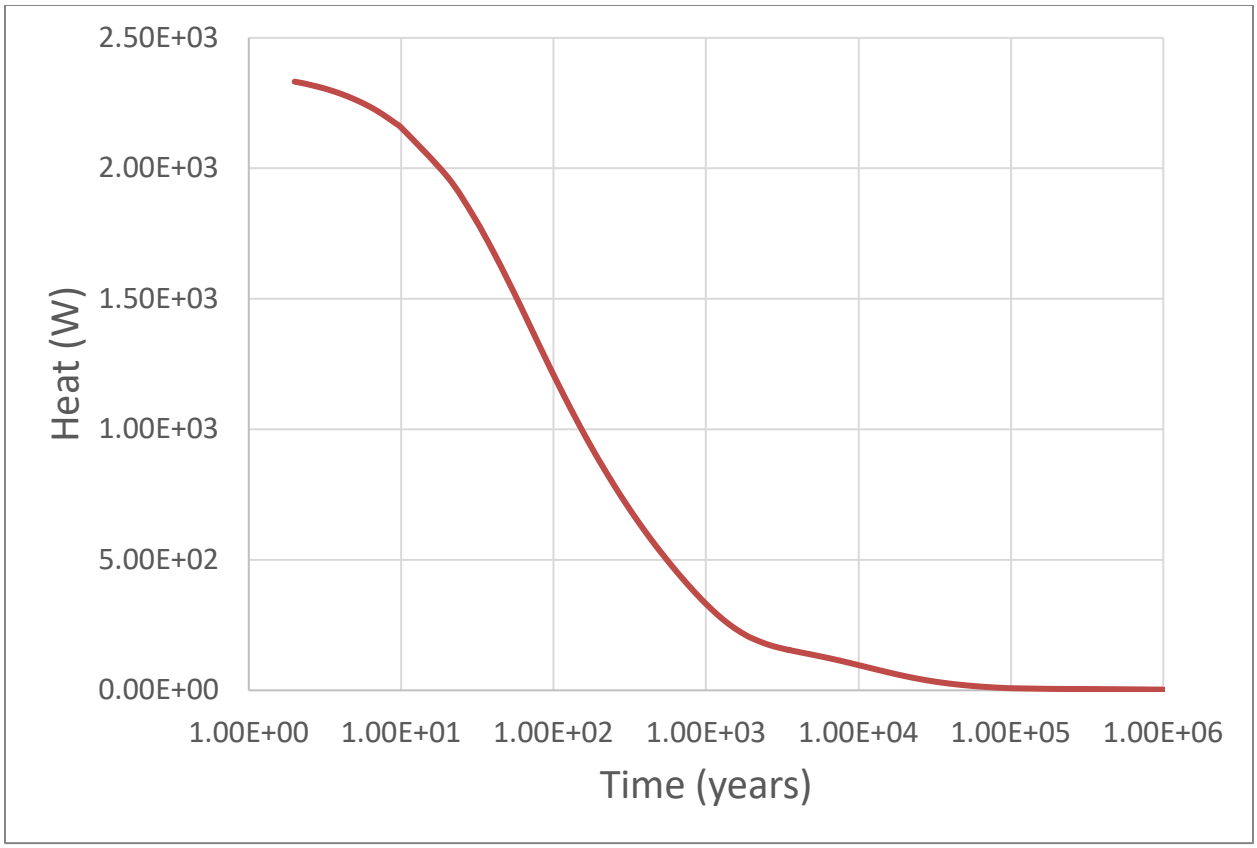

Figure 4-2. Heat vs. time for POLLUX-10 after 100 yr OoR; plotted using values in Table 4-2.

4.2.2 High Level Waste

The salt reference case includes vitrified high-level waste resulting from the reprocessing of spent nuclear fuel. The characteristics of the vitrified wasteform are based on the COGEMA vitrified waste from the Dutch fuel cycle (GRS 2012). In total, the operation of two nuclear power plants in the Netherlands is expected to result in 478 canisters of vitrified HLW. The reference case assumes a nominal inventory of 500 HLW canisters, each containing 400 kg of waste. The waste, which is 11.3% fission products and 2.2% actinides by mass, is aged 130 years before emplacement in the repository.

Selected radionuclide inventories at the time of emplacement (waste aged 130 y) expressed in Bq per canister, grams per canister, and grams per gram vitrified waste (glass) are given in Table 4-3.

The heat of decay versus time for an HLW canister containing 400 kg waste (Table 4-2) is calculated from the complete radionuclide inventories provided by (Kienzler et al., 2012). At the time of emplacement, the power output per canister is about 120 W.

The first stage of model development (flow and transport) does not require implementation of a heat source term.

See Section 4.3.3 for characteristics of the glass wasteform and the stainless-steel canister.

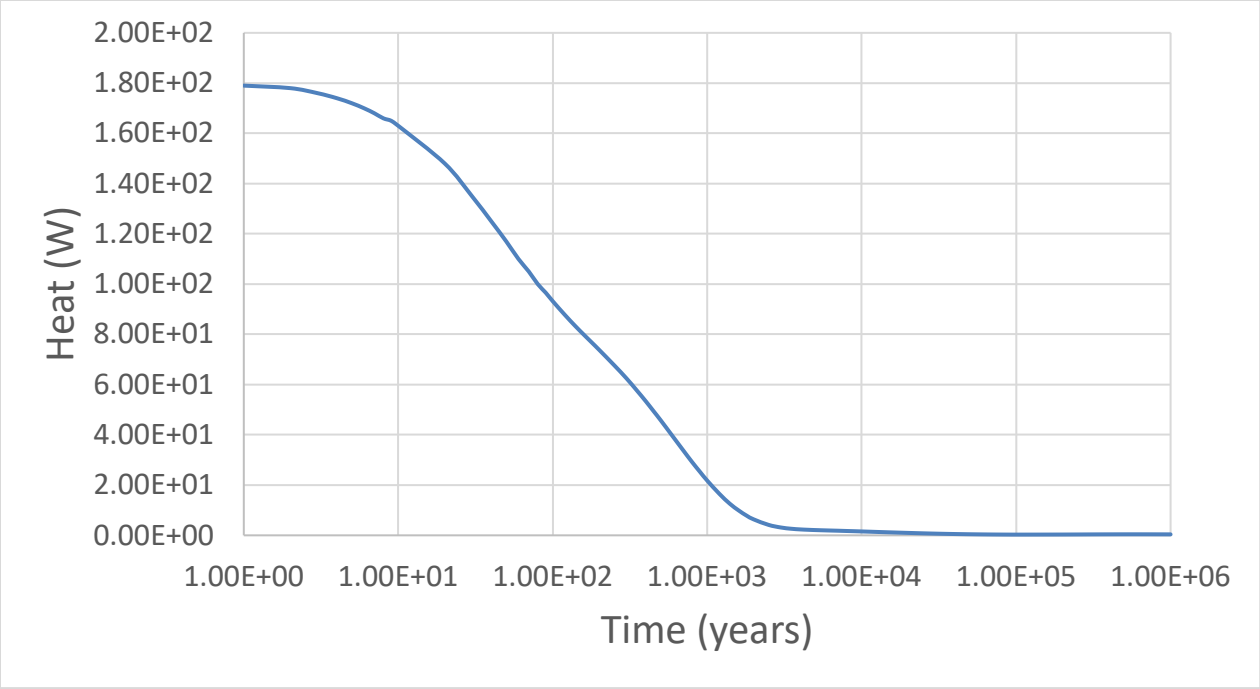

Figure 4-3. Heat vs. time for a single HLW canister aged 130 y; plotted using values in Table 4 4.

Table 4-3. Inventory of selected radionuclides in HLW aged 130y.

Isotope	Inventory (Bq/canister)[a]	Inventory (g/canister)	Inventory (g/g glass)[b,c]
^{241}Am	1.06E+14	8.35E+02	2.09E-03
^{243}Am	2.57E+12	3.48E+02	8.71E-04
^{238}Pu	4.78E+11	7.55E-01	1.89E-06
^{239}Pu	1.44E+11	6.26E+01	1.57E-04
^{240}Pu	2.31E+11	2.74E+01	6.85E-05
^{242}Pu	1.01E+09	7.15E+00	1.79E-05
^{237}Np	4.80E+10	1.84E+03	4.60E-03
^{233}U	3.20E+06	8.93E-03	2.23E-08
^{234}U	4.77E+08	2.06E+00	5.16E-06
^{236}U	4.21E+07	1.76E+01	4.40E-05
^{238}U	5.53E+07	4.45E+03	1.11E-02
^{229}Th	1.17E+04	1.49E-06	3.72E-12
^{230}Th	1.68E+05	2.25E-04	5.62E-10
^{226}Ra	1.03E+02	2.82E-09	7.04E-15
^{36}Cl	-	-	-
^{99}Tc	1.25E+12	1.99E+03	4.98E-03
^{129}I	-	-	-
^{135}Cs	3.01E+10	7.07E+02	1.77E-03

[a] Radionuclide inventory in COGEMA glass from GRS (2012).
[b] assuming 400 kg vitrified waste per canister
[c] Refer to Table 4-1 for atomic weights and decay constants.

Table 4-4. Predicted heat output per HLW canister as function of time.

Time (y) [a]	Heat (W)	Time (y) [a]	Heat (W)
0.0E+00	1.17E+02	1.4E+03	1.26E+01

1.0E+00	1.79E+02	1.6E+03	9.89E+00
2.0E+00	1.78E+02	1.8E+03	7.84E+00
3.0E+00	1.76E+02	2.0E+03	6.35E+00
4.0E+00	1.74E+02	2.5E+03	4.15E+00
5.0E+00	1.72E+02	3.0E+03	3.12E+00
6.0E+00	1.70E+02	3.5E+03	2.62E+00
7.0E+00	1.68E+02	4.0E+03	2.36E+00
8.0E+00	1.66E+02	4.5E+03	2.21E+00
9.0E+00	1.65E+02	5.0E+03	2.10E+00
1.0E+01	1.63E+02	6.0E+03	1.95E+00
2.0E+01	1.48E+02	7.0E+03	1.84E+00
3.0E+01	1.35E+02	8.0E+03	1.73E+00
4.0E+01	1.25E+02	9.0E+03	1.64E+00
5.0E+01	1.17E+02	1.0E+04	1.55E+00
6.0E+01	1.10E+02	1.5E+04	1.20E+00
7.0E+01	1.05E+02	2.0E+04	9.68E-01
8.0E+01	1.00E+02	2.5E+04	8.00E-01
9.0E+01	9.66E+01	3.0E+04	6.79E-01
1.0E+02	9.32E+01	3.5E+04	5.90E-01
1.2E+02	8.77E+01	4.0E+04	5.23E-01
1.4E+02	8.33E+01	4.5E+04	4.71E-01
1.6E+02	7.97E+01	5.0E+04	4.30E-01
1.8E+02	7.66E+01	6.0E+04	3.72E-01
2.0E+02	7.38E+01	7.0E+04	3.35E-01
2.5E+02	6.77E+01	8.0E+04	3.11E-01
3.0E+02	6.25E+01	9.0E+04	2.96E-01
3.5E+02	5.77E+01	1.0E+05	2.87E-01
4.0E+02	5.34E+01	2.0E+05	3.19E-01
4.5E+02	4.94E+01	3.0E+05	3.67E-01
5.0E+02	4.58E+01	4.0E+05	3.94E-01
6.0E+02	3.93E+01	5.0E+05	4.07E-01
7.0E+02	3.38E+01	6.0E+05	4.10E-01
8.0E+02	2.91E+01	7.0E+05	4.07E-01
9.0E+02	2.52E+01	8.0E+05	4.00E-01
1.0E+03	2.18E+01	9.0E+05	3.92E-01
1.2E+03	1.65E+01	1.0E+06	3.82E-01

[a] Time of emplacement (aged 130 y) is 0 y in this table.

4.2.3 Conservative Tracer Transport

In the next iteration of the reference case teams will model conservative transport of three tracers. Two for the SNF waste packages, and one for the HLW glass.

For the SNF Tracer 1 and 2 are the same two tracers as the crystalline case, but with inventory updated to be representative of the POLLUX®-10 containers. Tracer 1 and Tracer 2 are modeled after ^{129}I. Both have an atomic weight of 128.9 g/mol. The total inventory of the two tracers in each waste package is 1362.0 g (10.6 moles), equivalent to the expected inventory of ^{129}I in a waste package containing 10 pressurized water reactor assemblies. The inventory of Tracer 1 is 136.2 g (1.06 moles), or 10% of the total; it is instantly released at the start of the transport simulation. The inventory of Tracer 2 is 1226.0 g (9.50 moles), or 90% of the total; it is released congruently from the waste form as the waste form degrades at a fractional rate of 10^{-7}/year throughout the transport simulation. (Representative ^{129}I inventory is calculated from values in Table 4-1; instant release fraction and fractional rate of release are taken from Table 4-7 and Table 4-8, respectively.)

Tracer 3 is released from the HLW glass waste. It has properties representative of Technetium (Tc), as Tc has relatively low K_d, half-life in excess of 200,000 yr, and is present in reasonable quantities in the HLW packages (see Table 4-3). There is not expected to be any instant release of radionuclides from glass waste forms, so tracer is released at a fractional rate throughout the transport simulation. The tracer release rate is calculated according to the glass dissolution model and reactive surface area in Section 4.3.3.2, assuming a constant temperature of 38 C (311.15 K).

Table 4-5. Tracer inventories and release mechanisms for salt reference case simulations. Tracer 1 and 2 are released from SNF while Tracer 3 and 4 are released from HLW canisters.

	Atomic weight	Inventory per waste package or canister	Release mechanism
Tracer 1	128.9 g/mole	136.2 g	Instant
Tracer 2	128.9 g/mol	1226. g	10^{-7}/year
Tracer 3	98.91 g/mol	1990. g	3.8727×10^{-7}/year

4.3 Engineered Barrier System

4.3.1 Repository Layout

The floor of the repository is located at a depth of 850 m below the ground surface (-800 amsl). The repository is oriented so that the emplacement drifts are perpendicular to the orientation of the salt dome in Figure 4-1. With the repository oriented this way and positioned in the center of the salt dome it results in a line of symmetry through the repository and salt dome that modelers can choose to utilize to reduce the computational resources required for simulation. The repository is accessed by two shafts that extend vertically out of the salt dome formation through the cap rock and to the surface. The access shafts are designed this way based on the design of the shaft seal as it is specifically engineered to be an effective seal within a salt formation (see Section 4.3.7).

Within the repository there are three sets of 25 emplacement drifts with a drift spacing of 35 m center-to-center. For heat-generating waste, the waste package spacing is 3 m end-to-end in an emplacement drift 90 m long with a total of 10 waste packages per drift for a total of 500 POLLUX-10 waste packages. The vitrified waste emplacement area consists of 25 emplacement drifts with 35-m center-to-center drift spacing. Each 45-m-long drift contains 10 vertical boreholes with a center-to-center spacing of 4.5 m; two waste packages per borehole gives a total of 500 vitrified waste packages (Figure 4-4). The spacing of the drifts and waste packages (Table 4-6) should be sufficient to ensure that peak temperatures do not exceed 100°C (GRS 2020).

The dimensions of all emplacement drifts and access tunnels within the repository are the same, at 7 m width and 4 m height. The infrastructure has a total volume of 240,000 m^3, with dimensions of 240 m × 250 m × 4 m. The infrastructure is utilized during the construction and emplacement phases of disposal. During the post-closure phase this area is filled with gravel to allow for accumulation of excess fluid or gas.

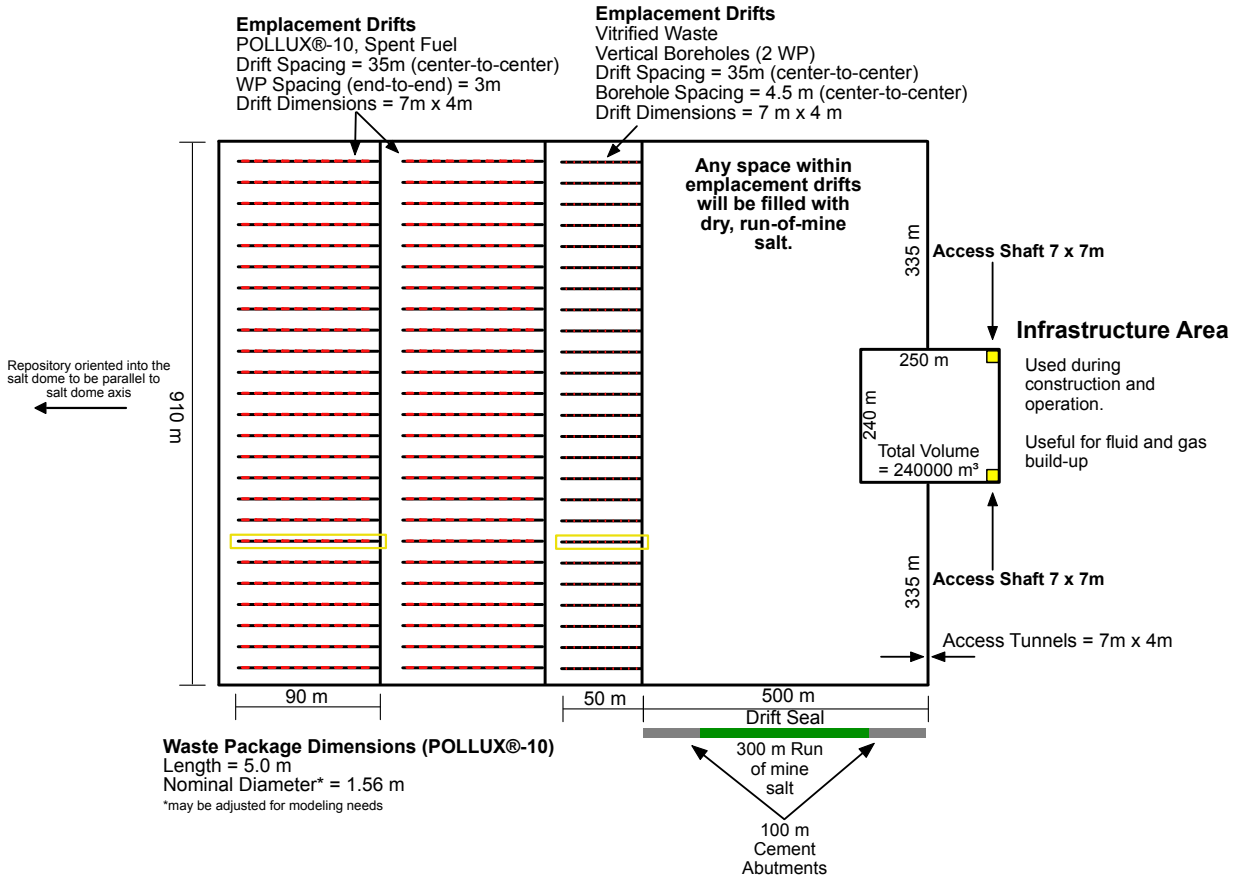

Figure 4-4. Schematic of the waste repository in a generic salt dome. The drifts outline in yellow will be for used for comparisons between each teams results.

Table 4-6. Dimensions for components of repository layout .

	Number	Width (m)	Height (m)	Length (m)	Spacing (m)
SNF Drifts	50	7	4	90	35 (center-to-center)
HLW Drifts	25	7	4	50	35 (center-to-center)
Access Shafts	2	7	850	7	240 – (7*2) (edge-to-edge)
Infrastructure Area	1	240	4	250	-
POLLUX-10	500	-	1.56*	5.0	3 (end-to-end)
Boreholes	250	1.5†	-	1.5†	4.5 (center-to-center)
Drift Seals	2	7	4	500	-

*diameter of POLLUX-10 container; may be adjusted for modeling needs
†diameter of borehole

4.3.2 Spent Nuclear Fuel Wasteform and Waste Container

4.3.2.1 SNF Wasteform

The SNF wasteform is spent uranium oxide (UO_2) fuel pellets encased in tubes of Zircaloy cladding. UO_2 is a polycrystalline ceramic material that is stable to high temperatures and has the potential for slow degradation in the disposal environment (Freeze et al. 2013). The reference case neglects any protection that the Zircaloy cladding may provide.

In the reactor, fuel undergoes physical changes due to heating, radiation damage, and the build-up of fission products. Concentration of lighter elements along margins of the UO_2 matrix and in gaps in the wasteform results in radionuclide release in two fractions: instant-release (upon failure of the waste canister) and slow-release (as the UO_2 matrix degrades).

Radioisotopes such as Nickel-60 accumulate in the metal components of a fuel assembly due to irradiation. These are neglected in this simplified comparison exercise.

Each waste container holds 4.35 MTHM of spent UO_2. Given a ratio of 1.44×10^6 g waste per initial MTHM, this quantity is equivalently expressed as 6264 kg of waste or (assuming the density of UO_2, 10,970 kg/m^3) 0.571 m^3 of waste.

Safety function: Slow degradation of the UO_2 wasteform limits radionuclide release.

4.3.2.2 Instant Release Fraction

The salt reference case considers two radionuclides having instant release fractions (IRF): ^{129}I and ^{135}Cs. The best estimate and pessimistic values for IRF of iodine and cesium from 60 GWd/MTHM-burnup SNF are 10% and 16% (Johnson et al. 2005 cited in Sassani et al. 2016). These values plus those for other light elements are listed in Table 4-7. The salt reference case assumes an IRF of 10% for both ^{129}I and ^{135}Cs.

Table 4-7. Instant release fractions from Johnson et al. (2005) cited in Sassani et al. (2016).

Element	Best Estimate IRF (%)	Pessimistic IRF (%)
C	10	–
Cl	5	–
Sr, Tc	7	11
I, Cs	10	16

4.3.2.3 UO2 Degradation Model

The reference case assumes that fuel matrix (UO_2) dissolution occurs when the POLLUX-10 container fails (and the disposal drift is liquid saturated). Dissolution proceeds at a fractional rate of 10^{-7}/yr. This rate is the mode of a log triangular distribution (Table 4-8) appropriate for fuel 3,000-10,000 years OoR and strongly reducing conditions (Werme et al. 2004; Ollila 2008); for a complete discussion refer to Sassani et al. (2016, Section 3.2.1). Congruent release of radionuclides is assumed, and radionuclide inventories in the wasteform are updated with time to account for decay and ingrowth.

Table 4-8. SNF dissolution rates; log triangular distribution from Werme et al. (2004) cited in Sassani et al. (2016, Section 3.2.1).

Parameter	Rate (yr^{-1})	Time to 50% dissolution (yr)	Time to 99% dissolution (yr)

Min	10^{-8}	6.93×10^{7}	4.61×10^{8}
Mode	10^{-7}	6.93×10^{6}	4.61×10^{7}
Max	10^{-6}	6.93×10^{5}	4.61×10^{6}

4.3.2.4 POLLUX-10 Container

A POLLUX® type container is utilized as the reference container. The POLLUX® container was conceived and designed for final disposal in salt (Figure 4-5). It consists of an inner and an outer container. The inner container is made of fine-grained structural steel and is tightly sealed by a bolted primary cover and a welded secondary cover. The interior is divided into several chambers, into each of which fuel rods of two PWR or six BWR assemblies can be inserted. Figure 4-5 shows an example of a POLLUX® container with the drawn fuel rods from ten PWR fuel assemblies (POLLUX®-10). The outer shielding vessel, like the primary and secondary covers, is made of nodular cast iron (material 0.7040). This shielding vessel has no sealing function to perform and is closed with a bolted cover. In the shell, rods made of polyethylene are inserted in radially distributed holes to reduce the neutron dose rate. The structural container design and the choice of materials ensure the basic requirements for retrievability in the operational phase. The POLLUX®-10 container is assumed to contain the waste for 500 years and to provide no containment after 500 years (BMU 2010).

The container shown below has a length of 5.517 m and a diameter of 1.56 m. For the reference case, a nominal length of 5.0 m is assumed. The diameter of 1.56 m is retained, although it is recognized that individual teams may need to adjust the cross-sectional area of the container to simplify modeling.

Each team is responsible for choosing how to represent the steel container in a porous media flow and transport model. For Stage 1 modeling, teams may need to assign porosity and permeability to the volumes occupied by POLLUX®-10 containers. As the staged modeling progresses, it is proposed that representative thermal and mechanical properties be based on the properties of nodular cast iron.

Safety function: The POLLUX®-10 container contains the waste for 500 years; it provides no safety function after 500 years.

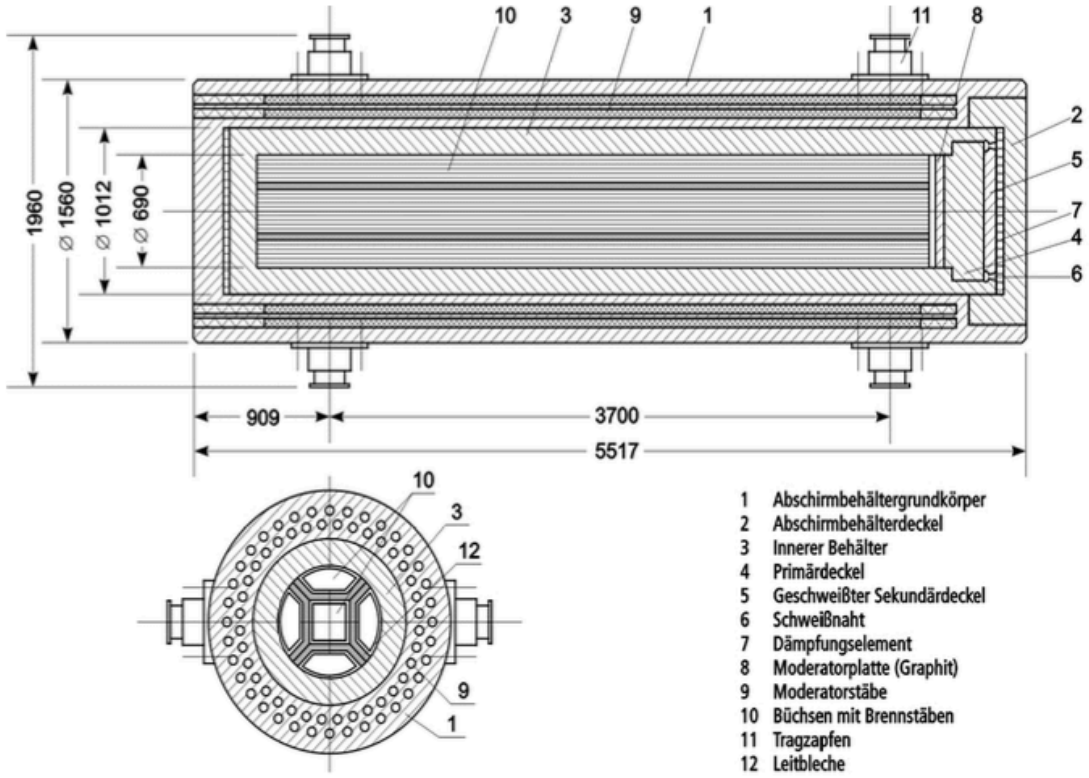

Figure 4-5. Schematic of the POLLUX-10 waste container. 1. Shielding body; 2. Shielding cover; 3. Inner tank; 4. Primary cover; 5. Secondary (welded) cover; 6. Welding seam; 7. Damping element; 8. Moderator plate (graphite); 9. Moderator staff; 10. Bushings with fuel rods; 11. Trunnion; 12. Guide plate (from Bertrams et al. 2020).

4.3.3 HLW Wasteform and Waste Container

4.3.3.1 Vitrified Glass in Stainless Steel Canister (Wasteform)

The vitrified (glass) waste is formed in stainless steel canisters with a height of 1.335 m and an outer diameter of 0.430 m (Figure 4-6). The canisters have a mass of 100 kg when empty. Each canister contains a nominal inventory of 400 kg of vitrified waste. The reference case assumes that the thin-walled stainless steel canister provides no containment function, i.e., the glass wasteform dissolves when brine saturation is 100%.

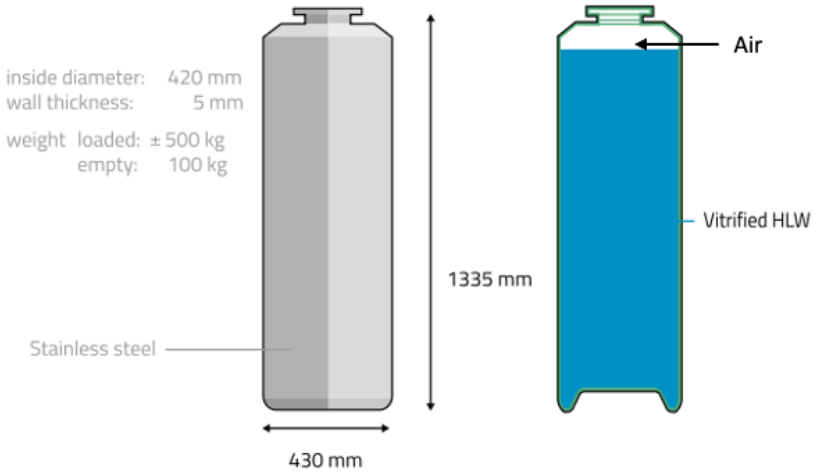

Figure 4-6. Stainless steel canister for vitrified HLW. See Figure 4-7 for overpack dimensions.

4.3.3.2 Glass dissolution model

Glass dissolution rate depends on many factors, including local pore fluid chemistry, temperature, and glass surface area; and will slow with time as pore fluids become saturated with $SiO_{2(aq)}$ and a surface alteration layer forms (Sassani et al. 2016, Section 3.2.2). This latter stage of dissolution (stage II dissolution, Vienna et al. 2013) is typically assumed to represent long-term dissolution rates for repository modeling (Sassani et al. 2016). The salt reference case uses an empirical rate law fitted to temperature (Kienzler et al. 2012) to model the long-term dissolution of glass:

$$R = 560 \times exp\left(\frac{-7397}{T}\right)$$

Where the dissolution rate, R, has the units kg m^{-2} d^{-1} and T is temperature in Kelvin. The rate law is appropriate for dilute and saline solutions. Initial flow and transport simulations assume a reference temperature of 38º C (Bauer et al. 2011).

The surface area of the glass is calculated from the cylindrical geometry of the glass and an exposure factor ($f_{exposure}$), a number greater than 1 that accounts for additional reactive surface area due to cracking and roughness (Sassani et al. 2016):

$$S = f_{exposure}A$$

where S is the reactive surface area of the glass and A is the geometric surface area of the glass. Surface area decreases with time, and can be calculated as a function of the specific geometric surface area (s_a [m^2/kg]) and the remaining mass of glass (M [kg]):

$$A = s_a M$$

Given a nominal density of 2754 kg/m^3 for COGEMA glass (Kienzler 2012), a mass of 400 kg, and a diameter of 0.42 m, the glass cylinder has a volume of 0.145 m^3 and a geometric surface area of 1.66 m^2. Kienzler et al. (2012) estimates $f_{exposure}$ = 10. Therefore, the specific geometric surface area is 0.004 m^2/kg and the specific reactive surface area is 10 times larger. A triangular distribution for $f_{exposure}$ is proposed by Strachan (2004) with a minimum and mode of 4 and a maximum of 17. This distribution may be applied to the reference case when we address uncertainty.

Congruent release of radionuclides is assumed, and radionuclide inventories in the wasteform are updated with time to account for decay and ingrowth.

Safety function: Slow dissolution of the glass wasteform limits radionuclide release.

4.3.3.3 HLW Emplacement

HLW Overpack

Each vitrified HLW canister is placed in an overpack. The overpack has a total length of 1.745 m, with a 0.20-m-long, air-filled crumple zone at the top (Figure 4-7).

Safety function: The HLW overpack is not assigned a post-closure safety function.

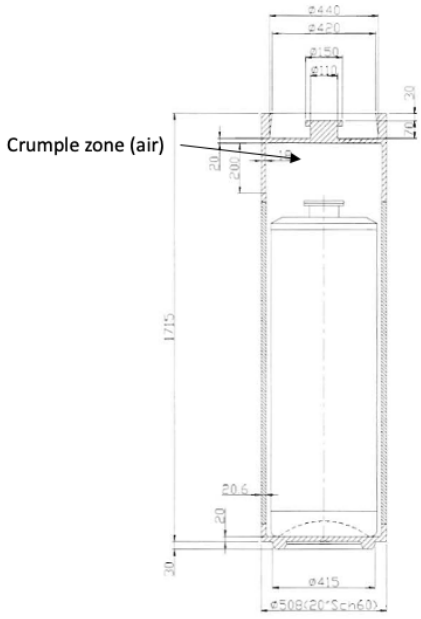

Figure 4-7. Canister dimensions for vitrified HLW.

Vertical Emplacement Borehole

Two overpacks are emplaced in a vertical borehole, one on top of the other, in the floor of a waste emplacement drift. The emplacement borehole is 14-m in length (Figure 4-8) (Poley 1999). The two overpacks sit in the lowest 4 m of the borehole, where the borehole is 0.7 m in diameter, lined with steel and backfilled with sand. A salt plug sits in the upper 10 m of the borehole, which is 1.5 m in diameter.

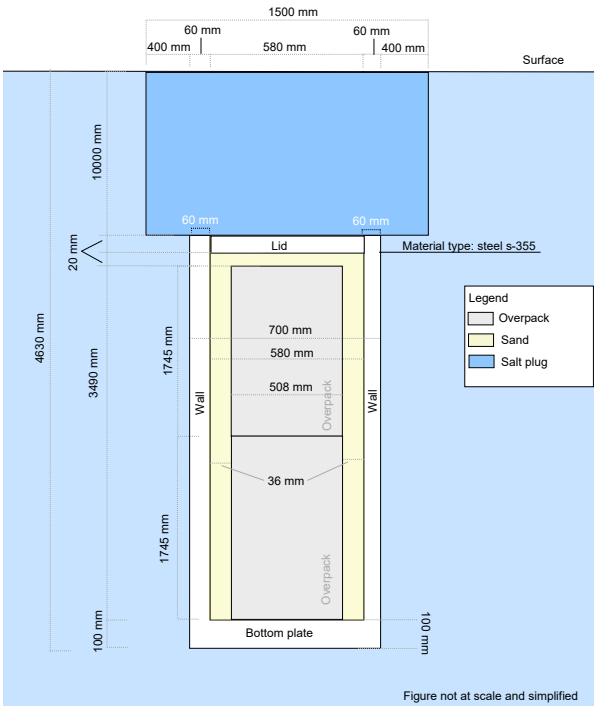

Figure 4-8. Dimensions for vertical borehole emplacement for vitrified HLW canisters.

Each team is responsible for determining how to represent the lower borehole (containing vitrified HLW in canisters and overpacks, sand backfill, and steel lining) in the porous media flow and transport model. For instance, teams could calculate bulk porosity from the void space in the HLW canister, overpack, and sand backfill. Permeability is left up to each modeling team to determine. As the staged modeling progresses, it is proposed that representative thermal and mechanical properties be based on the properties of borosilicate glass.

The salt plug is assigned the same properties as the run-of-mine salt that backfills the drift as discussed in the next section. This assumption results in conservatively high permeability and porosity, because in practice, the salt plug would be pre-compacted at the time of emplacement.

Safety function: The salt plug provides shielding during the operational phase of the repository and limits radionuclide transport after closure. Materials within the lower borehole have no post-closure safety function.

4.3.4 Emplacement and Access Tunnel Backfill

Emplacement drifts and access tunnels (except where drift seals are placed) are backfilled with dry run-of-mine salt. Due to the compaction of the run-of-mine salt backfill, the backfill will develop a sealing effect over time that is comparable to that of the surrounding, undisturbed geological barrier. The time required to reach the final state ranges from several tens to several thousands of years, depending on the convergence rate, moisture content and ambient temperature (Bertrams et al., 2020). Backfill properties have been adopted from Blanco-Martin et al. (2018) and are located in Table 4-9.

Safety function: Upon reconsolidation of the backfill, its low permeability and porosity limit the volume of water that comes in contact with waste and limit radionuclide transport.

4.3.5 Infrastructure Area Gravel Backfill

The shaft landing stations and the infrastructure area are backfilled with gravel which has negligible compaction capabilities, and which forms permanent pore storage to significantly delay an increase in brine pressure at the drift seals. Backfill properties are listed in Table 4-9.

Safety function: The gravel backfill provides a high porosity reservoir for fluids intruding from the host rock or via the shafts, thus allowing fluids to accumulate in the infrastructure area without causing increased pore fluid pressures in other areas of the repository.

4.3.6 Drift Seals

Two drift seals are placed in the 500-m long tunnels connecting the infrastructure area to the emplacement area. Each drift seal comprises two 100-m lengths of Sorel concrete, analogous to the lowest sealing element of the shaft closure (see Section 4.3.7), separated by a 300-m section filled with run-of-mine salt. The Sorel cement provides a seal immediate after closure of the repository, while the run-of-mine salt will consolidate to provide a seal at later times (Bertrams et al. 2020).

Although a typical drift seal design would call for moistening the run-of-mine salt to accelerate compaction, for the first stage of modeling, it is assumed that the run-of-mine salt in the drift seal is dry and has the same properties as the run-of-mine salt backfill in the emplacement drifts and other access tunnels. Properties for sorel cement can be found in Table 4-9.

Safety function: Provide long-term separation of surface, overburden, and/or formation waters from emplacement drifts, limiting the volume of water that comes in contact with waste and limiting radionuclide transport.

4.3.7 Shaft Design

Access to the repository is provided by two shafts connecting the infrastructure area to the ground surface. The shafts are 850 m tall with a 7 m by 7 m cross section. A layered shaft seal design shown in the illustration in Figure 4-9 is an option for teams with the capability for complex shaft models. This design contains segments designed to seal and segments designed to act as reservoirs. The uppermost sealing segment is bentonite, which limits advection due to its low permeability and retards radionuclide transport due to adsorption.

The first simulation option for flow and transport ignores distinct features of the shaft seal, and bulk hydrologic properties are assumed, as shown in Table 4-9. The assumed bulk permeability of the shaft seal changes at the time of failure: Prior to shaft seal failure, the bulk permeability is 8.6232×10^{-18} m^2; after shaft seal failure at 1000 years, the bulk permeability is 2.0606×10^{-16} m^2, which is necessary to be consistent with the post-failure average permeability in the heterogeneous model.

Some teams may wish to do a more detailed shaft model using the layered materials as shown in Figure 4-9. The porosity and permeability prior to shaft seal failure are given in Table 4-10. After shaft seal failure, the permeability of each layer in the shaft is assumed to increase by two orders of magnitude.

Safety function: The shaft seals limit ingress of water to the repository and limit advective radionuclide transport. In the shaft seal failure scenario, the shaft seals fail to perform these safety functions.

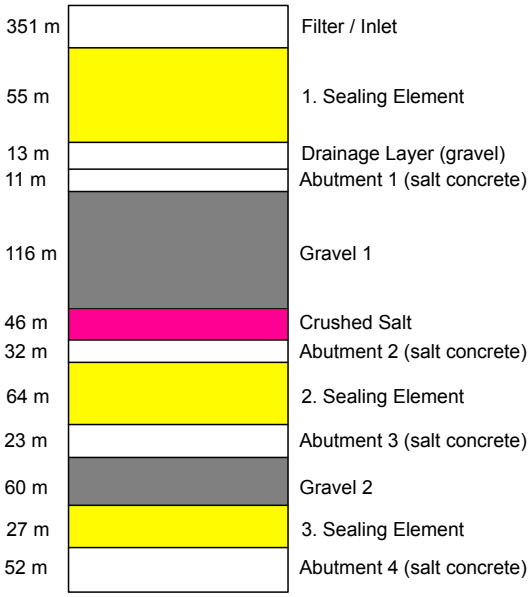

Figure 4-9. Shaft seal for generic salt dome repository (modified from Rübel et al. (2016) by Tanja Frank).

Properties of the engineered barrier system required for simulation of variably saturated flow and advective and diffusive transport are summarized in Table 4-9 and Table 4-12. These include (Table 4-9) intrinsic permeability, porosity, tortuosity (and the corresponding effective diffusion coefficient), compressibility, and (Table 4-12) relative permeability and capillary pressure functions. Grain density (assuming no sorption in the engineered barriers), specific heat capacity, and thermal conductivity although listed are not necessary until we add heat.

Table 4-9. Engineered barrier system material properties for use in initial flow and transport simulations.

	Intrinsic Permeability (m^2)	Porosity (-)	Tortuosity (-) [j]	Effective Diffusion Coefficient (m^2/s) [k]	Compressibility (1/Pa) [m]	Grain Density (kg/m^3)	Specific Heat Capacity (J/(kg*K))	Thermal Conductivity (W/(m*K))
POLLUX-10 container (bulk) [c]	TBD [a]	TBD [a]	TBD [a]	TBD [a]	TBD [a]	7000	506	32
HLW emplacement borehole (bulk) [d]	TBD [a]	0.14	0.14	4.5e-11	TBD [a]	2750	830	1.15
Crushed salt [e]	8.35E-15	0.1	0.1	2.3E-11	1.00E-08	2200	880	NA [b]
Sorel cement (drift seals) [f]	5.00E-17	0.13	0.13	3.9E-11	1.00E-09	2450	727	2.13
Gravel (infrastructure area) [g]	1.00E-14	0.3	0.3	2.1E-10	1.00E-08	2700	800	2
Shaft seals before failure [h]	8.6232E-18	0.24	0.24	1.3E-10	1.00E-08	NA [b]	NA [b]	NA [b]
Shaft seals after failure [h]	2.0606E-16	0.24	0.24	1.3E-10	1.00E-08	NA [b]	NA [b]	NA [b]

[a] To be determined by the individual modeling teams.

[b] These properties are not applicable to the initial flow and transport simulations and may require discussion.

[c] Generic values consistent with ductile cast iron (ASTM A536).

[d] Generic values consistent with properties of borosilicate glass.

[e] Estimated after 1000 years of reconsolidation from results in Blanco-Martin et al. 2018. Permeability (k [m^2]) is a function of porosity (ϕ): $k = 1.89 \times 10^{-10} \times \phi^{4.355}$.

[f] Permeability from GRS-415 (Rübel et al. 2016) and generic values consistent with MgO cement with silica sand aggregate (Zaleska et al. 2019).

[g] Permeability from GRS-415 and generic values consistent with properties of coarse quartz sand.

[h] Bulk permeability from GRS-415. Volume weighted average porosity estimated from shaft seal design in GRS 415.

[j] Tortuosity (τ) set equal to porosity (ϕ). (Tortuosity, defined in Section 6.3.4, is less than or equal to 1.)

[k] Effective diffusion coefficient, $D_e = D_m \phi \tau$, where D_m, the molecular diffusion coefficient in free water, = 2.3E-09 m²/s.

[m] Order of magnitude estimates, subject to future improvement

Table 4-10. Material properties for the detailed shaft model prior to seal failure. After shaft failure the permeability of each layer increases by two orders of magnitude.

	Intrinsic Permeability (m²)	Porosity (-)	Tortuosity (-) [j]	Effective Diffusion Coefficient (m²/s) [k]	Compressibility (1/Pa) [m]	Grain Density (kg/m³)	Specific Heat Capacity (J/(kg*K)	Thermal Conductivity (W/(m*K))
Filter/Inlet	1.00E-12	0.3	TBD [a]	TBD [a]	TBD [a]	TBD [a]	TBD [a]	TBD [a]
Sealing Element 1	1.00E-17	0.27	TBD [a]	TBD [a]	TBD [a]	TBD [a]	TBD [a]	TBD [a]
Drainage Layer 1	1.00E-12	0.25	TBD [a]	TBD [a]	TBD [a]	TBD [a]	TBD [a]	TBD [a]
Abutment 1	1.00E-12	0.1	TBD [a]	TBD [a]	TBD [a]	TBD [a]	TBD [a]	TBD [a]
Gravel 1	1.00E-09	0.23	TBD [a]	TBD [a]	TBD [a]	TBD [a]	TBD [a]	TBD [a]
Crushed Salt	1.30E-15	0.1	TBD [a]	TBD [a]	TBD [a]	TBD [a]	TBD [a]	TBD [a]
Abutment 2	2.00E-15	0.1	TBD [a]	TBD [a]	TBD [a]	TBD [a]	TBD [a]	TBD [a]
Sealing Element 2	7.00E-19	0.1	TBD [a]	TBD [a]	TBD [a]	TBD [a]	TBD [a]	TBD [a]
Abutment 3	2.00E-15	0.1	TBD [a]	TBD [a]	TBD [a]	TBD [a]	TBD [a]	TBD [a]
Gravel 2	1.00E-09	0.38	TBD [a]	TBD [a]	TBD [a]	TBD [a]	TBD [a]	TBD [a]
Sealing Element 3	5.00E-17	0.16	TBD [a]	TBD [a]	TBD [a]	TBD [a]	TBD [a]	TBD [a]
Abutment 4	5.00E-17	0.16	TBD [a]	TBD [a]	TBD [a]	TBD [a]	TBD [a]	TBD [a]

[a] To be determined by the individual modeling teams.

4.4 Natural Barrier System

The natural barrier system is comprised of the 5 simplified geologic units illustrated in Figure 4-1: the salt dome (which is the host rock); a mixed evaporite sequence flanking the salt dome; the caprock; the basin fill; and the overburden. The descriptions below are derived from the geologic units described by Bertrams et al. (2020) unless otherwise noted. Physical properties are summarized in Table 4-11 and Table 4-12.

4.4.1 Salt Host Rock

In the geological model of the salt dome, the host rock consists of homogeneous rock salt (halite), which has no flowable pore space and thus no permeability greater than 10^{-22} m^2. Due to the extremely low hydraulic permeability of the salt rock, advective mass transport is negligible, so that mass transport is determined solely by diffusion (Bertrams et al. 2020).

4.4.2 Mixed Evaporite Sequence

The flank areas of the salt structure consist of a potash seam, an evaporitic sequence of salt and anhydrite, and a clayey strata. These complicated alternating geologic formations are very common within salt dome architecture. As a result of this complexity a simplification is made in Figure 4-1 with this group of formations being represented by a single formation defined by bulk properties.

4.4.3 Caprock

A caprock with a thickness between 55 m to 80 m has formed above the salt structure. The model unit consists largely of gypsum or of the residual formations of the various evaporitic strata following the salt structure. With this formation being dominated by mainly evaporitic strata the permeability is assumed to be low.

4.4.4 Basin Fill

The basin fill, which is present on both sides of the salt structure and absent directly above the salt structure, mainly consists of a limestone to sandstone sequence with conglomerates throughout. Because of this sequence, this formation is assumed to have a higher permeability and effective porosity.

4.4.5 Overburden

Above the salt structure and cap rock, the overburden varies in thickness from 55 - 80 m. The overburden consists largely of unconsolidated sediments with higher pore volume relative to the deeper units. Therefore, this model unit is classified as a freshwater aquifer. Additionally, the permeability specified for this unit of 10^{-15} m^2 may allow for advection to occur. As a result, dispersion may need to be considered, which will be left up to the modelers because dispersivity will be dependent on grid discretization.

Table 4-11. Natural barrier system material properties for use in initial flow and transport simulations.

	Intrinsic Permeability (m^2)	Porosity	Tortuosity (-)[b]	Effective Diffusion Coefficient (m^2/s)[c]	Compressibility (1/Pa)[d]	Grain Density (kg/m^3)	Heat Capacity (J/kg*K)	Thermal Conductivity (W/m^2)[a]
Overburden	1.00E-15	0.2	0.2	9.2E-11	1.00E-08	2600	800	2.3
Caprock	1.00E-18	0.4	0.4	3.68E-10	1.00E-09	2200	950	2.2
Basin Fill	1.00E-17	0.25	0.25	1.44E-10	1.00E-08	2500	900	2.5
Anhydrite/Potash	1.00E-19	0.05	0.05	5.75E-12	1.00E-11	2700	750	2.6
Domal Salt	1.00E-22[a]	0.001[a]	0.0001	2.3E-15	1.00E-11	2200	880	5.5
Basement	1.00E-21[a]	0.01	0.01	2.3E-13	1.00E-12	3000	850	2.7

[a] from Bertrams et al., 2020
[b] Tortuosity (τ) set equal to porosity (ϕ). Order of magnitude estimates, subject to future improvement.
[c] Effective diffusion coefficient, $D_e = D_m \phi \tau$, where D_m, the molecular diffusion coefficient in free water, = 2.3E-09 m^2/s.
[d] Order of magnitude estimates, subject to future improvement.
All other parameters taken from general geologic property tables.

Table 4-12. Relative permeability parameters for salt, crushed salt, and shaft seal. Additional materials will be added as needed.

	Intact Salt[1]	Crushed Salt[1]	Shaft Seal[1]	Concrete[2]	Gravel[3]
Relative Permeability Function	Corey	Corey	Corey	Mualem - VG	VG
Residual Liquid Sat (S_{lr})	0.1	0.03	0.03	0.2	0.19
Residual Gas Sat (S_{gr})	0	0	0	0.1	0
Van Genuchten's	0.6	0.6	0.6	0.56	0.675
Van Genuchten's P_0 (MPa)	5.7	1.6	1.6	7.7	1.6
Van Genuchten's S_{lr}	0.01	0.02	0.02	0.0	0.0
[1]Blanco-Martín et al. (2018) [2]Ecay et al. (2020) [3]Osselin et al. (2015)					

4.5 Geochemical Environment

In a complex geologic system, solubility limits and adsorption behavior would be controlled by local porewater chemistry and mineral assemblage. For the salt reference case, simplifying assumptions are made.

4.5.1 Solubility

Radioelement solubility limits throughout the model domain are held constant at values calculated for a concentrated, reducing brine as in previous salt reference case simulations conducted in the U.S. (e.g., LaForce et al. 2020; Clayton et al. 2011). The calculated range of maximum dissolved concentration for each element is given as a triangular distribution in Table 4-13. The reference case uses the mode of the distribution as the nominal value.

Table 4-13. Element solubility calculated at T = 25° C in concentrated brine (Wang and Lee 2010 as cited in Clayton et al. 2011).

Element	Distribution Type	Maximum Dissolved Concentration (mol kg^{-1})		
		Min	Mode	Max
Am	Triangular	1.85×10^{-7}	5.85×10^{-7}	1.85×10^{-6}
Np	Triangular	4.79×10^{-10}	1.51×10^{-9}	4.79×10^{-9}
Pu	Triangular	1.40×10^{-6}	4.62×10^{-6}	1.53×10^{-5}
Sn	Triangular	9.87×10^{-9}	2.66×10^{-8}	7.15×10^{-8}
Tc	Log-triangular	4.56×10^{-10}	1.33×10^{-8}	3.91×10^{-7}
Th	Triangular	2.00×10^{-3}	4.00×10^{-3}	7.97×10^{-3}
U	Triangular	4.89×10^{-8}	1.12×10^{-7}	2.57×10^{-7}
Cs, I	N/A	Unlimited[a]		
[a]Assumed by Clayton et al. (2011)				

4.5.2 Adsorption

Adsorption is modeled using linear distribution coefficients (K_d). Distribution coefficients are material specific.

4.5.2.1 Host rock and repository

The reference case assumes that adsorption does not occur within the halite of the salt dome nor within any of the engineered materials in the repository. This assumption is likely conservative, because corrosion products associated with waste package degradation might provide sorption sites.

4.5.2.2 Mixed evaporite sequence and caprock

Clayton et al. (2011) compiled distribution coefficients for anhydrite and expressed them as uniform and log uniform distributions (Table 4-14). Adsorption in the mixed evaporite sequence and the caprock is modeled using a nominal K_d equal to the midpoint of each distribution. The midpoint is equivalent to the average of the minimum and maximum for a uniform distribution, or the value obtained by averaging the logs of the minimum and maximum for a log uniform distribution.

Table 4-14. Anhydrite Kds compiled by Clayton et al. (2011).

Element	Distribution	K_d [m^3/kg]		
		Min	Max	Mid
Ac	log uniform	5.0E-03	5.0E-01	5.0E-02
Am	uniform	2.5E-02	1.0E-01	6.3E-02

C	uniform	0.0E+00	6.0E-04	3.0E-04
Cl	constant	0.0E+00	0.0E+00	0.0E+00
Cm	log uniform	5.0E-03	5.0E-01	5.0E-02
Cs	uniform	1.0E-03	2.0E-02	1.1E-02
I	constant	0.0E+00	0.0E+00	0.0E+00
Nb	constant	1.0E-04	1.0E-04	1.0E-04
Np	uniform	1.0E-03	1.0E-02	5.5E-03
Pa	log uniform	1.0E-03	5.0E-01	2.2E-02
Pd	constant	1.0E-04	1.0E-04	1.0E-04
Pu	uniform	7.0E-02	1.0E-01	8.5E-02
Se	uniform	2.0E-04	5.0E-04	3.5E-04
Sn	uniform	2.0E-03	1.0E-02	6.0E-03
Sr	uniform	1.0E-03	8.0E-02	4.1E-02
Tc	uniform	0.0E+00	2.0E-03	1.0E-03
Th	uniform	1.0E-01	1.0E+00	5.5E-01
U	uniform	2.0E-04	1.0E-03	6.0E-04
Zr	log uniform	3.0E-03	5.0E-01	3.9E-02
Pb	constant	0.0E+00	0.0E+00	0.0E+00
Sb	constant	1.0E-02	1.0E-02	1.0E-02

4.5.2.3 Basin fill and overburden

Adsorption in the basin fill is modeled using K_ds calculated for the Brauner Dogger sandy limestone sequence (a geologic unit overlying the Opalinus clay). Baeyens et al. (2014) calculated values for a reference porewater composition, and three variants including a high salinity case (Table 4-15). The salt reference case assumes high salinity porewaters and reducing conditions in the basin fill. Therefore, the high salinity K_ds are adopted and reduced oxidation states are assumed for uranium and plutonium (U(IV) and Pu(III)).

Adsorption in the overburden is also modeled using K_ds calculated for the Brauner Dogger sandy limestone sequence. For the overburden, the reference K_ds and higher oxidation states (U(VI) and Pu(IV)) are chosen.

Table 4-15. Kds for basin fill and overburden (from Baeyens et al. 2014).

Element	**K_d [m^3/kg]**			
	Reference	High pCO2	Low pCO2	High salinity
I(-I)	0.00E+00	0.00E+00	0.00E+00	0.00E+00
Cs(I)	4.33E-01	4.31E-01	4.35E-01	2.88E-01
Th(IV)	7.59E+00	3.61E+00	1.67E+01	2.23E+01
U(IV) [a]	4.20E-02	1.51E-02	1.96E-01	3.08E-01

U(VI) [b]	7.89E-05	4.12E-05	2.41E-04	7.95E-04
Np(IV)	2.80E+01	2.80E+01	2.80E+01	2.80E+01
Pu(III) [a]	1.54E+00	9.22E-01	2.88E+00	1.49E+00
Pu(IV) [b]	7.28E-03	2.55E-03	3.25E-02	4.70E-03
Am(III)	1.54E+00	9.68E-01	2.87E+00	1.64E+00
[a] Use lower oxidation states in the basin fill.				
[b] Use higher oxidation states in the overburden.				

4.5.2.4 Shaft seal

Adsorption within the shaft seal is neglected for the initial simulations of flow and transport.

The upper shaft seal contains bentonite, which will sorb some radionuclide species. As staged model development progresses, adsorption in the bentonite will be modeled using K_ds calculated for MX-80 bentonite assuming equilibration with a high salinity porewater (Baeyens et al. 2014), as shown in Table 4-16. Reduced oxidation states are chosen for uranium and plutonium (U(IV) and Pu(III)).

Table 4-16. K_ds for the bentonite component of the shaft seal (from Baeyens et al. 2014).

Element	K_d [m^3/kg]
	High salinity
I(-I)	0.00E+00
Cs(I)	1.35E-02
Th(IV)	2.78E+02
U(IV)	3.90E+00
Np(IV)	3.75E+02
Pu(III)	6.68E+01
Am(III)	7.26E+01

4.6 Initial Conditions, Etc.

Initial conditions for this salt reference case are shown in Figure 4-10 and are summed up as follows:

1. Fluid pressure will be defined as hydrostatic. The scenario presented here focuses on the intrusion of water into the mined repository. However, depending on the equation-of-state (EOS) for the given code, density differences between the fluids may be neglected if the EOS lacks that capability.
2. Temperature will be established by setting a heat flux at the base of the model reflective of the regional heat flow in Germany around Gorleben Salt Dome (~110 mW/m^2; Hänel 1998) and setting a constant temperature boundary condition at ground surface at the average surface temperature (9°C) which will put the temperature at the depth of the repository ~38°C (Bräuer, et al. 2016).
3. Once hydrostatic conditions are calculated, the mined repository and access shafts will be added and are defined by unsaturated conditions at atmospheric pressure.

4. Initial saturation for each material in the mined repository and access shafts will be set at the residual liquid saturation that corresponds to the relevant relative permeability model (Table 4-12).

The flow rate (specific discharge or Darcy flux) in the aquifer (overburden) is 10^{-10} m/s (1.31×10^{-4} m/y).

Teams should run initial flow and transport simulations to 100,000 years.

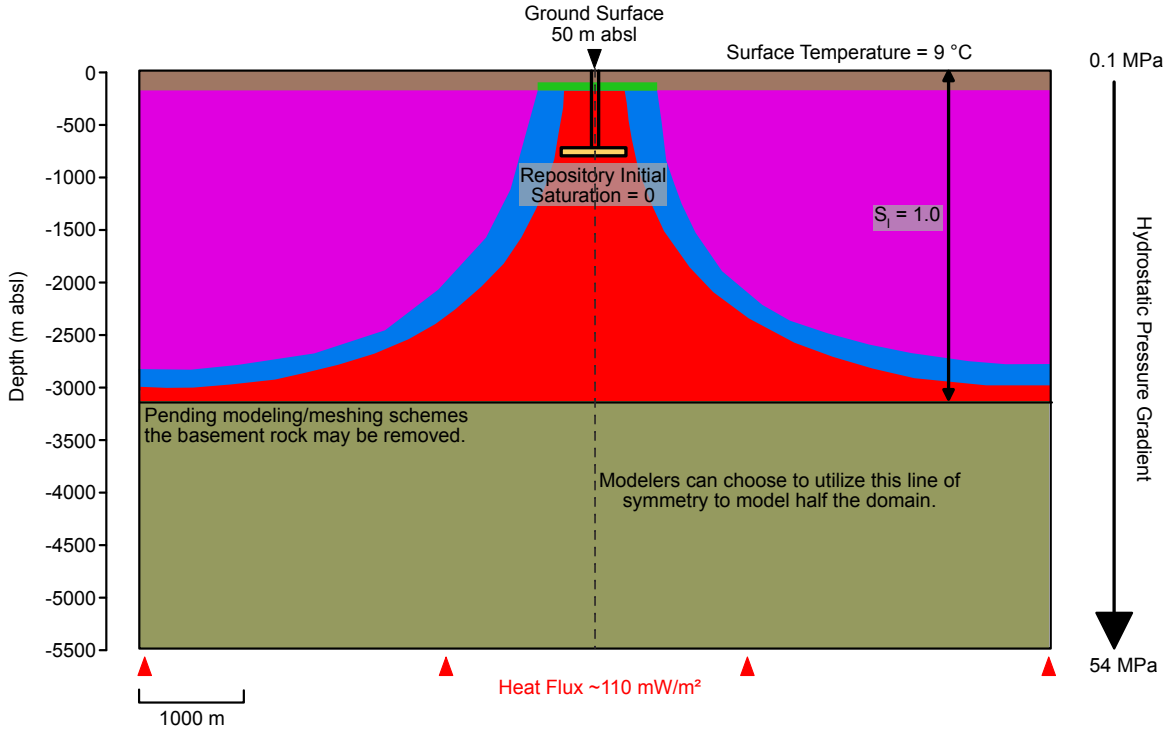

Figure 4-10. Schematic for initial conditions at t = 0 years after waste package emplacement. The orientation and design of the repository and geologic cross section were chosen to provide a symmetry boundary that modelers can choose to leverage to reduce the computational resources required for the presented scenario.

4.7 Outputs for Comparison

This section provides a list of outputs for comparison to compare/contrast modeling schemes, numerical codes, and assumptions made between the participating teams. Some output comparisons are made at a specific location while others are integrated over an area or averaged over a volume.

Initial comparisons will be conducted qualitatively. Each team should plot the following comparison quantities as a function of time

4.7.1 Transport comparisons

4.7.1.1 Radionuclide/Tracer Fluxes

- Lower Shaft(s): Plot as a function of time (years) the mass flow of each radionuclide (moles/second) across a plane in the shaft 25 m above the ceiling of the infrastructure area, integrated over the 7×7 m^2 cross section of the shaft.
- Upper Shaft(s): Plot as a function of time the mass flow of each radionuclide (moles/second) across a plane in the shaft at the base of the aquifer (overburden), integrated over the 7×7 m^2 cross section of the shaft.

- Drift Seal(s): Plot as a function of time the mass flow of each radionuclide (moles/second) across 4 planes in the drift seal, integrated over the 7 × 4 m^2 cross section, at both faces of each Sorel cement segment.

4.7.1.2 Radionuclide/Tracer mass

- Infrastructure Area: Plot as a function of time the total moles of each radionuclide in the 240 × 250 m^2 infrastructure area.
- Drift Seal(s): Plot as a function of time the total moles in each 100-m Sorel cement segment and in the 300-m run-of-mine salt section in the drift seal.
- Emplacement Drifts: Plot as a function of time the total moles of each radionuclide in the 90-m long SNF emplacement drift and in the 50-m long HLW emplacement drift highlighted in Figure 4-4. (Note: The group may decide to plot total moles of each radionuclide summed over all of the 90-m long SNF emplacement drifts and summed over all of the 50-m long HLW emplacement drifts instead.)

4.7.1.3 Radionuclide/Tracer concentration

- A comparison of radionuclide concentrations (moles/liter) in the aquifer is desirable. How best to achieve it will be discussed as teams begin to generate results.

4.7.1.4 Radionuclide/Tracer source term

- Plot as a function of time the rate of radionuclide release (moles/second) into one SNF and one HLW drift (highlighted in Figure 4-4).

4.7.2 Flow comparisons

4.7.2.1 Saturation and Pressure

- Infrastructure Area: Plot as a function of time the average liquid pressure (Pa) and saturation (unitless) in the 240 x 250 m^2 infrastructure area. If grid cells vary in volume, calculate the volume-weighted average.
- Drift Seal(s): Plot as a function of time the average liquid pressure and saturation in each 100-m Sorel cement segment and in the 300-m run-of-mine salt section of the drift seal. If grid cells vary in volume, calculate the volume-weighted average.
- Emplacement Drifts: Plot as a function of time the average liquid pressure and saturation in the 90-m long SNF emplacement drift and in the 50-m long HLW emplacement drift highlighted in Figure 4-4. If grid cells vary in volume, calculate the volume-weighted average.

4.7.2.2 Liquid Fluxes

- Plot as a function of time the volumetric flow of liquid (m^3/s) across all the same planes used to compare radionuclide mass flow.

5. Step 0C – Crystalline Reference Case Initial Description

5.1 Objectives

The objective of Step 0 is to fully describe and parameterize a single scenario, presumably the "canister failure by corrosion under temperate climate" scenario (Section 3.10.1). Participating teams will:

1. Agree on primary FEPs.
2. Divide the responsibility of gathering process model descriptions and tabulating necessary parameters.

Finalizing the hydrogeologic description of the fractured crystalline host rock will be prioritized, so that teams may progress through Step 1C when they are ready to do so.

5.2 Requirements

- The minimum description necessary to begin implementing models and running simulations is generated.
- A common set of quantities and units is used to characterize the system.
- Additional FEPs or alternate models may be added at a later date depending on results of the minimum description and interests of the participants.
- Additional scenarios may be added a later date depending on available time and interests of the participants.

5.3 Deadlines

November 2021

6. Step 1C – Crystalline Reference Case Process Model Comparison

6.1 Objectives

The objective of Step 1 is to compare performance measures or other outputs resulting from simple test cases or subsystem process models. These will be addressed in an order that facilitates sequential development of the complete repository system model. The focus will be on preparing to simulate the "canister failure by corrosion" scenario (Section 3.10.1). Test cases related to flow and transport (Section 6.3), radionuclide source term (Section 6.4), and buffer and canister processes (Section 6.5) provide an opportunity to:

1. understand differences in model implementation that affect how a problem can be specified, what results can be obtained, and which unit conversions will be necessary;
2. assess the influence of modeling choices on calculated values of performance measures in relatively simple systems.

6.2 Schedule

A tentative schedule for completion of test cases is proposed in Table 6-1.

Table 6-1. Tentative schedule for Step 1 test cases.

Section Heading	Test Cases related to:	Proposed Completion Date
6.3.1	Steady-state flow	July 2020
6.3.2	Transient advection/dispersion	July 2020
6.3.3	Matrix diffusion	November 2020
6.3.4	4-fracture network (deterministic)	November 2020
6.3.5	Stochastic fracture network	April 2021
6.4	Radionuclide source term	TBD
6.5	Buffer and canister processes	TBD

6.3 Flow and Transport

Flow and transport test cases will build toward comparison of flow and transport simulations using multiple realizations of a stochastically generated DFN in a 1-km^3 model domain. The objective is to understand how uncertainties due to the stochastic nature of the fracture network compare to differences in solution introduced by modelling choices, which may include, for instance, use of DFN versus ECPM, methods of upscaling to ECPM, use of particle tracking versus the advection/dispersion equation, and implementation of rock matrix diffusion.

6.3.1 Steady-state Flow

Steady-state, single-phase flow in 1, 2, and 3 dimensions will be compared to analytical solutions. The proposed test problems are adapted from Kolditz et al. (2015), and have been demonstrated using PFLOTRAN (Frederick 2018a). Whereas the OpenGeoSys simulations reported in Kolditz et al. (2015) neglected gravity by using zero liquid density, the PFLOTRAN simulations use constant liquid density and neglect gravity by setting the gravity vector to zero.

6.3.1.1 1-Dimensional (1-D) steady flow with boundary conditions of the first kind

The model domain is a 100 m × 10 m × 10 m beam extending in the positive *x* direction, discretized into 10 cubic grid cells, each 10 m × 10 m × 10 m. Constant pressure (Dirichlet) boundary conditions are held at either end of the beam (Figure 6-1). Material and fluid properties and boundary conditions are given in Table 6-2. The steady-state pressure solution is provided in Kolditz et al. (2015), Section 2.2.1.

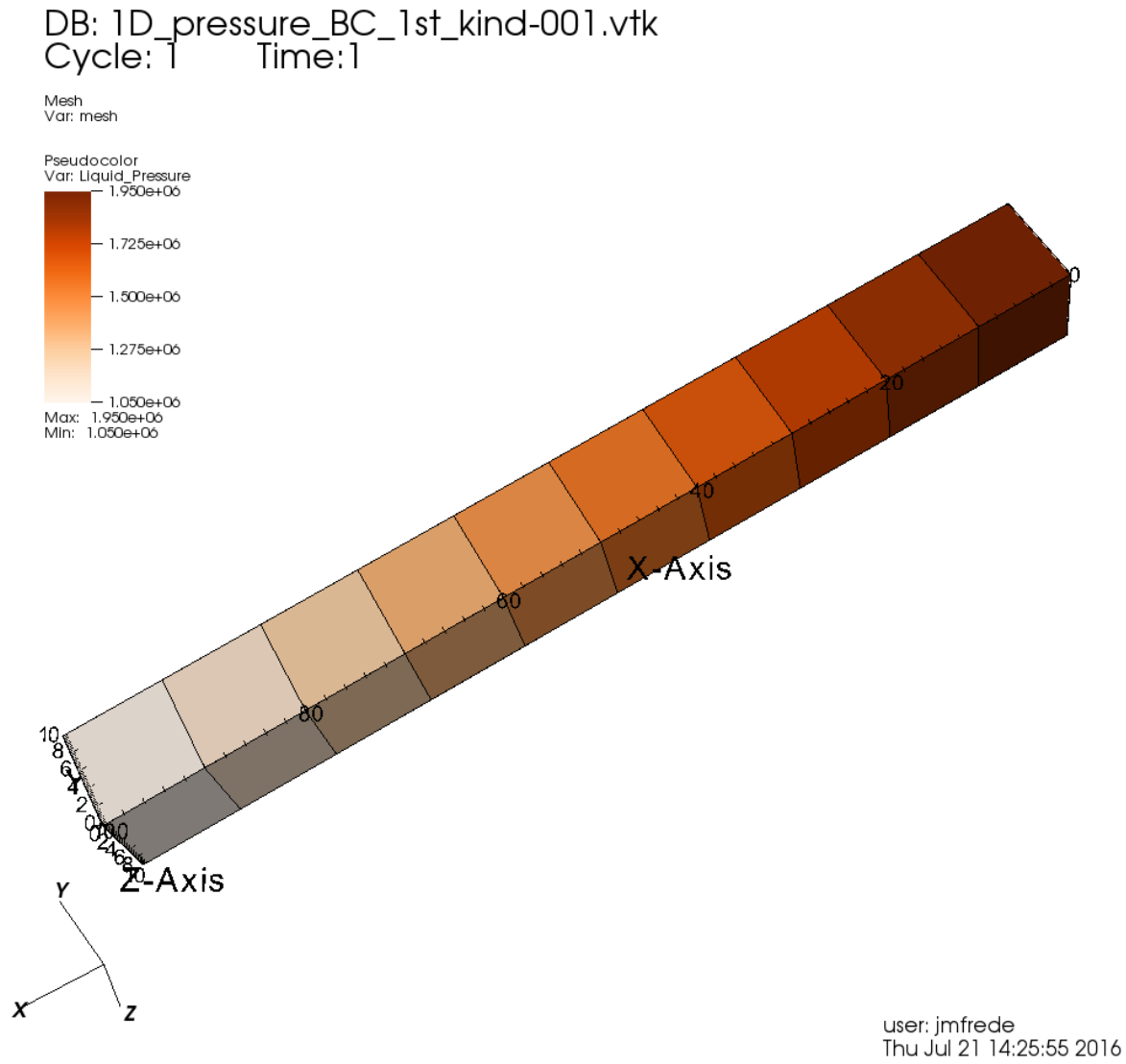

Figure 6-1. Model domain for simulation of 1-D steady flow with boundary conditions of the first kind (Frederick 2018a).

Table 6-2. Parameter values for simulation of 1-D steady flow with boundary conditions of the first kind.

Parameter	Value	Units
Permeability (k)	10^{-15}	m^2
Viscosity (μ)	10^{-3}	Pa-s
Density (ρ)	1000	kg/m^3

Pressure ($P_{x=0}$)	2×10^6	Pa
Pressure ($P_{x=100}$)	1×10^6	Pa

6.3.1.2 2-Dimensional (2-D) steady flow with boundary conditions of the first kind

The model domain is a 1 m × 1 m × 1 m slab extending in the positive x and y directions, discretized into 20 × 20 × 1 hexahedral grid cells, each 0.05 m × 0.05 m × 1 m. Constant pressure (Dirichlet) boundary conditions are held on the faces of the domain orthogonal to the x and y axes (Figure 6-2). Material and fluid properties and boundary conditions are given in Table 6-3. The steady-state pressure solution is provided in Kolditz et al. (2015), Section 2.2.3.

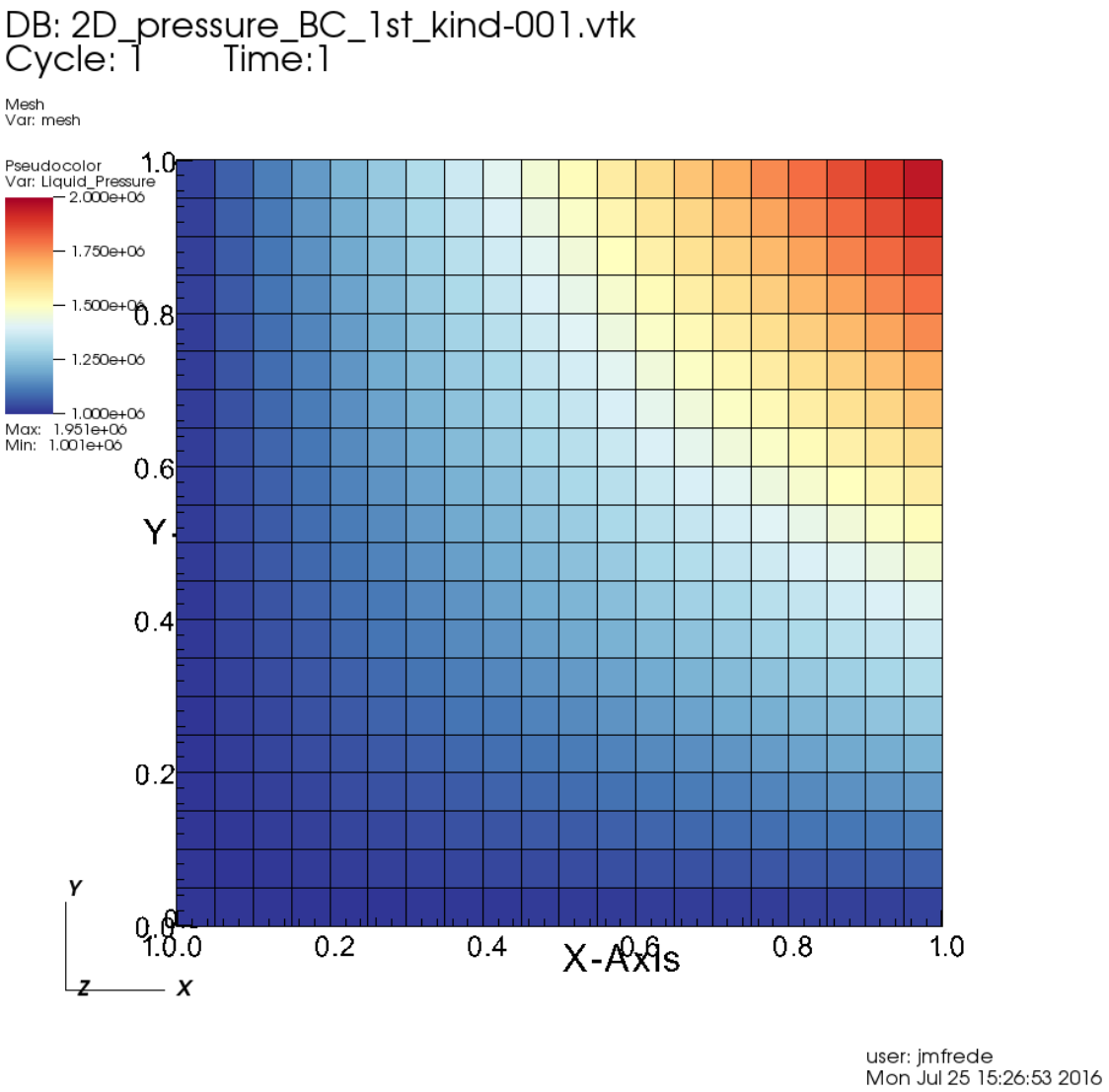

Figure 6-2. Model domain for simulation of 2-D steady flow with boundary conditions of the first kind (Frederick 2018a).

Table 6-3. Parameter values for simulation of 2-D steady flow with boundary conditions of the first kind.

Parameter	Value	Units

Permeability (k)	10^{-15}	m^2
Viscosity (μ)	10^{-3}	Pa-s
Density (ρ)	1000	kg/m^3
Pressure, $P(x = 0, y)$	1×10^6	Pa
Pressure, $P(x = L, y)$	$P_0 \frac{y}{L} + 1 \times 10^6$	Pa
Pressure, $P(x, y = 0)$	1×10^6	Pa
Pressure, $P(x, y = L)$	$P_0 \frac{x}{L} + 1 \times 10^6$	Pa
P_0	1×10^6	Pa
L	1	m

6.3.1.3 3-Dimensional (3-D) steady flow with boundary conditions of the first kind

The model domain is a 1 m × 1 m × 1 m cube extending in the positive x, y and z directions, discretized into cubic grid cells, each 0.1 m × 0.1 m × 0.1 m. Constant pressure (Dirichlet) boundary conditions are held on all six faces of the domain Figure 6-3). Material and fluid properties and boundary conditions are given in Table 6-4. The steady-state pressure solution is provided in Kolditz et al. (2015), Section 2.2.5.

Figure 6-3. Model domain for simulation of 3-D steady flow with boundary conditions of the first kind (Frederick 2018a).

Table 6-4. Parameter values for simulation of 3-D steady flow with boundary conditions of the first kind.

Parameter	Value	Units
Permeability (k)	10^{-10}	m^2
Viscosity (μ)	10^{-3}	Pa-s
Density (ρ)	1000	kg/m^3
Pressure, $P(x = 0, y, z)$	$P_0 \left(0 + \frac{y}{L} + \frac{z}{L}\right)$	Pa
Pressure, $P(x, y = 0, z)$	$P_0 \left(\frac{x}{L} + 0 + \frac{z}{L}\right)$	Pa
Pressure, $P(x, y, z = 0)$	$P_0 \left(\frac{x}{L} + \frac{y}{L} + 0\right)$	Pa
Pressure, $P(x = L, y, z)$	$P_0 \left(L + \frac{y}{L} + \frac{z}{L}\right)$	Pa
Pressure, $P(x, y = L, z)$	$P_0 \left(\frac{x}{L} + L + \frac{z}{L}\right)$	Pa

Pressure, $P(x, y, z = L)$	$P_0\left(\frac{x}{L} + \frac{y}{L} + L\right)$	Pa
P_0	1×10^6	Pa
L	1	m

6.3.2 Transient Transport

1-D transient advection and dispersion of three tracers (conservative, decaying, and adsorbing) will be compared to analytical solutions. The proposed test problem is adapted from Kolditz et al. (2015), Section 2.5.2.

The model domain is a 10 m × 1 m × 1 m beam extending in the positive x direction, discretized into 200 hexahedral grid cells, each 0.05 m × 1 m × 1 m (Figure 6-4). A steady-state flow field (constant specific discharge) is applied. At the inflow face ($x = 0$), concentrations of all three tracers are held at 1 mol/L from 0 to 15000 s, and zero afterward. Concentrations in the model domain are compared to the analytical solution at 20000 s. Material and fluid properties and boundary conditions are given in Table 6-5. Solutions are provided in Kolditz et al. (2015), Section 2.5.2.

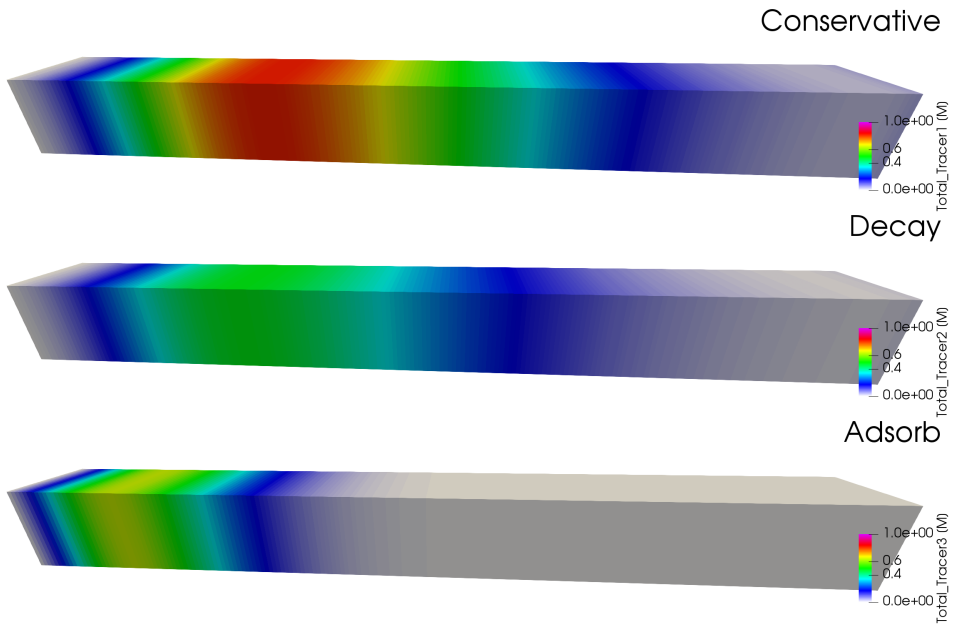

Figure 6-4. Model domain for simulation of transient advection and dispersion.

Table 6-5. Parameter values for simulation of transient advection and dispersion.

Parameter	Value	Units
Specific discharge (q)	10^{-4}	m/s
Dispersion coefficient (D)	10^{-4}	m^2/s
Porosity (ϕ)	0.4	–

Decay constant (λ)	5×10^{-5}	1/s
Linear distribution coefficient (K_d)	6.8×10^{-4}	m^3 H_2O / kg solid
Liquid density (ρ)	1000	kg/m^3
Solid grain density (ρ_s)	2000	kg/m^3

6.3.3 Fracture Transport with Matrix Diffusion

Matrix diffusion is the migration of dissolved solutes from flowing fractures into the pore space of the rock matrix (and vice versa). The proposed benchmark test is based on the analytical solution by Tang et al. (1981), for the problem of transport of a radionuclide in a single fracture, with diffusion into the rock matrix. The fracture-rock matrix system is represented in Figure 6-5. The governing equations are derived from mass conservation of the radionuclide and the following assumptions are made:

1. The width of the fracture is much smaller than its length.
2. Transverse diffusion and dispersion within the fracture assure complete mixing across the fracture width at all times.
3. The permeability of the porous matrix is very low and transport in the matrix will be mainly by molecular diffusion.
4. Transport along the fracture is much faster than transport within the matrix.

Concentration profiles along the fracture and the rock matrix (x >= b) are compared to the analytical solution at 100, 1000 and 10000 days over 101 cells. The first set is compared with v_1 along a 6 m domain for the fracture and at z = 2 m with a domain of 2 m for the matrix. A second set is compared with v_2 along a 60 m domain for the fracture and at z = 20 m with a domain of 1 m for the matrix.

The governing equations are:

$$\frac{\partial c}{\partial t} + \frac{v}{R}\frac{\partial c}{\partial z} - \frac{D}{R}\frac{\partial^2 c}{\partial z^2} + \lambda c + \frac{J}{bR} = 0 \quad (1)$$

$$\frac{\partial c'}{\partial t} - \frac{D'}{R'}\frac{\partial^2 c'}{\partial z^2} + \lambda c' = 0 \quad (2)$$

Where c, c' are the concentration of solute in solution in the fracture and rock matrix respectively (M/L^3). With v as average linear groundwater velocity in the fracture (L/T) and D is the hydrodynamic dispersion coefficient in the fracture given by:

$$D = \alpha_L v + D^* \quad (3)$$

The effective diffusion coefficient, D' is given by:

$$D' = \tau D^* \quad (4)$$

And the diffusive mass flux J ($M/L^2/T$), from the fracture in the rock matrix is given by, at x = b:

$$J = -\phi D' \frac{\partial c'}{\partial x} \tag{5}$$

The initial conditions are given by:

$$c(z,0) = c'(x,z,0) = 0$$

The boundary conditions are given by:

$$c(0,t) = c_0$$
$$c(\infty,t) = 0$$

$$c'(b,z,t) = c(z,t)$$
$$c'(\infty,z,t) = 0$$

Material and fluid properties are given in Table 6-6.

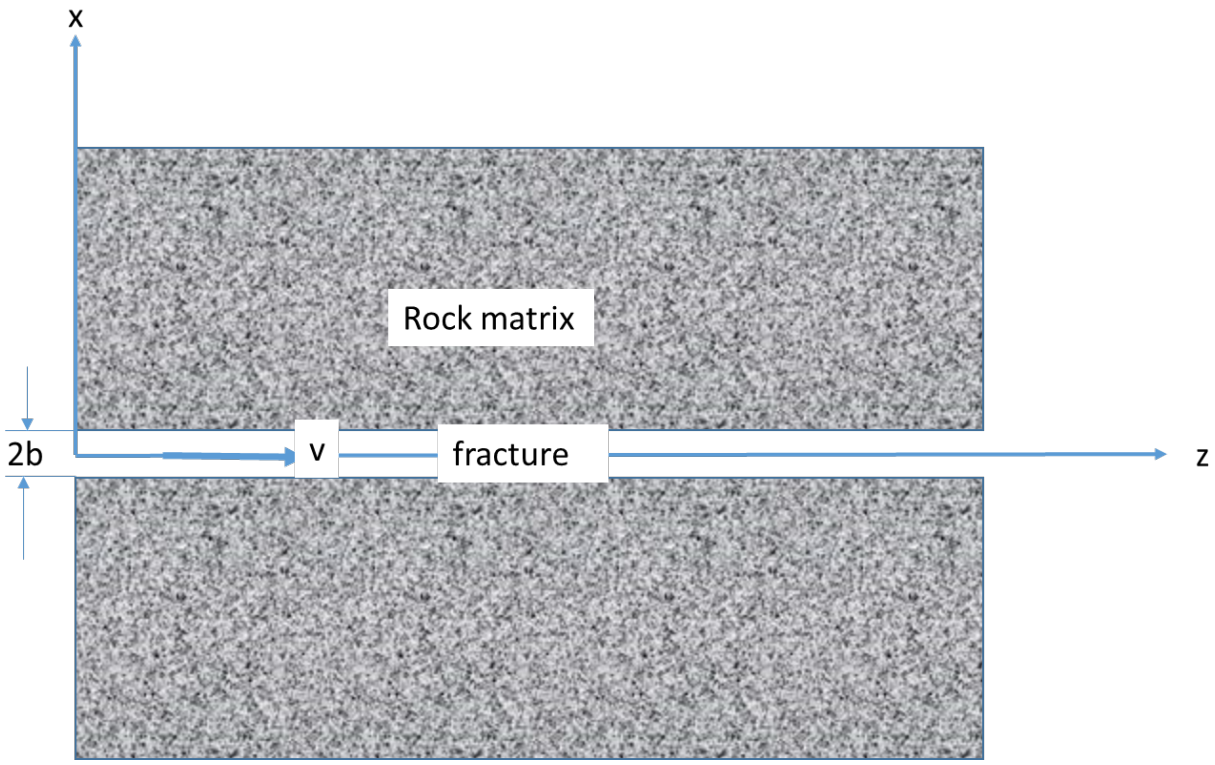

Figure 6-5 Fracture/rock matrix system

Table 6-6. Parameter values for simulation of fracture transport in matrix diffusion.

Parameter	Value	Units
Diffusion coefficient in water (D^*)	1.6×10^{-9}	m^2/s
Tortuosity (τ)	0.1	–
Fracture width ($2b$)	10^{-4}	m
Dispersivity (α_L)	0.5	m
Half-life ($t_{1/2}$), equivalent to Decay constant (λ)	12.35 1.779×10^{-9}	y s
Retardation factor in matrix (R')	1.0	–
Retardation factor in fracture (R)	1.0	–
Porosity (ϕ)	0.01	–
Concentration, c_0 (z=0)	1.0	mol/L
Average linear velocity (v_1)	0.01	m/d
Average linear velocity (v_2)	0.1	m/d

6.3.4 Transport in a 4-Fracture DFN

The four-fracture test problem will provide an opportunity for teams to practice generating deterministic fractures and to test methods for upscaling to ECPM or simulating particle tracking (if desired). The test problem (built based on an example provided with dfnWorks (Hyman et al. 2015)) models advection and diffusion of a conservative tracer through four fractures within a cubic domain. It is assumed flow and transport only occur in the fractures; matrix diffusion is neglected. Groundwater flow is simulated by a steady state (saturated, single-phase) flow driven by a pressure gradient along the x-axis. Constant pressure (Dirichlet) boundary conditions are applied on the inflow and outflow faces. For simplicity, gravity is not included. No-flow boundary conditions are applied at all other faces of the domain.

An initial pulse of tracer is inserted uniformly along the single fracture on the west face (x = -500) of the domain at time zero; the concentration at the west face is zero for all other times. The tracer then exits the domain through the two fractures on the east face (x = 500). The tracer can be modeled using particle tracking (Lagrangian reference frame) or with the advection-dispersion equation (Eulerian reference frame). In particle tracking, the mass of each particle is equal and 1.0 x 10^4 particles were introduced on the inflow face. For comparison, normalized breakthrough curves (total mass that's crossed the east face divided by the initial mass at the west face) are generated at the outflow face and compared over 30 years. Since breakthrough curves are normalized to initial mass, the concentration of the initial pulse is inconsequential.

The governing equation for advective-diffusive transport is,

$$\frac{\partial}{\partial t}(\phi\psi) + \nabla \cdot \Omega = 0 \tag{6}$$

With ϕ as porosity and ψ denoting total concentration. The total flux Ω is given by,

$$\Omega = (q - D_e \cdot \nabla)\psi \tag{7}$$

With D_e representing the effective diffusion coefficient which is defined as,

$$D_e = \phi\tau D_m \tag{8}$$

Where D_m is the molecular diffusion coefficient in free water [m^2/s] and τ is tortuosity. Tortuosity is defined as $(L/L_e)^2$, where L is the straight-line length and L_e is the average length of a tortuous path through a porous medium (Bear 1972). Using this definition, tortuosity is a value less than or equal to one.

Pressure is modeled according to Darcy's law,

$$q = -\frac{k}{\mu}\nabla(P) \tag{9}$$

Where k is permeability [m^2], μ is viscosity [Pa s] and P is pressure [Pa].

Details can be found in Table 6-7 and vertex coordinates for the domain and fractures can be found in Table 6-8.

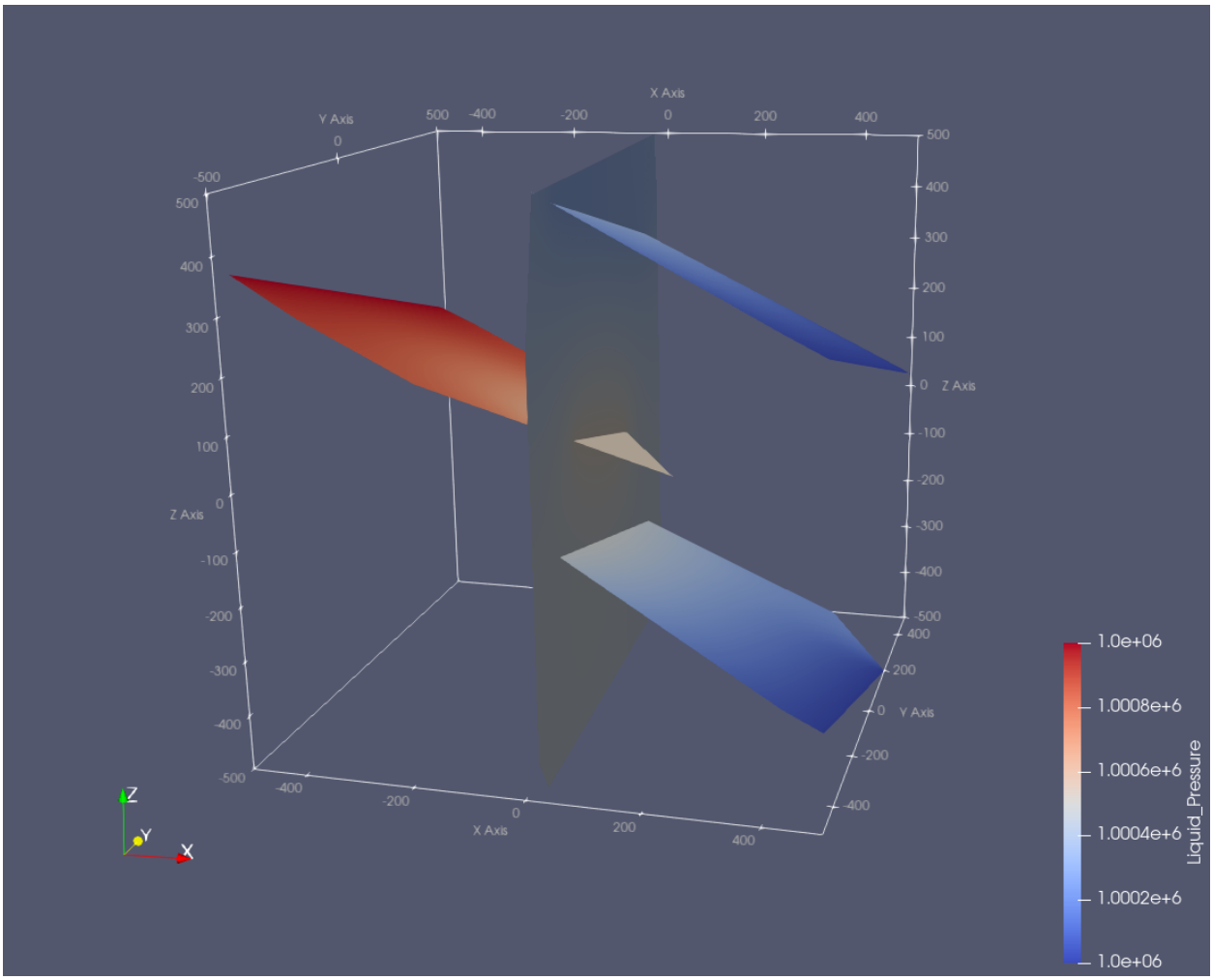

Figure 6-6 Four-fracture pressure simulation.

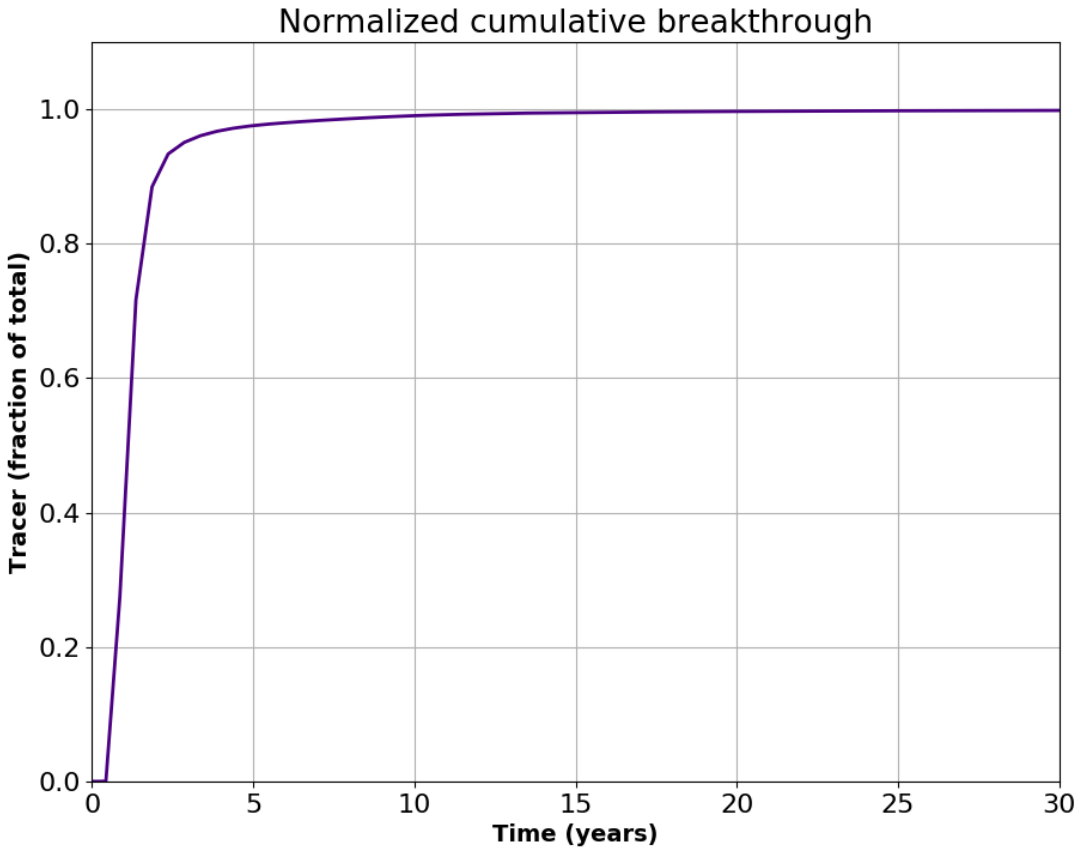

Figure 6-7 Example breakthrough curve

Table 6-7 Parameter values for four-fracture problem.

Parameter	Value	Units
Pressure (inlet, x = -500)	1.001×10^{6}	Pa
Pressure (outlet, x = 500)	1×10^{6}	Pa
Fracture 1 Aperture	1×10^{-3}	m
Fracture 2 Aperture	1×10^{-3}	m
Fracture 3 Aperture	1×10^{-3}	m
Fracture 4 Aperture	5×10^{-4}	m
Fracture 1 Permeability	8.333×10^{-8}	m^2
Fracture 2 Permeability	8.333×10^{-8}	m^2
Fracture 3 Permeability	8.333×10^{-8}	m^2

Fracture 4 Permeability	2.083×10^{-8}	m^2
Porosity in a fracture (ϕ)	1.0	–
Tortuosity in a fracture (τ)	1.0	–
Diffusion coefficient in water (D_m)	1.6×10^{-9}	m^2/s

Table 6-8 Coordinates for domain and fractures

Feature	Vertex
Domain	{-500, -500, -500} {-500, -500, 500} {-500, 500, 500} {-500, 500, -500} {500, -500, -500} {500, 500, -500} {500, 500, 500} {500, -500, 500}
Fracture 1	{-162.354, -500.000, 206.177} {138.978, -30.511, -61.861} {-229.987, 500.000, -10.007} {-417.374, 500.000, 83.687} {-500.000, 475.093, 131.227} {-500.00, -446.814, 361.704} {-367.607, -500.000, 308.800}
Fracture 2	{26.316, -500.000, -431.524} {23.472, -445.963, -500.000} {-21.371, 406.045, -500.000} {-26.316, 500.000, -397.831} {-26.316, 500.000, 392.163} {-25.312, 480.928, 500.000} {23.070, -438.334, 500.000} {26.316, -500.000, 261.673}
Fracture 3	{500.000, -500.000, 275.000} {500.000, 500.000, 25.000}

	{382.626, 500.000, 83.687} {-53.977, 368.388, 334.891} {-18.109, -319.021, 488.810} {432.393, -500.000, 308.804}
Fracture 4	{500.000, -500.000, -325.000} {500.000, 200.000, -500.000} {354.273, 491.453, -500.000} {-53.977, 368.388, -265.109} {-18.109, -319.021, -111.190} {432.393, -500.000, -291.196}

6.3.5 Transport in a 4-Fracture DFN with Stochastic Fractures

A note about Revision 4: This problem specification and associated files have been corrected in Revision 4. The discrete fracture network in "vertices.txt" provided with Revision 3 was generated with incorrect fracture orientations. When the fracture orientations were corrected, additional changes to model inputs were also made. These include: 1) the pressure at the west face of the domain has been increased to 1.1 MPa; the half-life of the decaying tracer has been decreased to 100 y; the retardation coefficient in the fractures (see Equation 12) has been increased to 5. Additionally, hydrologic properties of the matrix have been added to the problem description, and the inputs necessary to generate the fracture network using dfnWorks (Hyman et al. 2015) and to upscale it using mapdfn.py (Stein et al. 2017) have been provided separately.

The four-fracture benchmark case is extended by adding stochastically-generated fracture sets to the model domain. The stochastic fractures are generated based on Central Hydraulic Unit West (CHUW) Case A distributions from Posiva WR 2012-42 (Hartley et al. 2012, Table D-4) corresponding to Depth Zone 4, which applies at repository depth (Hartley et al. 2016, Table 3-1). The domain, including stochastically-generated fractures, will be provided to the teams. The problem models advection and diffusion of conservative, decaying, and adsorbing tracers according to Equation 6 (Section 6.3.4), through the four fractures and stochastic fractures within a cubic domain. The problem uses the same assumptions for flow and transport as the four-fracture benchmark case and the domain coordinates remain the same.

Three fracture families, two subvertical and one subhorizontal, are defined. For each fracture family, fracture radius is sampled from a truncated power law distribution, and fracture orientation is sampled from a Fisher distribution. (Although a bivariate Bingham distribution is given for the subhorizontal fracture family, the option isn't yet implemented in dfnWorks, so for this initial test problem we proceed by substituting a Fisher distribution.) Fractures are assumed to be randomly distributed in space, with a fracture intensity for each fracture family expressed as fracture area per unit volume of rock (P_{32}).

Posiva employed truncated power law distributions with a minimum radius of 0.04 m and a maximum radius of 564 m in calibrating P_{32} and fracture transmissivity to borehole flow measurements (Hartley et al. 2011), but employed larger minimum fracture radii (8.46 m in the far field and 0.5 m in the vicinity of the repository) in generating DFNs for flow and transport modeling (Hartley et al. 2012). Similarly, to

generate fractures for this test problem, we increased the minimum fracture radius to 30 m and adjusted P_{32} accordingly using the method in Hedin (2008).

In this test problem, fracture transmissivity (T [m^2/s]) is correlated with fracture radius (r [m]) according to:

$$T = ar^b \tag{10}$$

In Equation 10, *a* and *b* are dimensionless constants with values equal to 2.2e-9 and 0.8, respectively (Hartley et al. 2012, Table D-4).

Fracture aperture is calculated from transmissivity using the cubic law (as in Bear et al. 1993):

$$T = \frac{\rho g}{\mu}\frac{B^3}{12} \tag{11}$$

In Equation 11, *B* is fracture aperture [m] (equal to 2*b* in Figure 6-5), ρ is the density of water [kg/m^3], g is acceleration due to gravity [m/s^2], and μ is the viscosity of water [Pa s].

An initial pulse of tracer is inserted uniformly along the fractures on the west face (x = -500) of the domain at time zero; the concentration at the west face is zero for all other times. The tracer then exits the domain through the fractures on the east face (x = 500). For comparison, normalized breakthrough curves (total mass that has crossed the east face divided by the initial mass at the west face) are generated at the outflow face and compared over 1000000 years. Since breakthrough curves are normalized to initial mass, the concentration of the initial pulse is inconsequential. The tracer can be modeled using particle tracking (Lagrangian reference frame) or with the advection-dispersion equation (Eulerian reference frame). The decaying tracer has a half-life of 100 years. The adsorbing tracer has a retardation coefficient in the fracture of 5. If a team's software requires a linear distribution coefficient instead of a retardation coefficient, Equations 12 and 13 will assist in the conversion. The retardation coefficient (R [-]) is defined as (Tang et al. 1981):

$$R = 1 + \frac{K_f}{b} \tag{12}$$

In Equation 12, *b* is half the fracture aperture, and K_f is the linear distribution coefficient in the fracture, defined as (Freeze and Cherry 1979):

$$K_f = \frac{\text{mass sorbed} / \text{area fracture}}{\text{mass dissolved} / \text{volume water}}. \tag{13}$$

The parameters necessary for teams to generate their own stochastic fracture sets will be given in future problems. For this problem, teams will use identical fracture networks. dfnWorks input files are provided to create the fracture network as well as input (mapdfn2pflotran.py) to upscale to an ECPM using mapdfn.py. Output files are provided for both the DFN and ECPM as well. Coordinates of the fracture vertices are provided in the text file polygons.dat. Fracture apertures and permeabilities are provided respectively in the text files aperture.dat and perm.dat. Coordinates of the fracture centers are provided in the text file translations.dat; fracture radii are provided in radii_Final.dat; and normal vectors for each fracture are provided in normal_vectors.dat.

Details for flow and transport parameters can be found in Table 6-9. The problem specification does not include fracture-matrix diffusion (such as might be simulated using a dual-porosity model). Hydrologic properties of the matrix are included for teams that choose to include the matrix in upscaling to an ECPM. These values correspond to the inputs given in mapdfn2pflotran.py associated with this problem; however, to minimize advection and diffusion in ECPM cells not intersected by fractures, teams may prefer to choose smaller values for matrix permeability and tortuosity or to deactivate matrix cells during simulations.

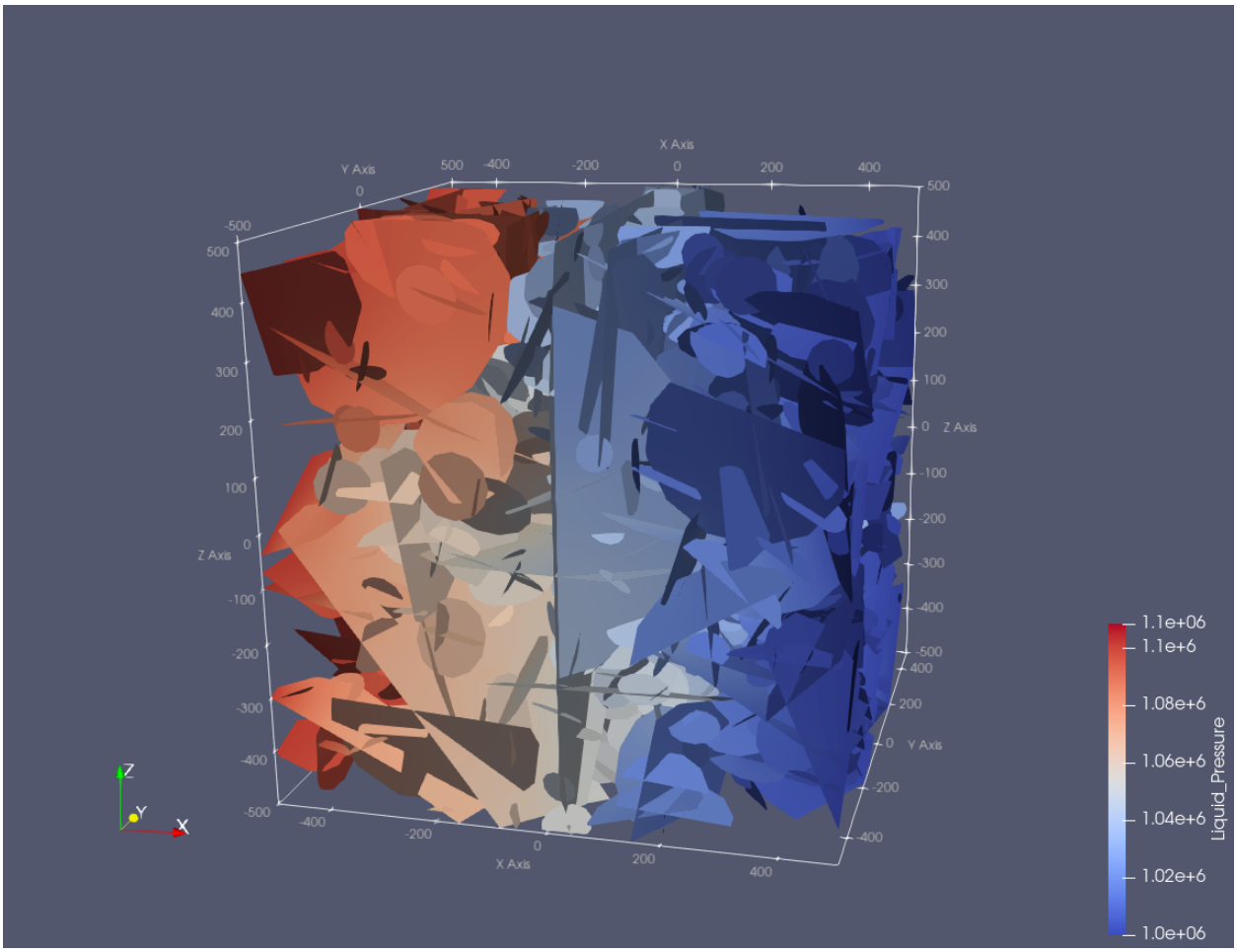

Figure 6-8 Four-fracture with stochastic fractures pressure simulation.

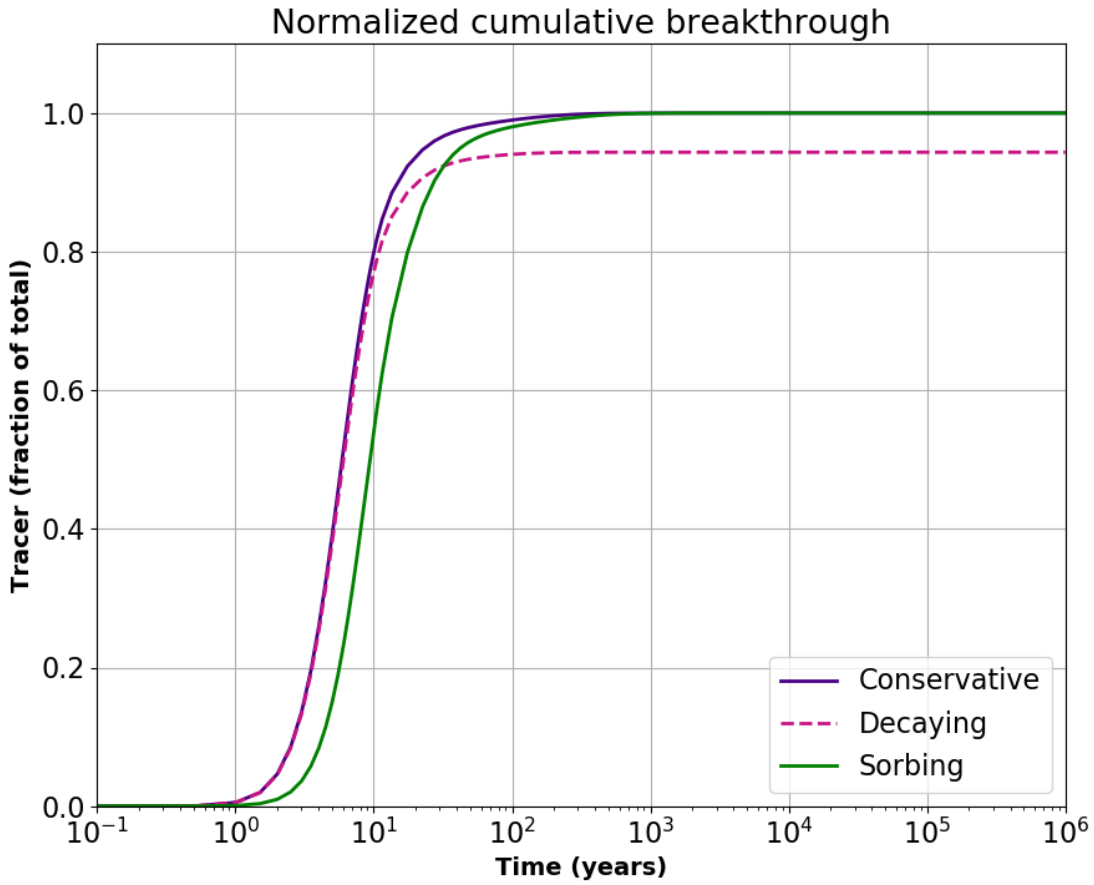

Figure 6-9 Example breakthrough curve

Table 6-9 Parameters for four fracture problem with stochastic fractures

Parameter	Value	Units
Pressure (inlet, x = -500)	1.1×10^6	Pa
Pressure (outlet, x = 500)	1×10^6	Pa
Porosity in a fracture	1.0	–
Tortuosity in a fracture	1.0	–
Matrix porosity	0.005	–
Matrix tortuosity[a]	0.2	–
Matrix permeability	10^{-18}	m^2
Diffusion coefficient in water (D_m)	1.6×10^{-9}	m^2/s

Half-life ($t_{1/2}$)	100	years
Retardation factor in fracture (R)	5	–
[a] The effective diffusion coefficient in the rock matrix is 1.6×10^{-12} m^2 (see Equation 8).		

6.3.6 Revised Transport in a 4-Fracture DFN with Stochastic Fractures

The 4-Fracture DFN with stochastic fractures benchmark has been revised to be more consistent with the 4-Fracture DFN benchmark in Section 6.3.4. The apertures and permeabilities of the four deterministic fractures can now be found in Table 6-10. The four deterministic fractures represent the first four fractures listed in aperture.dat and perm.dat. The inlet pressure boundary condition has also been revised to 1.001 x 10^6 Pa (Table 6-10). An example breakthrough curve can be seen in Figure 6-10. The stochastic fractures and all other parameters remain the same as section 6.3.5.

Table 6-10 Revised parameters for four fracture problem with stochastic fractures

Parameter	Value	Units
Pressure (inlet, x = -500)	1.001×10^6	Pa
Pressure (outlet, x = 500)	1×10^6	Pa
Deterministic Fracture 1 Aperture	1×10^{-3}	m
Deterministic Fracture 2 Aperture	1×10^{-3}	m
Deterministic Fracture 3 Aperture	1×10^{-3}	m
Deterministic Fracture 4 Aperture	5×10^{-4}	m
Deterministic Fracture 1 Permeability	8.333×10^{-8}	m^2
Deterministic Fracture 2 Permeability	8.333×10^{-8}	m^2
Deterministic Fracture 3 Permeability	8.333×10^{-8}	m^2
Deterministic Fracture 4 Permeability	2.083×10^{-8}	m^2

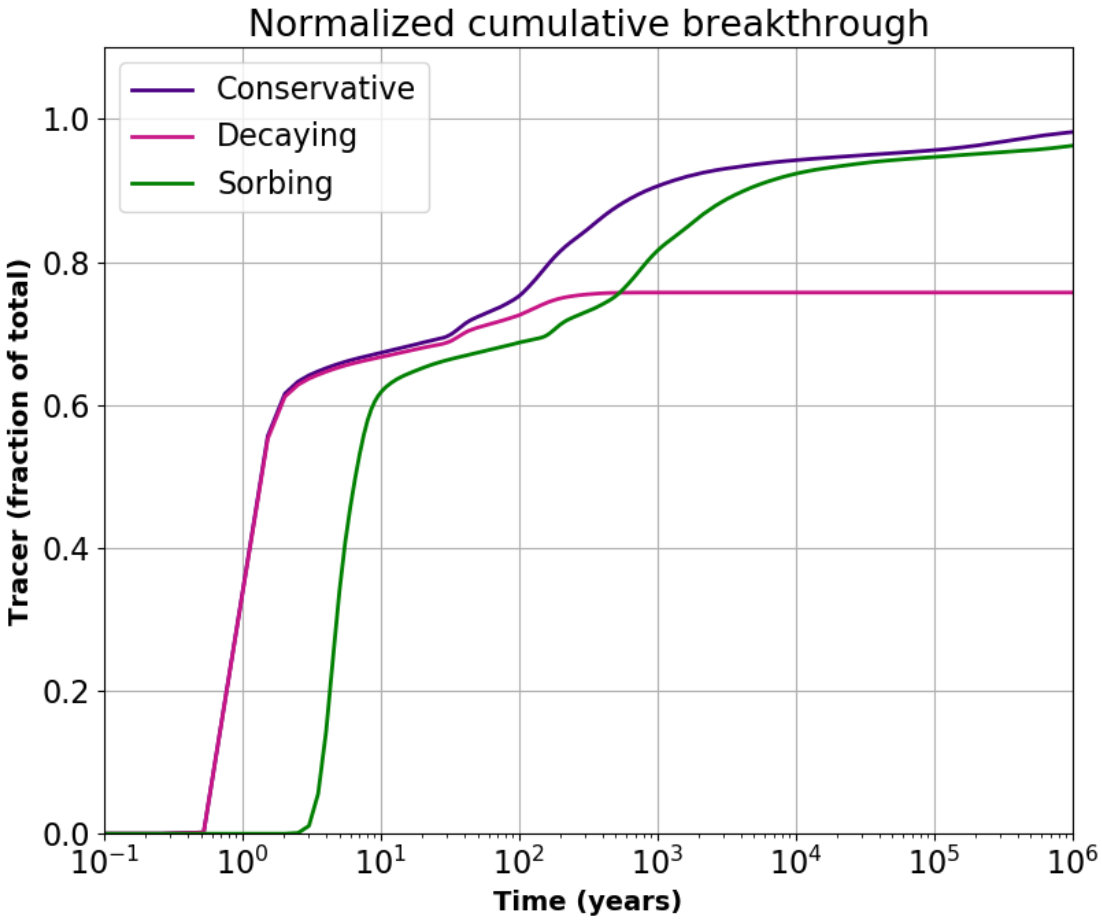

Figure 6-10 Example breakthrough curve

6.4 Radionuclide Source Term

The radionuclide source term depends on rates of radioactive decay and ingrowth and on the degradation rate of SNF. Depending on implementation, limits on radionuclide solubility within the waste canister may be accounted for in the source term model or considered separately. Comparisons aimed at ensuring consistency between radionuclide source term models will consider (similar to Frederick 2018b):

- Radioactive decay and ingrowth
- Rate-controlled release of radionuclides
- Radionuclide solubility limits

6.5 Buffer and Canister Processes

A series of test problems related to buffer saturation and erosion and canister corrosion will also be developed.

7. Steps 2C – 4C

Steps 2 – 4 of the crystalline reference case will be described in detail progressively, and will take into account the interests of the participants, the results of the test cases in Step 1, and the experience had by the participating teams when tackling the test cases in Step 1. The high-level schedule presented in Section 2.1 may be modified to incorporate simulation of more than one scenario, if sufficient time and interest exists.

8. Step 0S – Salt Reference Case Initial Description

8.1 Objectives

The objective of Step 0 is to fully describe and parameterize a single scenario, the "shaft seal failure" scenario (Section 4). Participating teams will:

3. Agree on primary FEPs.
4. Divide the responsibility of gathering process model descriptions and tabulating necessary parameters.

8.2 Requirements

- The minimum description necessary to begin implementing models and running simulations is generated.
- A common set of quantities and units is used to characterize the system.
- Additional FEPs or alternate models may be added at a later date depending on results of the minimum description and interests of the participants.
- Additional scenarios may be added a later date depending on available time and interests of the participants.

8.3 Deadlines

November 2021

9. Step 1S – Salt Reference Case Process Model Comparison

9.1 Objectives

The objective of Step 1 is to compare performance measures or other outputs resulting from simple test cases or subsystem process models. These will be addressed in an order that facilitates sequential development of the complete repository system model. The focus will be on preparing to simulate the "shaft seal failure" scenario (Section4). Test cases related to flow and transport, radionuclide release, and other processes provide an opportunity to:

3. understand differences in model implementation that affect how a problem can be specified, what results can be obtained, and which unit conversions will be necessary;
4. assess the influence of modeling choices on calculated values of performance measures in relatively simple systems.

9.2 Schedule

A tentative schedule for completion of test cases is proposed in Table 6-1.

Table 9-1. Tentative schedule for Step 1 test cases.

Section Heading	Test Cases related to:	Proposed Completion Date
6.3.2	1D transient advection/dispersion	November 2021
9.3.1	2D transient advection/dispersion	November 2021
9.4	Radionuclide source term	TBD
9.4	Others as motivated by the staged development of the reference case	TBD

9.3 Flow and Transport

1-D transient advection and dispersion of three tracers (conservative, decaying, and adsorbing) will be compared to analytical solutions. The 1-D transport benchmarks are the same as those completed for the crystalline case.

A 2-D transient advection and dispersion benchmark, a point source in a 2-D flow field, mimics the geometry of a shaft intersecting an aquifer. This benchmark is described in the following section.

9.3.1 2-D Transient Transport

An analytical benchmark for code comparison is needed for the salt case. Transport of radionuclides to the overburden by shaft-seal failure is considered as the disruptive scenario for the DECOVALEX salt case. Thus, the proposed benchmark problem has been chosen to be a simplified model of transport of tracers through a semi-infinite domain from a line source. The analytical solution is one of the example models from Section 3.3.2.2 of Batu (2006).

9.3.1.1 Analytical model

The conceptual model for the benchmark is shown in Figure 9-1. The assumptions of the analytical model are (after Batu 2006):

1) Unidirectional steady-state groundwater velocity field with flow in the x-direction.
2) Solute source is located at x = 0, planar and perpendicular to the velocity of the flow field.
3) Source concentration is a function of z-coordinate and time through an exponential function.
4) The medium is infinite in the x-direction and z is in the range (0,Z).

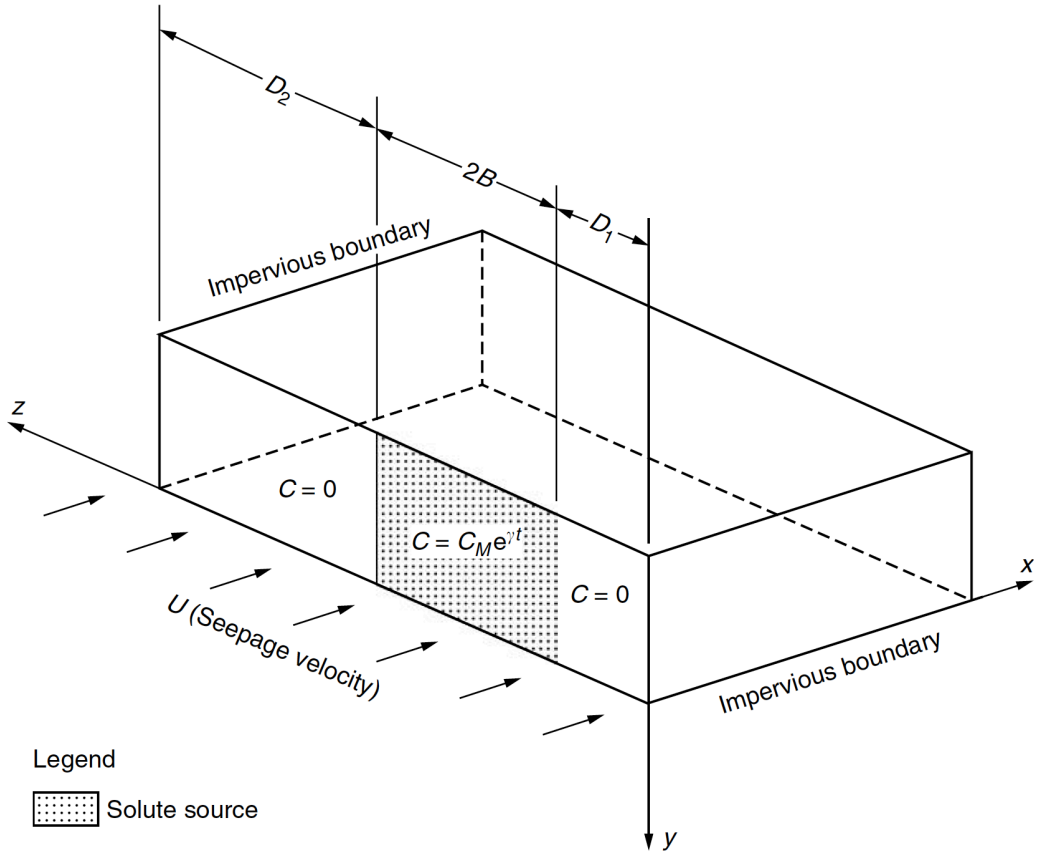

Figure 9-1. Schematic of chemical diffusion and transport from a planar source in a uniform flow field. Taken from Batu (2006).

The governing equation is:

$$\frac{\partial C}{\partial t} = \frac{D_x}{R_d}\frac{\partial^2 C}{\partial x^2} + \frac{D_z}{R_d}\frac{\partial^2 C}{\partial z^2} - \frac{U}{R_d}\frac{\partial C}{\partial x} - vC \qquad (9\text{-}1)$$

The initial condition is

$$C(x,z,0) = 0 \qquad (9\text{-}2)$$

,

and the boundary condition is

$$C(0,z,t) = \begin{cases} C_m \exp(\gamma t) & D_1 < z < D_1 + 2B \\ 0 & \text{otherwise} \end{cases} . \tag{9-3}$$

In this equation C_m is the initial tracer concentration at the source, U is the groundwater seepage velocity, v is the interstitial velocity, γ is the chemical decay rate of the source, R_d is the retardation factor. D_1 is the distance of the source from the z = 0 axis, D_2 is the distance from the z = Z outer boundary of the model, and B is the half-length of the planar source. $R_d = 1$ for flow without adsorption and $\gamma = 0$ for a constant rate tracer source.

The solution to this equation is:

$$\begin{aligned} C(x,z,t) = {} & C_m P_1 \left[\exp(-P_2)\operatorname{erfc}(P_3 - P_4) + \exp(P_2)\operatorname{erfc}(P_3 + P_4)\right] \\ & + \frac{C_m}{\pi} P_5 P_6 \sum_{n=1}^{\infty} P_{7_n} \left[\exp(-P_{8_n})\operatorname{erfc}(P_3 - P_{9_n}) + \exp(P_{8_n})\operatorname{erfc}(P_3 + P_{9_n})\right] \end{aligned} \tag{9-4}$$

where

$$P_1 = \frac{B}{D_1 + 2B + D_2} \exp\left(\gamma t + \frac{Ux}{2D_x}\right) \qquad P_2 = \left(\frac{vR_d}{D_x} + \frac{U^2}{4D_x^2} + \frac{\gamma R_d}{D_x}\right)^{\frac{1}{2}} x$$

$$P_3 = \frac{R_d x}{2(D_x R_d t)^{\frac{1}{2}}} \quad P_4 = \left[\left(v + \frac{U^2}{4D_x R_d} + \gamma\right) t\right]^{\frac{1}{2}} \qquad P_5 = \exp\left(\frac{Ux}{2D_x}\right)$$

$$P_6 = \exp(\gamma t) \qquad P_{7_n} = \frac{1}{n}\left\{\sin\left[\lambda_n (D_1 + 2B)\right] - \sin(\lambda_n D_1)\right\}\cos(\lambda_n z)$$

$$P_{8_n} = \left(\frac{vR_d}{D_x} + \frac{D_z}{D_x}\lambda_n^2 + \frac{U^2}{4D_x^2} + \frac{\gamma R_d}{D_x}\right)^{\frac{1}{2}} x \qquad P_{9_n} = \left[\left(v + \frac{D_z}{R_d}\lambda_n^2 + \frac{U^2}{4D_x R_d} + \gamma\right) t\right]^{\frac{1}{2}}$$

$$\lambda_n = \frac{n\pi}{D_1 + 2B + D_2}, \quad n = 1, 2, \ldots$$

The analytical model is based on Example 3-9 of Batu (2006). Parameters are shown in Table 9-2. The domain for the analytical solution is infinite in the x-direction (flow direction), but concentrations will only be calculated up to X = 900 m downstream of the shafts. The model is Z= 2,010 m in the z-direction with $D_1 = D_2 = 1{,}000$ m and 2B = 10 m. The porous medium is 10 m thick and porosity $\phi = 0.25$. The background flux rate is U = 0.15 m/day and the overburden is assumed to be completely water-saturated. Dispersion is anisotropic with longitudinal dispersivity $\alpha_l = 21.3$ m and transverse dispersivity $\alpha_t = 4.3$ m.

Effective molecular diffusion is assumed to be negligible, so that $D^* = 0$ m^2/day, and directional dispersion is $D_x = D^* + U\alpha_l$ and $D_z = D^* + U\alpha_t$ All parameters are shown in Table 9-2.

The analytical solution is also calculated for a tracer with retardation factor greater than one and a decaying rate source. A reference partition coefficient, K_d, value representative of Cs(I) in the overburden at neutral conditions is chosen (see Table 4-15). $K_d = 0.433$ m^3/kg so that $R_d=1+K_d/\phi = 2.732$. The decay rate of the source assigned the value $\gamma = -0.001$ day^{-1}, as in Example 3-9 of Batu (2006).

Table 9-2. Hydraulic, thermal, and mechanical parameters for DECOVALEX Task F salt analytical benchmark. Height and permeability are only needed for simulations.

Parameter	Value
Distance to source, D_1 [m]	1000
Half-width of source, B [m]	5
Width of the model in z-direction, Z [m]	2,010
Length of the model in x-direction, X [m]	9,000
Interstitial velocity [m/day]	0.15
Longitudinal dispersivity, a_l [m]	21.3
Transverse dispersivity, a_t [m]	4.3
Diffusion coefficient, D^* [m^2/day]	0.0
Concentration at source, C_m [kg/m^3]	1.0
Retardation factor for Case 2, R_d [m^3/kg]	2.732
Decay rate for Case 3, g [day^{-1}]	-0.001
Porosity [-]	0.25
Permeability [m^2]	1×10^{-15}
Height [m]	10

9.3.1.2 Solution

The analytical solution is scripted in python3 for comparison with simulated results and will be provided separately. The series solution shown in Eq. 9-4 is challenging to compute numerically. A large number of terms in the infinite series are required for convergence and all analytical solutions shown have n = 500 terms of the series. Furthermore, many of the exponential and error functions contain very large arguments, especially at late time. It is not always possible to use regular python float variables because of overflow, and the 'decimal.getcontext().prec' library is required.

The analytical solution for Case 1 with no retardation or decay in the source after 20 years is shown in Figure 9-2, and is identical to the contours in Figure 3-24 of Batu (2006). The analytical solution for Case 2 at 20 years is in Figure 9-3, and shows that the tracer stays much closer to the source with retardation in the model. Figure 9-4 shows the analytical solution for Case 3 after 10 years and is identical to Figure 3-27 in Batu (2006).

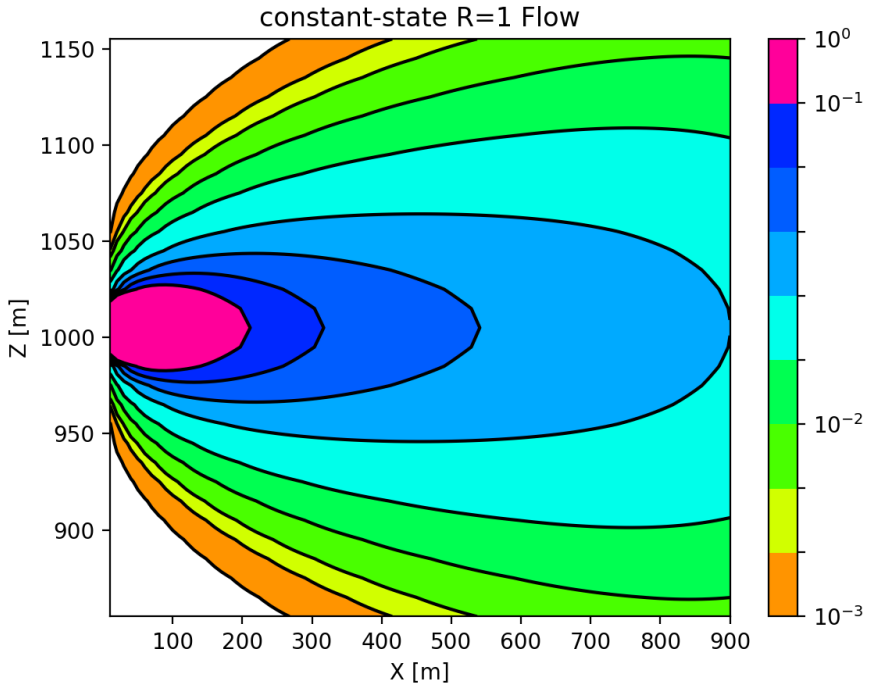

Figure 9-2. Tracer distribution [kg/m^3] for proposed salt analytical benchmark problem with no retardation and constant-rate source after 20 years.

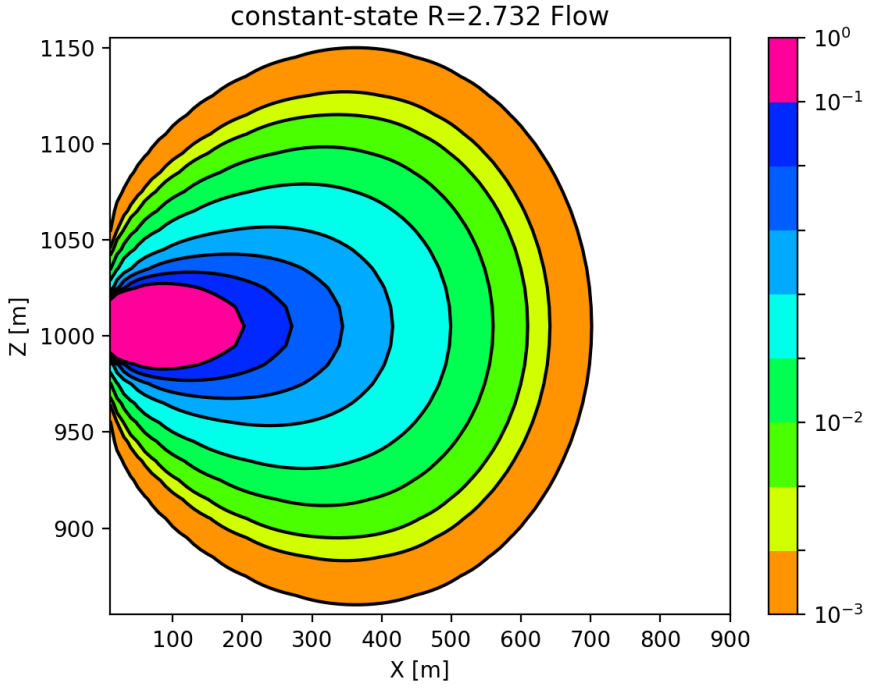

Figure 9-3. Tracer distribution [kg/m^3] for proposed salt analytical benchmark problem with retardation factor R_d = 2.732 m^3/kg, representative of Cs(I) retardation and no decay in the tracer source after 20 years.

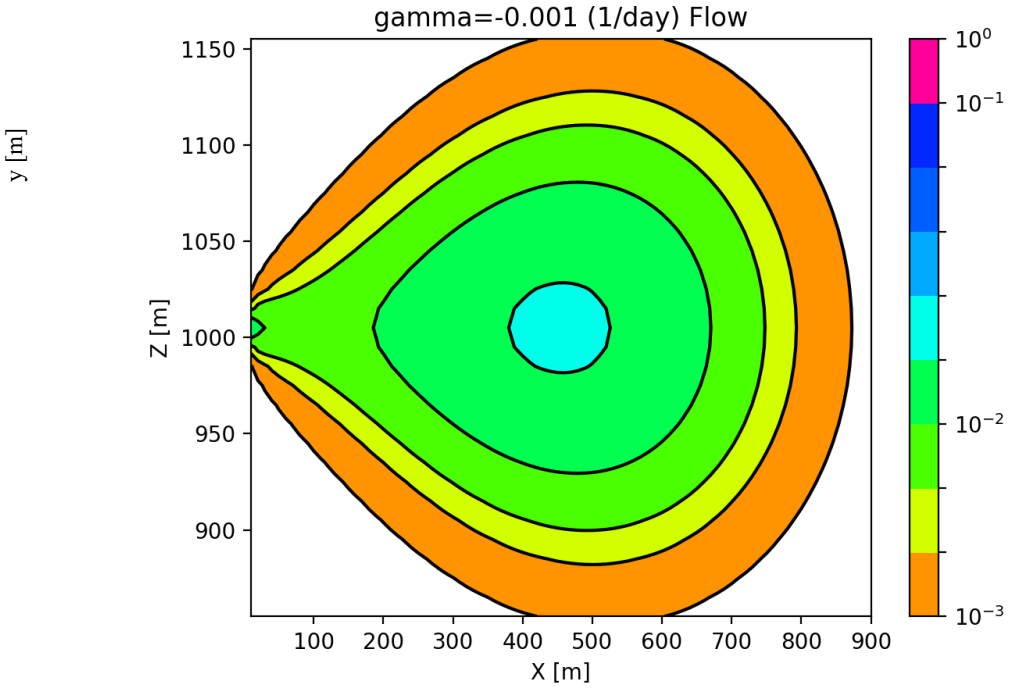

Figure 9-4. Tracer distribution [kg/m^3] for proposed salt analytical benchmark problem without retardation and with time-dependent tracer source γ = -0.001 (1/day) after 10 years.

9.3.1.3 Comparison quantities

In order to allow teams to choose different resolutions for their simulations, comparison of simulated solutions with the analytical model will be done at snapshots in time and discrete points in the domain. The proposed comparison quantities are:

Cross sections at 5 years and 10 years:

- X parallel section at the mid-point of the source in the Z-direction (Z=1005 m)
- X parallel section at Z=1055m
- Z parallel sections at X=100, 200 and 500 m.

Analytical cross sections for each of the three benchmark cases are shown in Figure 9-5 to Figure 9-7.

Profiles at a point as a function of time from 0 to 20 years at the intersection of the cross sections:

- (X,Z) = (100,1005)
- (X,Z) = (200,1005)
- (X,Z) = (100,1055)
- (X,Z) = (200,1055)

Profiles in time for each of the three benchmark cases are shown in Figure 9-8 to Figure 9-10.

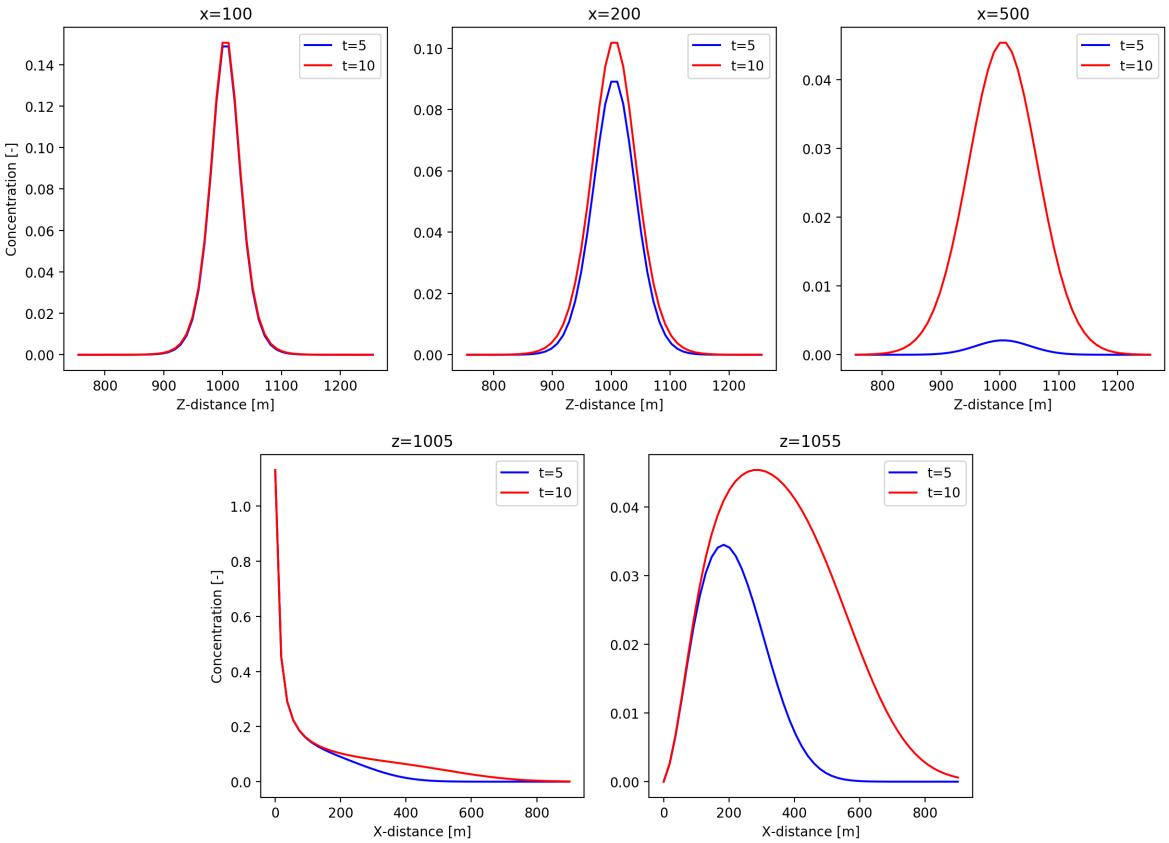

Figure 9-5 Analytical cross-sections for model with R=1 and a constant tracer source at time t=5 years (blue) and t=10 years (red). Top row: Concentration as a function of the z-coordinate on the line x = 100 m (left), x= 200 m (middle), x = 500 m (right). Bottom row: Concentration as a function of the z-coordinate on the line z = 1005 m (left), z = 1055 m (right).

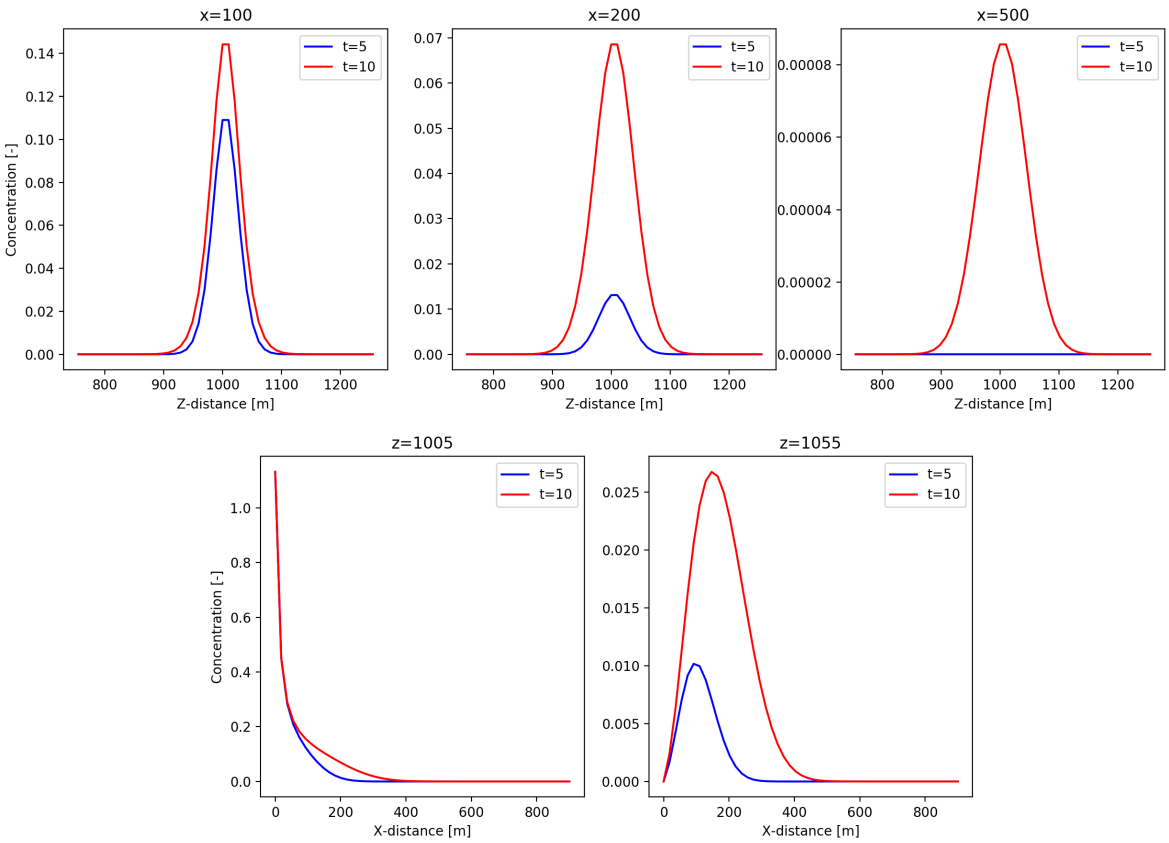

Figure 9-6 Analytical cross-sections for model with R = 2.732 and a constant tracer source at time t=5 years (blue) and t=10 years (red). Top row: Concentration as a function of the z-coordinate on the line x = 100 m (left), x= 200 m (middle), x = 500 m (right). Bottom row: Concentration as a function of the z-coordinate on the line z = 1005 m (left), z = 1055 m (right).

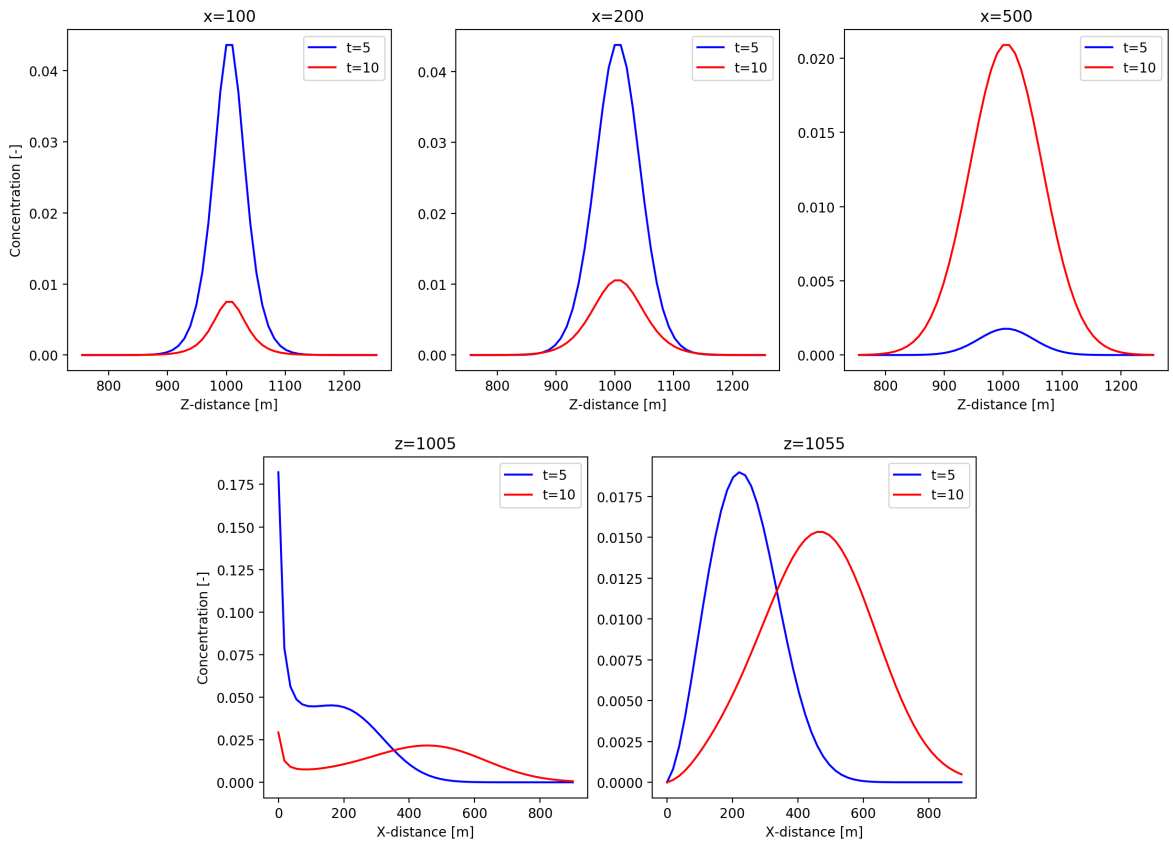

Figure 9-7 Analytical cross-sections for model with R = 1 and decaying tracer source with rate γ = -0.001 (1/yr) at time t=5 years (blue) and t=10 years (red). Top row: Concentration as a function of the z-coordinate on the line x = 100 m (left), x= 200 m (middle), x = 500 m (right). Bottom row: Concentration as a function of the z-coordinate on the line z = 1005 m (left), z = 1055 m (right).

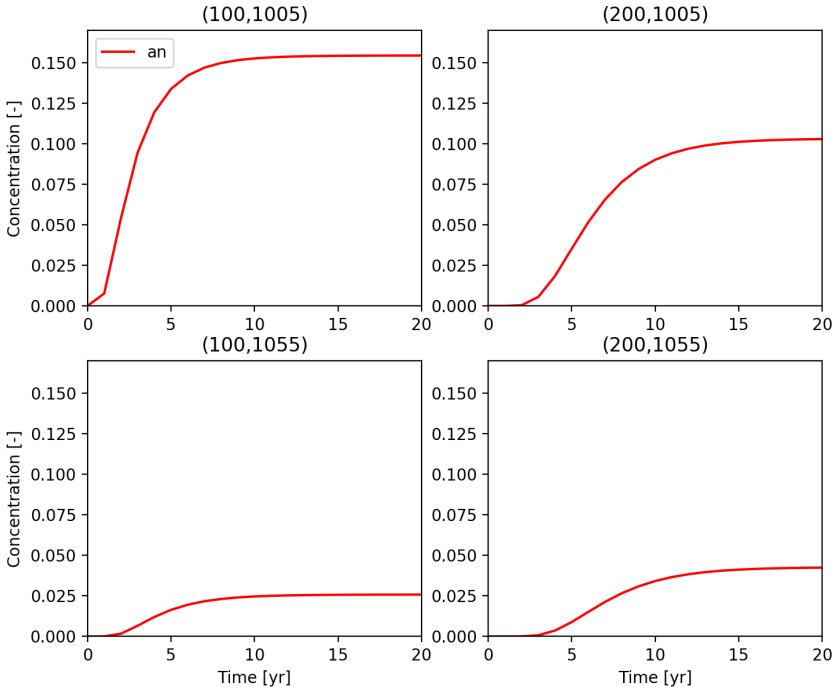

Figure 9-8 Analytical profile for model with R=1 and a constant tracer source as a function of time at four points in the domain. Top left: (100,1005) m. Top right: (200,1005) m. Bottom left: (100,1055) m. Bottom right: (200,1055) m.

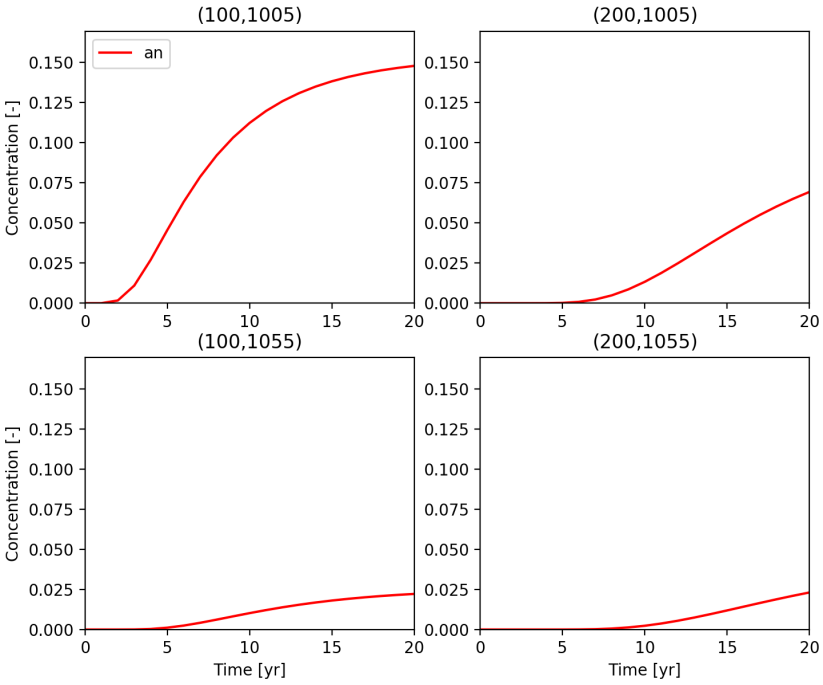

Figure 9-9 Analytical profile for model with R=2.732 and a constant tracer source as a function of time at four points in the domain. Top left: (100,1005) m. Top right: (200,1005) m. Bottom left: (100,1055) m. Bottom right: (200,1055) m.

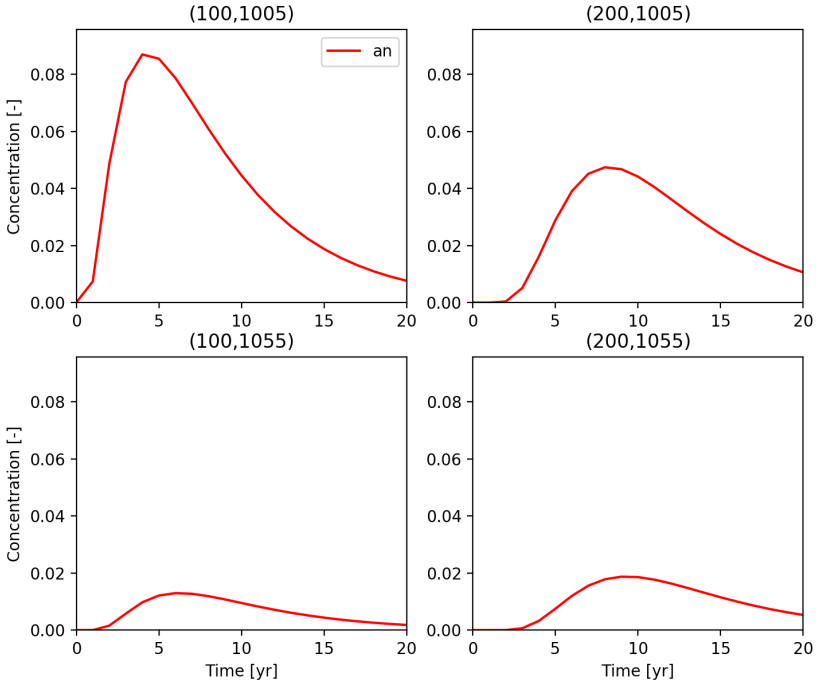

Figure 9-10 Analytical profile for model with R=1 and source decay rate γ=-0.001 (1/yr) as a function of time at four points in the domain. Top left: (100,1005) m. Top right: (200,1005) m. Bottom left: (100,1055) m. Bottom right: (200,1055) m.

9.4 Other Benchmarks

Radionuclide source term benchmarks describing the rate of release of radionuclides from each of the two wasteforms (SNF and vitrified HLW) in the salt reference case will be developed. The SNF source term benchmark may be identical to that used for the crystalline case.

Staged development of the salt reference case is expected to motivate the development of additional benchmarks.

10. Steps 2S – 4S

Steps 2 – 4 of the salt reference case will be described in detail progressively, and will take into account the interests of the participants, the results of the test cases in Step 1, and the experience had by the participating teams when tackling the test cases in Step 1. The high-level schedule presented in Section 2.1 may be modified to incorporate simulation of more than one scenario, if sufficient time and interest exists.

11. Appendix -Input decks

PFLOTRAN input decks for flow and transport test cases are presented here.

```
SIMULATION
  SIMULATION_TYPE SUBSURFACE
  PROCESS_MODELS
    SUBSURFACE_FLOW flow
      MODE RICHARDS
    /
  /
END

SUBSURFACE

#========================== discretization ===================================
GRID
  TYPE structured
  NXYZ 10 1 1
  BOUNDS
    0.d0 0.d0 0.d0
    100d0 1d0 1d0
  END
END

#==========================regions=============================================
REGION all
  COORDINATES
    0.0d0 0.0d0 0.0d0
    100d0 1d0 1d0
  /
END

REGION left_end
  FACE WEST
  COORDINATES
    0.d0 0.d0 0.d0
    0.d0 1d0 1d0
  /
END

REGION right_end
  FACE EAST
  COORDINATES
    100d0 0.d0 0.d0
    100d0 1d0 1d0
  /
END

#========================== material properties ==============================
MATERIAL_PROPERTY beam
```

```
  ID 1
  POROSITY 0.50d0
  TORTUOSITY 1.d0
  ROCK_DENSITY 2.8E3
  CHARACTERISTIC_CURVES cc1
  PERMEABILITY
    PERM_X 1.d-15
    PERM_Y 1.d-15
    PERM_Z 1.d-15
  /
END

#=========================saturation functions===============================
CHARACTERISTIC_CURVES cc1
  SATURATION_FUNCTION VAN_GENUCHTEN
    LIQUID_RESIDUAL_SATURATION 0.5d-1
    M 0.75
    ALPHA 1.d-3
  /
  PERMEABILITY_FUNCTION MUALEM
    LIQUID_RESIDUAL_SATURATION 0.1d0
    M 0.5d0
  /
  PERMEABILITY_FUNCTION MUALEM_VG_GAS
    LIQUID_RESIDUAL_SATURATION 0.1d0
    GAS_RESIDUAL_SATURATION 0.1d0
    M 0.5d0
  /
END

#========================== fluid properties ================================
EOS WATER
 DENSITY CONSTANT 1000.d0 kg/m^3
 VISCOSITY CONSTANT 1.0d-3 Pa-s
END

FLUID_PROPERTY
  DIFFUSION_COEFFICIENT 1.d-9
END

#========================== stratigraphy couplers============================
STRATA
  REGION all
  MATERIAL beam
END

#=========================times=============================================
TIME
  FINAL_TIME 10 day
```

```
  INITIAL_TIMESTEP_SIZE 1.d-4 day
  MAXIMUM_TIMESTEP_SIZE 1.d0 day at 0.d0 day
END

#==========================output options=================================
OUTPUT
  SNAPSHOT_FILE
    NO_PRINT_INITIAL
    FORMAT HDF5
  /
END

#========================== flow conditions ================================
FLOW_CONDITION initial
  TYPE
    PRESSURE dirichlet
  /
  PRESSURE 1.5 MPa
END

FLOW_CONDITION left_end
  TYPE
    PRESSURE dirichlet
  /
  PRESSURE 2 MPa
END

FLOW_CONDITION right_end
  TYPE
    PRESSURE dirichlet
  /
  PRESSURE 1 MPa
END

#========================== condition couplers ============================
INITIAL_CONDITION initial
  REGION all
  FLOW_CONDITION initial
END

BOUNDARY_CONDITION left_end
  REGION left_end
  FLOW_CONDITION left_end
END

BOUNDARY_CONDITION right_end
  FLOW_CONDITION right_end
  REGION right_end
END
```

```
END_SUBSURFACE
```

Figure 11-1. PFLOTRAN input deck for simulation of 1-D steady flow with boundary conditions of the first kind.

```
SIMULATION
  SIMULATION_TYPE SUBSURFACE
  PROCESS_MODELS
    SUBSURFACE_FLOW flow
      MODE RICHARDS
    /
  /
END

SUBSURFACE

#=========================== discretization ===================================
GRID
  TYPE structured
  NXYZ 20 20 1
  BOUNDS
    0.d0 0.d0 0.d0
    1d0 1d0 1d0
  END
END

#==========================regions=============================================
REGION all
  COORDINATES
    0.0d0 0.0d0 0.0d0
    1d0 1d0 1d0
  /
END

REGION west_face
  FACE WEST
  COORDINATES
    0.d0 0.d0 0.d0
    0.d0 1d0 1d0
  /
END

REGION east_face
  FACE EAST
  COORDINATES
    1d0 0.d0 0.d0
    1d0 1d0 1d0
  /
END
```

```
REGION north_face
  FACE NORTH
  COORDINATES
    0.d0 1d0 0.d0
    1d0 1d0 1d0
  /
END

REGION south_face
  FACE SOUTH
  COORDINATES
    0.d0  0.d0  0.d0
    1d0 0.d0 1d0
  /
END


#========================== material properties ==============================
MATERIAL_PROPERTY plate
  ID 1
  POROSITY 0.5
  TORTUOSITY 1.d0
  ROCK_DENSITY 2.8E3
  CHARACTERISTIC_CURVES cc1
  PERMEABILITY
    PERM_X 1.d-15
    PERM_Y 1.d-15
    PERM_Z 1.d-15
  /
END


#==========================saturation functions==============================
CHARACTERISTIC_CURVES cc1
  SATURATION_FUNCTION VAN_GENUCHTEN
    LIQUID_RESIDUAL_SATURATION 0.5d-1
    M 0.75
    ALPHA 1.d-3
  /
  PERMEABILITY_FUNCTION MUALEM
    LIQUID_RESIDUAL_SATURATION 0.1d0
    M 0.5d0
  /
  PERMEABILITY_FUNCTION MUALEM_VG_GAS
    LIQUID_RESIDUAL_SATURATION 0.1d0
    GAS_RESIDUAL_SATURATION 0.1d0
    M 0.5d0
  /
END
```

```
#========================== stratigraphy couplers=============================
STRATA
  REGION all
  MATERIAL plate
END

#========================== fluid properties =================================
FLUID_PROPERTY
  DIFFUSION_COEFFICIENT 1.d-9
END

EOS WATER
 DENSITY CONSTANT 1000.d0 kg/m^3
 VISCOSITY CONSTANT 1.0d-3 Pa-s
END

#==========================times=========================================
TIME
  FINAL_TIME 1 yr
  INITIAL_TIMESTEP_SIZE 1.d-4 day
  MAXIMUM_TIMESTEP_SIZE 0.1 yr at 0.d0 yr
END

#==========================output options=================================
OUTPUT
  SNAPSHOT_FILE
    NO_PRINT_INITIAL
    #NO_PRINT_FINAL
    FORMAT HDF5
  /
END

#==========================datasets=======================================
DATASET pressure_bc_x
  HDF5_DATASET_NAME x_line_node_centered
  FILENAME dataset.h5
END

DATASET pressure_bc_y
  HDF5_DATASET_NAME y_line_node_centered
  FILENAME dataset.h5
END

#========================== flow conditions ==============================
FLOW_CONDITION initial
  TYPE
    PRESSURE dirichlet
  /
  PRESSURE 1.d0 MPa
```

```
END

FLOW_CONDITION west_face
  TYPE
    PRESSURE dirichlet
  /
  PRESSURE 1.d0 MPa
END

FLOW_CONDITION east_face
  TYPE
    PRESSURE dirichlet
  /
  PRESSURE DATASET pressure_bc_y
END

FLOW_CONDITION north_face
  TYPE
    PRESSURE dirichlet
  /
  PRESSURE DATASET pressure_bc_x
END

FLOW_CONDITION south_face
  TYPE
    PRESSURE dirichlet
  /
  PRESSURE 1.d0 MPa
END


#========================== condition couplers ==================================
INITIAL_CONDITION initial
  REGION all
  FLOW_CONDITION initial
END

BOUNDARY_CONDITION west_face
  REGION west_face
  FLOW_CONDITION west_face
END

BOUNDARY_CONDITION south_face
  REGION south_face
  FLOW_CONDITION south_face
END

BOUNDARY_CONDITION east_face
  FLOW_CONDITION east_face
  REGION east_face
END
```

```
BOUNDARY_CONDITION north_face
  FLOW_CONDITION north_face
  REGION north_face
END

END_SUBSURFACE
```

Figure 11-2. PFLOTRAN input deck for simulation of 2-D steady flow with boundary conditions of the first kind.

```
SIMULATION
  SIMULATION_TYPE SUBSURFACE
  PROCESS_MODELS
    SUBSURFACE_FLOW flow
      MODE RICHARDS
    /
  /
END

SUBSURFACE

#========================== discretization ===================================
GRID
  TYPE structured
  NXYZ 10 10 10
  DXYZ
   0.1d0
   0.1d0
   0.1d0
  END
END

#==========================regions=============================================
REGION all
  COORDINATES
    0.0d0 0.0d0 0.0d0
    1d0 1d0 1d0
  /
END

REGION west_face
  FACE WEST
  COORDINATES
    0.d0 0.d0 0.d0
    0.d0 1d0 1d0
  /
END

REGION east_face
```

```
  FACE EAST
  COORDINATES
    1d0 0.d0 0.d0
    1d0 1d0 1d0
  /
END

REGION north_face
  FACE NORTH
  COORDINATES
    0.d0 1d0 0.d0
    1d0 1d0 1d0
  /
END

REGION south_face
  FACE SOUTH
  COORDINATES
    0.d0 0.d0 0.d0
    1d0 0.d0 1d0
  /
END

REGION bottom_face
  FACE BOTTOM
  COORDINATES
    0.d0 0.d0 0.d0
    1d0 1d0 0.d0
  /
END

REGION top_face
  FACE TOP
  COORDINATES
    0.d0 0.d0 1d0
    1d0 1d0 1d0
  /
END


#========================== material properties ============================
MATERIAL_PROPERTY cube
  ID 1
  POROSITY 0.5
  TORTUOSITY 1.d0
  ROCK_DENSITY 2.8E3
  CHARACTERISTIC_CURVES cc1
  PERMEABILITY
    PERM_X 1.d-10
    PERM_Y 1.d-10
    PERM_Z 1.d-10
```

```
  /
END

#==========================saturation functions===============================
CHARACTERISTIC_CURVES cc1
  SATURATION_FUNCTION VAN_GENUCHTEN
    LIQUID_RESIDUAL_SATURATION 0.5d-1
    M 0.75
    ALPHA 1.d-3
  /
  PERMEABILITY_FUNCTION MUALEM
    LIQUID_RESIDUAL_SATURATION 0.05d0
    M 0.5d0
  /
  PERMEABILITY_FUNCTION MUALEM_VG_GAS
    LIQUID_RESIDUAL_SATURATION 0.05d0
    GAS_RESIDUAL_SATURATION 0.1d0
    M 0.5d0
  /
END

#========================== stratigraphy couplers=============================
STRATA
  REGION all
  MATERIAL cube
END

#========================== fluid properties ================================
FLUID_PROPERTY
  DIFFUSION_COEFFICIENT 1.d-9
END

EOS WATER
 DENSITY CONSTANT 1000.d0 kg/m^3
 VISCOSITY CONSTANT 1.0d-3 Pa-s
END

#==========================times=============================================
TIME
  FINAL_TIME 1 yr
  INITIAL_TIMESTEP_SIZE 1.d-4 day
  MAXIMUM_TIMESTEP_SIZE 0.10 yr at 0.d0 yr
END

#==========================output options====================================
OUTPUT
  SNAPSHOT_FILE
    NO_PRINT_INITIAL
```

```
    FORMAT HDF5
  /
END

#==========================datasets=======================================
DATASET pressure_bc_west
  HDF5_DATASET_NAME node_centered_surf_west
  FILENAME kolditz_225_dataset.h5
END

DATASET pressure_bc_east
  HDF5_DATASET_NAME node_centered_surf_east
  FILENAME kolditz_225_dataset.h5
END

DATASET pressure_bc_north
  HDF5_DATASET_NAME node_centered_surf_north
  FILENAME kolditz_225_dataset.h5
END

DATASET pressure_bc_south
  HDF5_DATASET_NAME node_centered_surf_south
  FILENAME kolditz_225_dataset.h5
END

DATASET pressure_bc_bottom
  HDF5_DATASET_NAME node_centered_surf_bottom
  FILENAME kolditz_225_dataset.h5
END

DATASET pressure_bc_top
  HDF5_DATASET_NAME node_centered_surf_top
  FILENAME kolditz_225_dataset.h5
END

#========================== flow conditions ================================
FLOW_CONDITION initial
  TYPE
    PRESSURE dirichlet
  /
  PRESSURE 1.0 MPa
END

FLOW_CONDITION west_face
  TYPE
    PRESSURE dirichlet
  /
  PRESSURE DATASET pressure_bc_west
END
```

```
FLOW_CONDITION east_face
  TYPE
    PRESSURE dirichlet
  /
  PRESSURE DATASET pressure_bc_east
END

FLOW_CONDITION north_face
  TYPE
    PRESSURE dirichlet
  /
  PRESSURE DATASET pressure_bc_north
END

FLOW_CONDITION south_face
  TYPE
    PRESSURE dirichlet
  /
  PRESSURE DATASET pressure_bc_south
END

FLOW_CONDITION bottom_face
  TYPE
    PRESSURE dirichlet
  /
  PRESSURE DATASET pressure_bc_bottom
END

FLOW_CONDITION top_face
  TYPE
    PRESSURE dirichlet
  /
  PRESSURE DATASET pressure_bc_top
END


#========================== condition couplers ==================================
INITIAL_CONDITION initial
  REGION all
  FLOW_CONDITION initial
END

BOUNDARY_CONDITION west_face
  REGION west_face
  FLOW_CONDITION west_face
END

BOUNDARY_CONDITION east_face
  FLOW_CONDITION east_face
  REGION east_face
END
```

```
BOUNDARY_CONDITION north_face
  REGION north_face
  FLOW_CONDITION north_face
END

BOUNDARY_CONDITION south_face
  FLOW_CONDITION south_face
  REGION south_face
END

BOUNDARY_CONDITION bottom_face
  REGION bottom_face
  FLOW_CONDITION bottom_face
END

BOUNDARY_CONDITION top_face
  FLOW_CONDITION top_face
  REGION top_face
END

END_SUBSURFACE
```

Figure 11-3. PFLOTRAN input deck for simulation of 3-D steady flow with boundary conditions of the first kind.

```
SIMULATION
  SIMULATION_TYPE SUBSURFACE
  PROCESS_MODELS
    SUBSURFACE_TRANSPORT transport
      MODE GIRT
    /
  /
END

SUBSURFACE

#=========================== specific discharge =================================
SPECIFIED_VELOCITY #Darcy flux / specific discharge (vol/area/time)
  UNIFORM? YES
  DATASET 1.d-4 0.d0 0.d0 m/s
END

#==========================chemistry=============================================
CHEMISTRY
  PRIMARY_SPECIES
    Tracer1
    Tracer2
    Tracer3
  /
  RADIOACTIVE_DECAY_REACTION
```

```
    REACTION Tracer2 <->
    RATE_CONSTANT 5.0d-5 # 1/s, half life = 3.85 hrs
  /
  SORPTION
    ISOTHERM_REACTIONS
      Tracer3
        DISTRIBUTION_COEFFICIENT 816.d0 #6.8e-4 m^3/kg
        # Kd(kgH2O/m^3bulk) = Kd(m^3H2O/kgsoil)*H2Odensity*(1-porosity)*soildensity
      /
    /
  /
  DATABASE hanford.dat
  LOG_FORMULATION
  OUTPUT
    TOTAL
    ALL
  /
END

#========================== solver options===================================
NUMERICAL_METHODS TRANSPORT
  LINEAR_SOLVER
    SOLVER DIRECT
  /

  TIMESTEPPER
    TS_ACCELERATION 13
  /
END
#========================== discretization ==================================
GRID
  TYPE structured
  NXYZ 200 1 1
  BOUNDS
    0.d0 0.d0 0.d0
    10.d0 1.d0 1.d0
  /
END

#=========================times=============================================
TIME
  FINAL_TIME 20000. s
  INITIAL_TIMESTEP_SIZE 60. s
  MAXIMUM_TIMESTEP_SIZE 120. s
END

#========================== output options==================================
OUTPUT
  SNAPSHOT_FILE
    TIMES s 10000. 15000. 20000.
    FORMAT HDF5
```

```
  /
END

#========================== fluid properties ================================
FLUID_PROPERTY
  DIFFUSION_COEFFICIENT 1.0d-4 #m^2/s includes dispersion
END

#========================== material properties =============================
MATERIAL_PROPERTY soil1
  ID 1
  POROSITY 0.4d0
  TORTUOSITY 1.d0
  ROCK_DENSITY 2000. #kg/m^3
END

#==========================regions=============================================
REGION all
  COORDINATES
    -1.d20 -1.d20 -1.d20
     1.d20  1.d20  1.d20
  /
END

REGION west
  FACE WEST
  COORDINATES
    0.d0 0.d0 0.d0
    0.d0 1.d0 1.d0
  /
END

REGION east
  FACE EAST
  COORDINATES
    10.d0 0.d0 0.d0
    10.d0 1.d0 1.d0
  /
END

#========================== transport conditions ============================
TRANSPORT_CONDITION initial
  TYPE DIRICHLET_ZERO_GRADIENT
  CONSTRAINT_LIST
    0.d0 initial
  /
END

TRANSPORT_CONDITION west
  TYPE DIRICHLET
  CONSTRAINT_LIST
```

```
    0.d0 inlet
   1.5d4 initial #at 15000 s
  /
END

#========================== constraints ===================================
CONSTRAINT inlet
  CONCENTRATIONS
    Tracer1 1.d0      T
    Tracer2 1.d0      T
    Tracer3 1.d0      T
  /
END

CONSTRAINT initial
  CONCENTRATIONS
    Tracer1 1.d-20     T
    Tracer2 1.d-20     T
    Tracer3 1.d-20     T
  /
END

#========================== condition couplers ==============================
INITIAL_CONDITION initial
  REGION all
  TRANSPORT_CONDITION initial
END

BOUNDARY_CONDITION west
  REGION west
  TRANSPORT_CONDITION west
END

BOUNDARY_CONDITION east
  REGION east
  TRANSPORT_CONDITION initial
END
#========================== stratigraphy couplers ===========================
STRATA
  REGION all
  MATERIAL soil1
END

END_SUBSURFACE
```

Figure 11-4. PFLOTRAN input deck for simulation of transient advection and dispersion.

12. References

Adeniyi, A., Howard, R., Banerjee, K., Bhatt, S. 2020. *GDSA Waste Package Reference Physical and Thermal Characteristics*. M3SF-20OR010304072, Oak Ridge National Laboratory, Oak Ridge, TN.

Baeyens, B., T. Thoenen, M. H. Bradbury and M. Marques Fernandes 2014. *Sorption Data Bases for Argillaceous Rocks and Bentonite for the Provisional Safety Analyses for SGT-E2*. NAGRA Technical Report. National Cooperative for the Disposal of Radioactive Waste (NAGRA), Wettingen, Switzerland.

Batu, V. 2006. *Applied Flow and Solute Transport Modelling in Aquifers*. CRC Taylor and Francis.

Bear, J. 1972. *Dynamics of Fluids in Porous Media*, American Elsevier Publishing, Inc., New York, NY.

Bear J. 1993. *Flow and Contaminent Transport in Fractured Rocks,* Academic Press: 1-37.

Bertrams, N., Bollingerfehr, W., Eickemeier, R., Fahland, S. Flügge, J., Frenzel, B., Hammer, J., Kindlein, J. Liu, W., Maßmann, J., Mayer, K.-M., Mönig, J., Mrugalla, S., Müller-Hoeppe, N., Reinhold, K., Rübel, A., Schubarth-Engel- schall, N., Simo, E., Thiedau, J., Thiemeyer, T., Weber, J.R., Wolf, J. 2020. *Grundlagen zur Bewertung eines Endlagersystems in flach lagernden Salzformationen (S1) - Ergebnisse aus dem Vorhaben RESUS*. BGE TEC 2020.

Beuth, T., Bracke, G., Buhmann, D., Dresbach, C., Keller, S., Krone, J., Lommerzheim, A., Mönig, A., Mrugalla, S., Rübel, A., and Wolf, J. 2012. *Szenarienentwicklunng: Methodic und Anwendung. Bericht zum Arbeitspaket 8. Vorläufige Sicherheitsanalyse für den Standort Gorleben*, Gesellschaft für Anlagen und Reaktorsicherheit (GRS) mbH, GRS-284, Köln, ISBN 978-3-939355-60-1.

Blanco-Martin, L., J. Rutqvist, A. Battistelli, and J.T. Birkholzer 2018. Coupled processes modeling in rock salt and crushed salt including halite solubility constraints: Application to disposal of heat-generating nuclear waste. Transport in Porous Media 124: 159-182.

Bollingerfehr, W., Filbert, W., Pöhler, M., Tholen, M., and Wehrmann, J. 2008. *Konzeptionelle Endlagerplanung und Zusammen- stellung des endzulagernden Inventars (Design planning of a final repository and summary of the inventory to be stored) – Project ISIBEL*, Peine, April 2008.

Bollingerfehr, W., Bertrams, N., Buhmann, D., Eickemeier, R., Fahland, S., Filbert, W., Hammer, J., Kindlein, J., Knauth, M., and Wenting, L., 2018. *Concept developments for a generic repository for heat-generating waste in bedded salt formations in Germany*. Synthesis Report (No. BGE TEC 2018-13). BGE TECHNOLOGY GmbH.

Bollingerfehr, W., Buhmann, D. and Doerr, S., 2017. *Evaluation of methods and tools to develop safety concepts and to demonstrate safety for an HLW repository in salt*. Final Report (No. TEC-03-2017-AB). DBE Technology GmbH.

Bundesministerium für Umwelt (BMU), 2010. *Naturschutz und Reaktorsicherheit: Sicherheitsanforderungen an die Endlagerun wärmeentwickelnder radioaktiver Abfälle. Bundesministerium für Umwelt*, Naturschutz und Reaktorsicherheit. Stand: 30, September 2010.

Börgesson, L., T. Sandén, L.-E. Johannesson, J. Autio, X. Pintado, and P. Smith 2017. *KBS-3H Summary*. SKB P-16-18. Svensk Kärnbränslehantering AB, Stockholm, Sweden.

Bräuer, S. and Urquhart, A., 2016. Thermal and physical properties of reconsolidated crushed rock salt as a function of porosity and temperature. *Acta Geotechnica*, *11*(4), pp.913-924.

Carter, J., A. J. Luptak, J. Gastelum, C. T. Stockman, and A. Miller 2013. *Fuel Cycle Potential Waste Inventory for Disposition*. FCR&D-USED-2010-000031 Rev 6. Savannah River National Laboratory, Aiken, SC.

Chang, C.-C., H.-T. Chang and S. Yu-Hsiang, *Specifications of the draft Taiwan's repository facility*. Presented to the Task F crystalline group, August 24, 2021.

Choi, H. J., J. Y. Lee, and J. Choi 2013. "DEVELOPMENT OF GEOLOGICAL DISPOSAL SYSTEMS FOR SPENT FUELS AND HIGH-LEVEL RADIOACTIVE WASTES IN KOREA". *Nuclear Engineering and Technology, 45*(1), 29-40. doi: 10.5516/net.06.2012.006

Clayton, D., G. Freeze, T. Hadgu, E. Hardin, J. Lee, J. Prouty, R. Rogers, W. M. Nutt, J. Birkholzer, H. H. Liu, L. Zheng, and S. Chu 2011. *Generic Disposal System Modeling - Fiscal Year 2011 Progress Report*. SAND 2011-5828P; FCRD-USED-2011-000184. Sandia National Laboratories, Albuquerque, NM.

Croff, A.G. 1983. "ORIGEN2: A Versatile Computer Code for Calculating the Nuclide Compositions and Characteristics of Nuclear Materials," *Nuclear Technology*, 62(3), 335-352. doi: dx.doi.org/10.13182/NT83-1.

Ecay, L., Grégoire, D., and Pijaudier-Cabot G. 2020. On the prediction of permeability and relative permeability from pore size distributions. *Cement and Concrete Research*, 133: 106074.

Follin, S., L. Hartley, P. Jackson, D. Roberts, N. Marsic, and K. Konsult 2008. *Hydrogeological conceptual model development and numerical modelling using CONNECTFLOW, Forsmark modelling stage 2.3*. SKB R-08-23. Svensk Kärnbränslehantering AB, Stockholm, Sweden.

Follin, S., L. Hartley, P. Jackson, S. Joyce, D. Roberts, and B. Swift 2007. *Hydrogeological characterization and modeling of deformation zones and fracture domains, Forsmark modelling stage 2.2*. SKB R-07-48. Svensk Kärnbränslehantering AB, Stockholm, Sweden.

Frederick, J. M. 2018a. PFLOTRAN QA Test Suite. Retrieved April 25, 2020, from qa.pflotran.org

Frederick, J. M. 2018b. *PFLOTRAN-RepoTREND Source Term Comparison Summary*. SAND2018-2427. Sandia National Laboratories, Albuquerque, NM.

Freeze, R. A. and J. A. Cherry, 1979. *Groundwater*, Prentice-Hall, Englewood Cliffs, NJ.

Freeze, G., M. Voegele, P. Vaughn, J. Prouty, W.M. Nutt, E. Hardin, and S.D. Sevougian 2013a. Generic Deep Geologic Disposal Safety Case. FCRD-UFD-2012-000146 Rev. 1, SAND2013-0974P. Sandia National Laboratories, Albuquerque, NM.

GRS, 2012. Radionuclide Inventory of Vitrified Waste after Spent Nuclear Fuel Reprocessing at La Hague. Gesellschaft für Anlagen- und Reaktorischerhet, Germany. GRS-294.

Hartley, L., P. Appleyard, S. Baxter, J. Hoek, D. Roberts, and D. Swan 2013. *Development of a Hydrogeological Discrete Fracture Network Model for the Olkiluoto Site Descriptive Model 2011*. Working Report 2012-32. Posiva Oy, Eurajaki, Finland.

Hartley, L., J. Hoek, D. Swan, P. Appleyard, S. Baxter, D. Roberts, and T. Simpson 2013. *Hydrogeological Modelling for Assessment of Radionuclide Release Scenarios for the Repository System 2012*. Working Report 2012-42. Posiva Oy,

Hartley, L., P. Appleyard, S. Baxter, J. Hoek, S. Joyce, K. Mosley, T. Williams, A. Fox, M. Cottrell, P. La Pointe, S. Gehör, C. Darcel, R. Le Goc, I. Aaltonen, O. Vanhanarkaus, J. Löfman, and A. Poteri 2018. *Discrete Fracture Network Modelling (Version 3) in Support of Olkiluoto Site Description 2018*. Working Report 2017-32. Posiva Oy, Eurajoki, Finland.

Hartley, L., S. Baxter, and T. Williams 2016. *Geomechanical Coupled Flow in Fractures during Temperate and Glacial Conditions*. Working Report 2016-08. Posiva Oy, Eurajoki, Finland.

Hyman, J. D., S. Karra, N. Makedonska, C. W. Gable, S. L. Painter, and H. S. Viswanathan 2015. "DFNWORKS: A discrete fracture network framework for modeling subsurface flow and transport". *Computers & Geosciences*, 84, 10-19. doi: 10.1016/j.cageo.2015.08.001

Johnson, L. R., C. Ferry, C. Poinssot and P. Lovera 2005. Spent fuel radionuclide source term model for assessing spent fuel performance in geological disposal. Part I: Assessment of the Instant Release Fraction. Journal of Nuclear Materials 346: 66-77.

Joyce, S., L. Hartley, D. Applegate, J. Hoek, and P. Jackson 2014. "Multi-scale groundwater flow modeling during temperate climate conditions for the safety assessment of the proposed high-

level nuclear waste repository site at Forsmark, Sweden". *Hydrogeology Journal, 22*(6), 1233-1249. doi: 10.1007/s10040-014-1165-6

Joyce, S., T. Simpson, L. Hartley, D. Applegate, J. Hoek, P. Jackson, D. Swan, N. Marsic, and S. Follin 2010. *Groundwater flow modelling of periods with temperate climate conditions - Forsmark*. SKB R-09-20. Svensk Kärnbränslehantering AB, Stockholm, Sweden.

Kärnbränslehantering, S. 2011. *Long-term safety for the final repository for spent nuclear fuel at Forsmark. Main report of the SR-Site project.* No. SKB-TR—11-01 (V.2). Swedish Nuclear Fuel and Waste Management Co.

Kienzler, B., M. Altmaier, C. Bube and V. Metz 2012. *Radionuclide Source Term for HLW Glass, Spent Nuclear Fuel, and Compacted Hulls and End Pieces (CSD-C Waste)*. KIT Scientific Reports 7624. Karlsruhe Institute of Technology, Baden-Württemberg, Germany.

Kolditz, O., H. Shao, W. Wang, and S. Bauer 2015. *Thermo-Hydro-Mechanical-Chemical Processes in Fractured Porous Media: Modelling and Benchmarking Closed-Form Solutions* (O. Kolditz, H. Shao, W. Wang, & S. Bauer Eds.). Switzerland: Springer International Publishing.

LaForce, T., Chang, K.W., Perry, F.V., Lowry, T.S., Basurto, E., Jayne, R., Brooks, D., Jordan, S., Stein, E., Leone, R., and Nole, M., 2020. *GDSA Repository Systems Analysis Investigations in FY2020*. M2SF-20SN010304052, SAND2020-12028 R. Sandia National Laboratories, Albuquerque, NM.

Mariner, P. E., W. P. Gardner, G. Hammond, S. D. Sevougian, and E. R. Stein 2015. *Application of Generic Disposal System Models*. FCRD-UFD-2015-000126; SAND2015-10037R. Sandia National Laboratories, Albuquerque, NM.

Mariner, P. E., E. R. Stein, J. M. Frederick, S. D. Sevougian, G. E. Hammond, and D. G. Fascitelli 2016. *Advances in Geologic Disposal System Modeling and Application to Crystalline Rock*. FCRD-UFD-2016-000440 / SAND2016-9610R. Sandia National Laboratories, Albuquerque, NM.

Mariner, P. E., E. R. Stein, J. M. Frederick, S. D. Sevougian, and G. E. Hammond 2017. *Advances in Geologic Disposal System Modeling and Shale Reference Cases*. SFWD-SFWST-2017-000044 / SAND2017-10304R. Sandia National Laboratories, Albuquerque, NM.

Martín, L.B., Rutqvist, J., and Birkholzer, J.T. 2015. Long-term modeling of the thermal-hydraulic-mechanical response of a generic salt repository for heat-generating nuclear waste. Engineering Geology, 193: 198–211.

NWMO 2012. *Used Fuel Repository Conceptual Design and Postclosure Safety Assessment in Crystalline Rock*. NWMO TR-2012-16. Nuclear Waste Management Organization, Toronto, Ontario.

OCRWM 1990. *Performance Assessment Strategy Plan for the Geologic Repository Program*. DOE-RW-0266P. U.S. Department of Energy, Office of Civilian Radioactive Waste Management, Washington, DC.

Ollila, K. 2008. *Dissolution of unirradiated UO2 and UO2 doped with 233U in low- and high-ionic strength NaCl under anoxic and reducing conditions*. Working Report 2008-50. Posiva Oy, Eurajoki, Finland.

Osselin, F., Fabbri, A., Fen-Chong, T., Pereira, J., Lassin, A., and Dangla, P. 2015. Experimental Investigation of the Influence of Supercritical State on the Relative Permeability of Vosges Sandstone. *Comptes Rendus Mécanique*, 343: 495-502.

Pettersson, S. and B. Lönnerberg 2008, 16-18 June 2008. *Final Repository for Spent Nuclear Fuel in Granite - The KBS-3V Concept in Sweden and Finland.* Paper presented at the International Conference Underground Disposal Unit Design & Emplacement Processes for a Deep Geological Repository, Prague.

Prij, J., van Dalen, A., Englund-Borowiec, G., Glasbergen, P., de Haas, J.B.M., Jong, C.T.J., de Jong, E.J., Köster, H.W., Nijhoff-Pan, I., Roodbergen, H.A., Slagter, W., van Weers, A.W., and

Znastra, D.A., 1989. *Safety Evaluation of Disposal Concepts in Rock Salt*. Final Report (IL 369; OPLA 89-08)

Prij, J., Blok, B.M., Laheij, G.M.H., van Rheenen, W., Slagter, W., Uffink, G.J.M., Uijt de Haag, P., Wildenborg, A.F.B., and Zanstra, D.A., 1993. *PRObablistic Safety Assessment*. Final Report (OPLA-1A)

Poley, A.D., 1999. Concept ontwerp terughaalbare opslag van radioactief afval in diepe boorgaten in steenzout (Torad-B) 1–54.

Rübel, A., Buhmann, D., Kindlein, J. and Lauke, T., 2016. *Performance assessment of sealing systems. Conceptual and integrated modelling of plugs and seals* (No. GRS-415). Gesellschaft fuer Anlagen-und Reaktorsicherheit (GRS) gGmbH.

Sassani, D., C. F. Jove Colon, P. Weck, J. L. Jerden, K. E. Frey, T. Cruse, W. L. Ebert, E. C. Buck, and R. S. Wittman 2013. *Used Fuel Degradation: Experimental and Modeling Report*. SAND2013-9077P. Sandia National Laboratories, Albuquerque, NM.

Sevougian, S. D., E. R. Stein, M. B. Gross, G. E. Hammond, J. M. Frederick, and P. E. Mariner 2016. *Status of Progress Made Toward Safety Analysis and Technical Site Evaluations for DOE Managed HLW and SNF.* SAND2016-11232R. Sandia National Laboratories, Albuquerque, NM.

SKB (Svensk Kärnbränslehantering AB) 2010a. *Design, production and initial state of the canister*. SKB TR-10-14. Svensk Kärnbränslehantering AB, Stockholm, Sweden.

SKB (Svensk Kärnbränslehantering AB) 2010b. *Design, production and initial state of the buffer*. SKB TR-10-15. Svensk Kärnbränslehantering AB, Stockholm, Sweden.

SKB (Svensk Kärnbränslehantering AB) 2010c. *Design, production and initial state of the backfill and plug in deposition tunnels*. SKB TR-10-16. Svensk Kärnbränslehantering AB, Stockholm, Sweden.

SKB (Svensk Kärnbränslehantering AB) 2010d. *THM modelling of buffer, backfill and other system components*. SKB TR-10-44. Svensk Kärnbränslehantering AB, Stockholm, Sweden.

SKB (Svensk Kärnbränslehantering AB) 2010e. *Radionuclide transport report for the safety assessment SR-Site*. SKB TR-10-50. Svensk Kärnbränslehantering AB, Stockholm, Sweden.

SKB (Svensk Kärnbränslehantering AB) 2010e. *Data report for the safety assessment SR-Site*. SKB TR-10-52. Svensk Kärnbränslehantering AB, Stockholm, Sweden.

SKB (Svensk Kärnbränslehantering AB) 2011. *Long-term safety for the final repository for spent nuclear fuel at Forsmark*. SKB TR-11-01. Svensk Kärnbränslehantering AB, Stockholm, Sweden.

Stein, E. R., J. M. Frederick, G. E. Hammond, K. L. Kuhlmann, P. E. Mariner, and S. D. Sevougian 2017, April 9-13, 2017. *Modeling Coupled Reactive Flow Processes in Fractured Crystalline Rock*. Paper presented at the International High-Level Radioactive Waste Management Conference, Charlotte, NC.

Strachan, D. 2004. *Defense HLW Glass Degradation Model*. ANL-EBS-MD-000016 REV 02. Sandia National Laboratories, Albuquerque, New Mexico.

Sudicky, E. A. and E. O. Frind 1982. "CONTAMINANT TRANSPORT IN FRACTURED POROUS-MEDIA - ANALYTICAL SOLUTIONS FOR A SYSTEM OF PARALLEL FRACTURES". *Water Resources Research*, 18(6), 1634-1642. doi: 10.1029/WR018i006p01634

Sudicky, E. A. and E. O. Frind 1984. "CONTAMINANT TRANSPORT IN FRACTURED POROUS-MEDIA - ANALYTICAL SOLUTIONS FOR A SYSTEM OF PARALLEL FRACTURES - REPLY". *Water Resources Research*, 20(9), 1323-1324. doi: 10.1029/WR020i009p01323

Swiler, L. P., J. C. Helton, E. Basurto, D. M. Brooks, P. E. Mariner, L. M. Moore, S. Mohanty, S. D. Sevougian, and E. R. Stein 2019. *Status Report on Uncertainty Quantification and Sensitivity Analysis Tools in the Geologic Disposal Safety Assessment (GDSA) Framework*. SAND2019-13835 R. Sandia National Laboratories, Albuquerque, NM.

Swiler, L. P., E. Basurto, D. M. Brooks, A.C. Eckert, P. E. Mariner, T. Portone, and E. R. Stein 2020. *Advances in Uncertainty Quantification and Sensitivity Analysis Methods and Applications in GDSA Framework*. SAND2020-10802 R. Sandia National Laboratories, Albuquerque, NM.

Tang DH, Frind, EO and Sudicky EA, 1981. "Contaminant transport in fracture porous media: analytical solution for a single fracture". *Water Resources Research,* 17(3), 555-564. doi: 10:1029/WR017i003p00555

TPC (Taiwan Power Company) 2017. *The Technical Feasibility Assessment Report on Spent Nuclear Fuel Final Disposal*. Main Report. Taiwan Power Company, Taipei, Taiwan.

Vienna, J. D., J. V. Ryan, S. Gin and Y. Inagaki (2013). Current understanding and remaining challenges in modeling long-term degradation of borosilicate nuclear waste glasses. International Journal of Applied Glass Science 4(4): 283-294.

Von Mises-Fisher distribution (accessed 23 October 2021) https://en.wikipedia.org/wiki/Von_Mises%E2%80%93Fisher_distribution

Weast, R. C. and M. J. Astle, Eds. (1981). CRC Handbook of Chemistry and Physics. Boca Raton, Florida, CRC Press, Inc.

Werme, L. O., L. H. Johnson, V. M. Oversby, F. King, K. Spahiu, B. Grambow, and D. W. Shoesmith 2004. *Spent fuel performance under repository conditions: A model for use in SR-Can*. SKB TR-04-19. Svensk Kärnbränslehantering AB, Stockholm, Sweden.

Winterle, J. 1998. *Matrix Diffusion Summary Report*. Center for Nuclear Waste Regulatory Analyses, San Antonio, TX.

Zaleska, M., M. Pavlikova, and Z. Pavlik (2019). Structural, Mechanical and Thermal Properties of Lightweight Magnesium Oxychloride Cement Concrete. AIP Conference Proceedings 2170(1), published online 05 November 2019.

Appendix A

DOE Crystalline Reference Case

A-1. Model Set Up

Stochastic and deterministic fractures are generated using Los Alamos National Laboratories (LANL) dfnWorks (Hyman et al. 2015). dfnWorks takes inputs of probability distributions for fracture radius and orientation, fracture density, and fracture transmissivity. Fracture orientation is sampled from a Fisher distribution which is parameterized by mean direction (characterized by mean trend φ, the angle the projection of the pole onto the x-y plane makes with the x axis and mean plunge θ, the angle the pole makes with x-y plane), and a concentration parameter κ. Fracture radius is sampled through a truncated power law distribution, with the form of (Follin et al. 2007),

$$f(r) = \frac{k r_0^k}{r^{k+1}}$$

where r_0 is the minimum radius and k is a constant, respectively. Fracture intensity is expressed as fracture area per unit volume of rock (P_{32} [m^2/m^3]). The P_{32} values for the task specification assumes r_0 = 0.04 m and maximum radius (r_{max}) of 564 m. P_{32} is related to the average number of fractures per unit volume of rock (n_0) by (Swiler et al. 2020):

$$P_{32} = n_0 \int_{r_0}^{r_{upper}} p(r)\pi r^2 dr = n_0 \int_{r_0}^{r_{upper}} \frac{k r_0^k}{r^{k+1}} \pi r^2 dr = \frac{n_0 \pi k r_0^k}{2-k} [r^{2-k}]_{r=r_0}^{r=r_{upper}}.$$

The P_{32} over the range r_0 = 0.04 m to r_{max} = 564 m is equivalent to billions of fractures per km^3, the vast majority of which have radii < 1 m. We calculated the P_{32} for a smaller range of radii (e.g., minimum radius, r_{min} = 30 m to r_{max} = 564 m), by integrating the above over the range r_{min} to r_{max} (Swiler et al. 2020):

$$P_{32}[r_{min}, r_{max}] = \frac{\pi n_0 k r_0^k}{2-k} [r_{max}^{2-k} - r_{min}^{2-k}].$$

Fracture transmissivity (T [m^2/s]) is a function of fracture radius. The reference case uses the fully-correlated relationship defined in Follin et al. (2007):

$$\log T = \log a r^b$$

Where r is radius [m] and the coefficients a and b are dimensionless constants. Fracture aperture is calculated from the transmissivity using the cubic law (Bear et al. 1993):

$$aperture = \left(12T \frac{\mu}{\rho g}\right)^{\frac{1}{3}}$$

Where μ is viscosity of water [Pa s], ρ is density of water [kg/m^3], and g is the acceleration due to gravity [m/s^2]. Permeability (k [m^2], not to be confused with the exponent in the power law) is defined as,

$$k = \frac{aperture^2}{12}$$

The dfnWorks output must be post processed to allow for the depth dependent transmissivity, aperture, and permeability. Deterministic fractures are entered by specifying normal vectors, radii, and translation

from the origin. Stochastic fractures are randomly distributed in the domain until the target fracture density is reached. Isolated fractures and fracture clusters not connected to faces in the domain are discarded. Fracture apertures, permeabilities, normal vectors, and coordinates are outputs. Figure 12-1 shows an image of the DFNs generated from one realization.

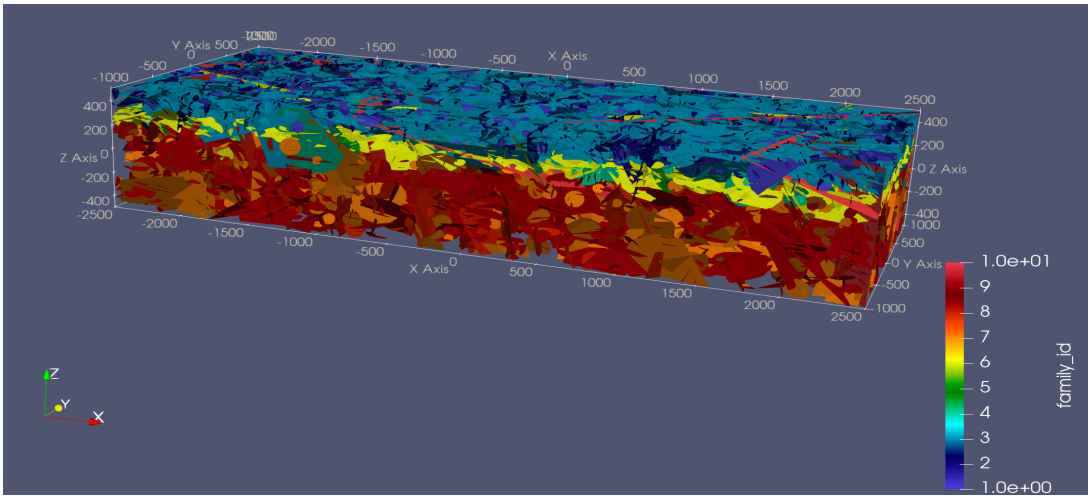

Figure 12-1 dfnWorks output of fracture families for one realization (stochastic and deterministic).

Fractures are upscaled using a python script called mapdfn.py (Stein et al. 2017). mapDFN takes dfnWorks input and ECPM model domain and discretization (origin, domain, length, and length of cubic grid cells) and outputs grid cell permeability, porosity, and tortuosity. Cell properties are calculated by determining the fractures that extend over the ECPM grid cell. For each fracture in a cell, intrinsic transmissivity (T_f[m^3]) is calculated as,

$$T_f = k_f b_f$$

Where k_f is fracture permeability [m^2] and b_f is fracture aperture [m]. Intrinsic transmissivity is described as a diagonal transmissivity tensor, where the coordinates are then rotated into the coordinates of the grid. Off-diagonal terms are discarded, and the diagonal tensor describe cell permeability is calculated as

$$\begin{bmatrix} k_{xx} & & \\ & k_{yy} & \\ & & k_{zz} \end{bmatrix} = \frac{1}{d}\sum \begin{bmatrix} T_{xx} & & \\ & T_{yy} & \\ & & T_{zz} \end{bmatrix}_f$$

Where d is the length of the cell side, and the sum is over all fractures intersecting the cell. A stairstep correction may be added to the permeability which accounts for the artificially low flux calculated from the ECPM due to fractures being characterized as stair-cases. The correction is derived from Sweeney et al. 2020, where the amount of correction needed is determined by the dot product between each fracture in the grid cell and the normal vector to each coordinate axis and is applied based on the angle closest to 45°. Fracture porosity for each grid cell is calculated as,

$$\phi = \frac{1}{d}\sum b_f$$

And cell tortuosity (τ) is calculated so the effective diffusion coefficient (D_e) is homogeneous everywhere in the fractured rock. In PFLOTRAN tortuosity is a number less than one so that,

$$D_e = \phi \tau D_m$$

Where D_m is the molecular diffusion coefficient in water. Cells not intersected by fractures are assigned matrix permeability and porosity. For the reference case, an upscaled grid cell size of 20 or 25 m will be used (Figure 12-2).

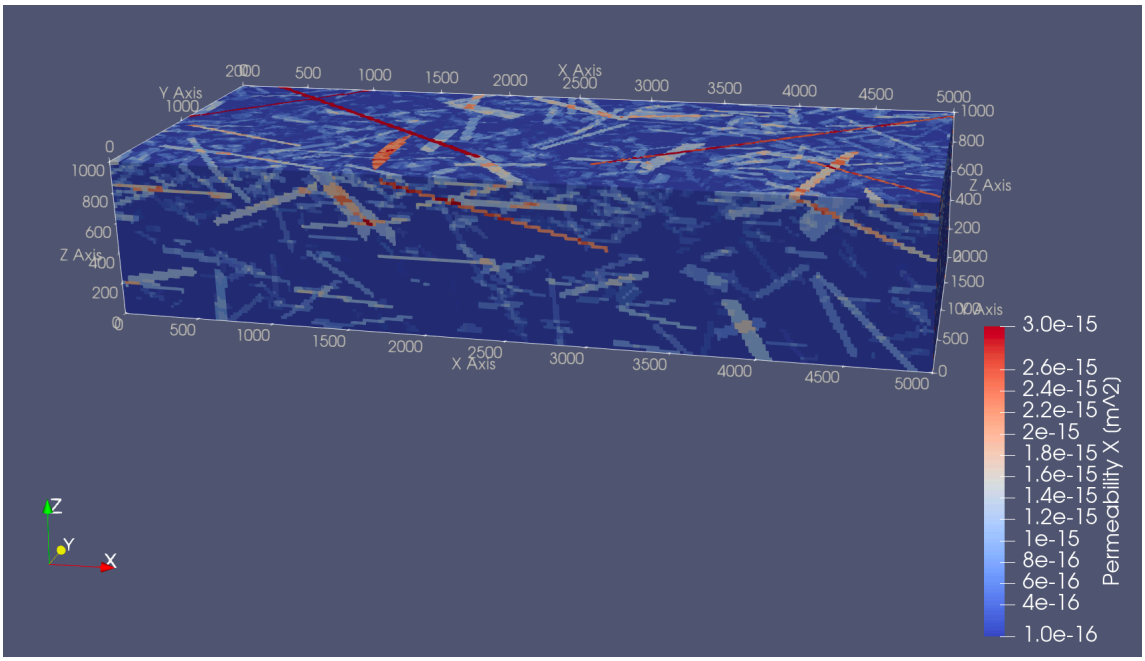

Figure 12-2 Upscaled fracture domain using cell size of 20 m

The repository is discretized using Cubit and converted to an unstructured mesh that can be entered into into PFLOTRAN, a massively parallel flow and reactive transport model (Hammond et al. 2014). Figure 12-3 shows an image in Paraview of the drifts and deposition holes in the repository. The deposition holes and waste packages will be discretized to 25/27 or 20/27 m, the deposition drifts will be discretized to 25/9 or 20/9 m, and the near field will be discretized to 25/3 or 20/3 m (Figure 12-4).

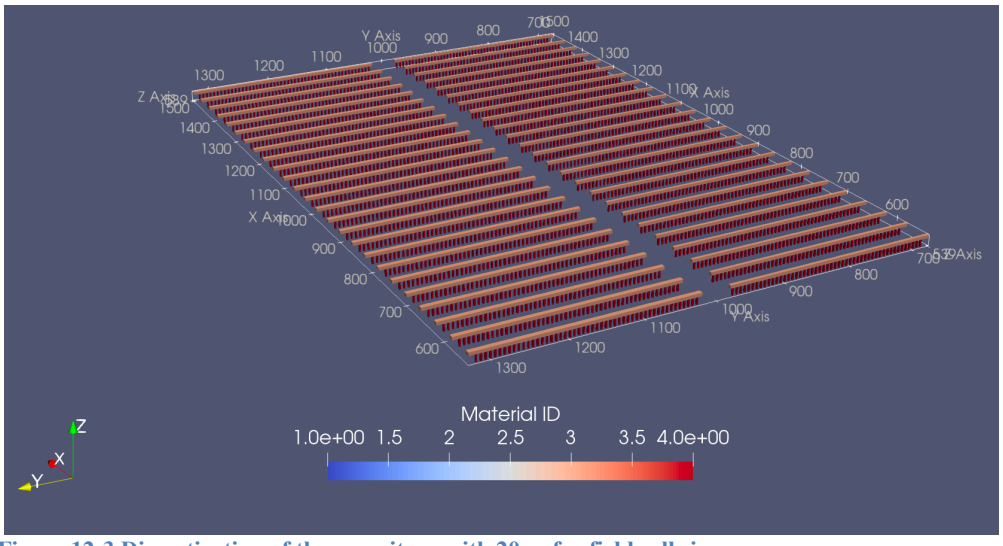

Figure 12-3 Discretization of the repository with 20 m far field cell size.

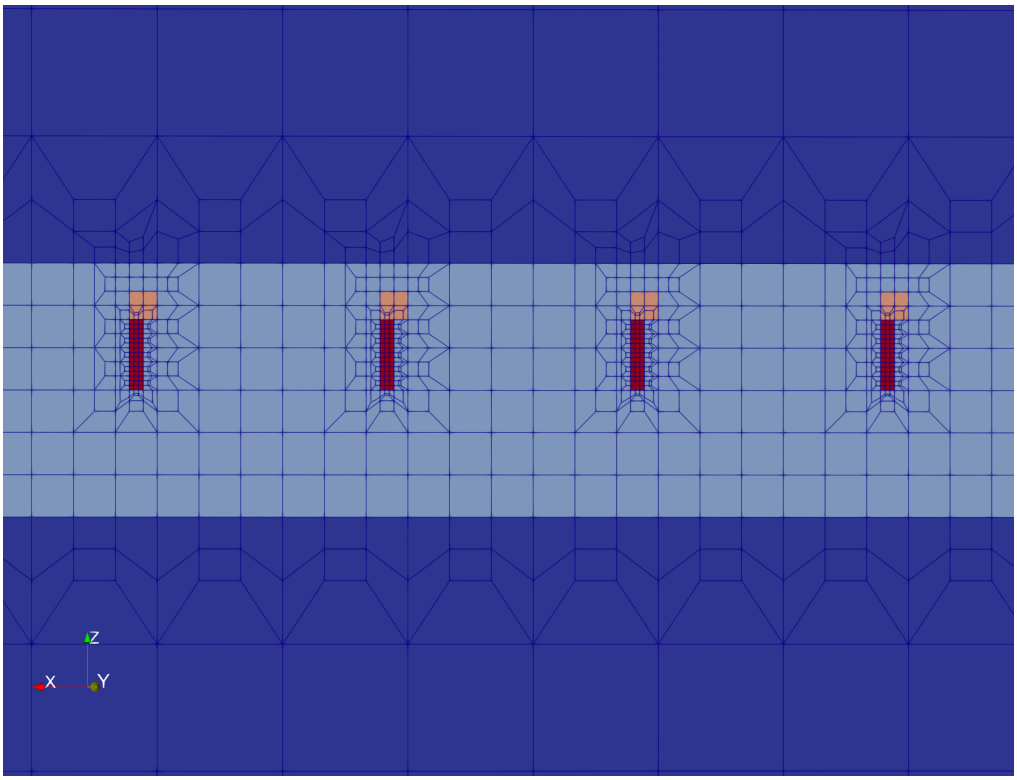

Figure 12-4 Discretization of deposition holes and drifts with 20 m far field cell size

A minimum radius of 10 m will be used to generate the fractures in the near field and then upscaled to a 25/3 or 20/3 m grid (Figure 12-5).

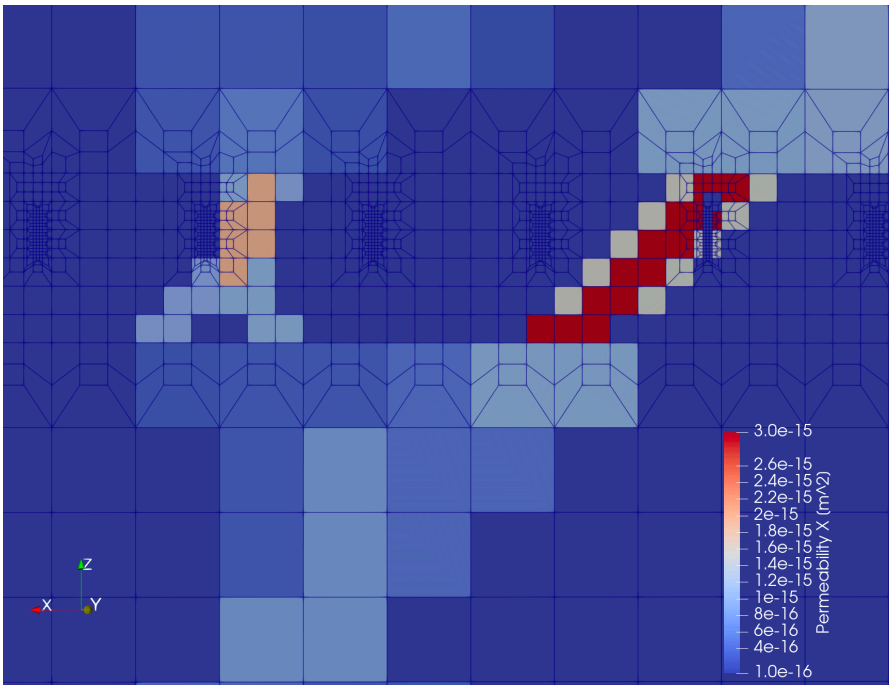

Figure 12-5 Upscaled repository using cell size of 20/3 m.

Table 12-1 shows the grid value of each parameter based on a 20 or 25 m grid size vs the value specified in the task specification. The 20 m grid cell size results in closer sizing to the task specification for all parameters except for the volume of the canister. Therefore, both grid sizes will be implemented and tested to see if the smaller volume of canister in the 20 m grid affects the transport results.

Table 12-1 Sizes of parameters meshed in cubit vs Task Specification

Parameter	Value with Grid Size 20 m [m]	Value with Grid Size 25 m	Value in Task Specification [m]
Deposition hole spacing	5.93	5.55	6
Canister dimensions	0.74 x 5.18	0.9 x 5.55	1.05 x 4.9
Drift spacing	40	41.66	40
Drift floor (z value)	551.11	550	550
Drift tunnel dimensions	4.44 x 4.44	5.55 x 5.55	4.2 x 4.8
Deposition hole dimensions	2.22 x 8.88	2.77 x 8.33	1.75 x 8.155

Steady state flow will be implemented using PFLOTRAN Richards mode and transport will be simulated using PFLOTRAN reactive transport mode. The initial conditions will be created by running the top pressure boundary condition on a 2D model to steady state (Figure 12-6). The tracer will advect out of the top boundary condition while zero-gradient boundary conditions will be applied to all other faces.

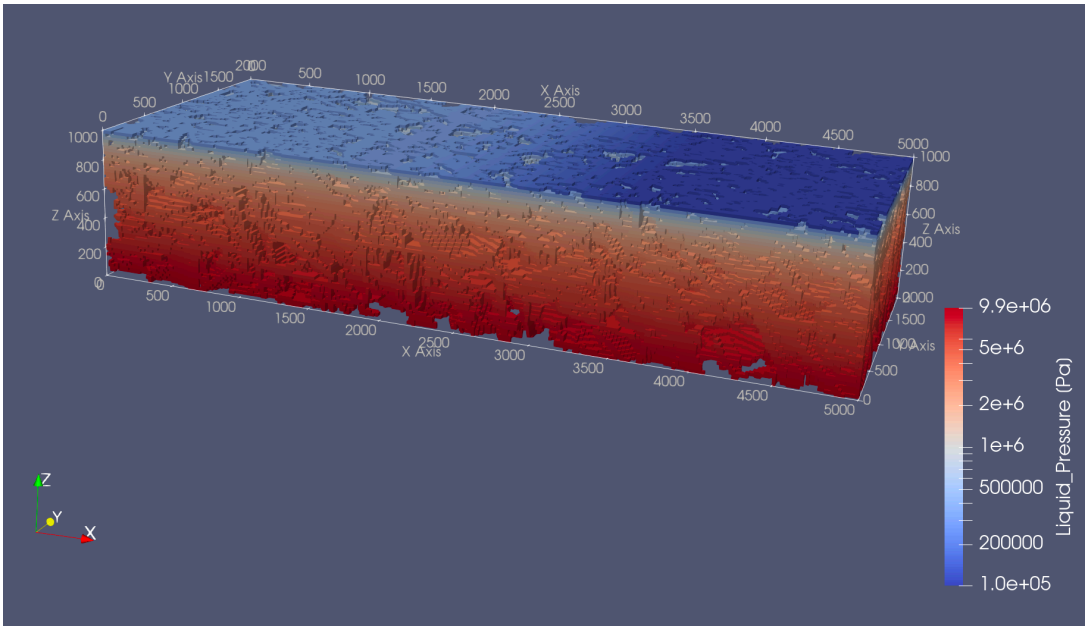

Figure 12-6 Steady state flow solution

The source terms for the tracers will be simulated in PFLOTRAN using the Waste Form Process Model. The model contains three main components: the waste form canister, waste form object, and the waste form release mechanism. The waste form canister controls the timing of the canister breach and performance of the canister after the breach. The waste form object contains only information required by all waste form types (such as location, volume, and exposure factor) and points to the waste form

mechanism and stores concentrations of the radionuclide inventory. Once the canister breaches, the waste form object degrades according to the degradation model defined by the waste form mechanism. The waste form mechanism contains information which defines behavior of each specific waste form type and contains the density, initial radionuclide concentrations, and pointer to the waste form degradation model. Below is an example how the Waste Form Process Model will be specified in the input deck.

```
WASTE_FORM_GENERAL
 WASTE_FORM
   REGION 4pwr0_13
   EXPOSURE_FACTOR 1.d0
   CANISTER_BREACH_TIME 0.d0 yr
   VOLUME 2.28d-01 #4*.435MTHM*1.44e3kgwaste/MTHM*(m3/10970kgUO2),
   MECHANISM_NAME pwr_60GWdMTU_50yOoR
  /
 PRINT_MASS_BALANCE
 MECHANISM CUSTOM
  NAME pwr_60GWdMTU_50yOoR
   FRACTIONAL_DISSOLUTION_RATE 1.d-7 1/yr
    MATRIX_DENSITY 10970.
    SPECIES
    !isotope, atomic wt (g/mol), decay constant 1/s, g/g waste, instant release fraction, daughter
     Tracer1  128.90d0  0.0d0  2.18d-04  0.10d0  #no_daughter
     Tracer2  128.90d0  0.0d0  1.96d-03. 0.00d0  #no_daughter
    /
    CANISTER_DEGRADATION_MODEL
     CANISTER_MATERIAL_CONSTANT 1500.
    /
 END #MECHANISM CUSTOM
END_WASTE_FORM_GENERAL
```

A-2. Calculation of Outputs for Comparison

The tracer mass flow and steady state liquid flow across specified surfaces with time will be calculated via the INTEGRAL_FLUX keyword in PFLOTRAN:

```
INTEGRAL_FLUX X_at_1
 PLANE
   1. 0. 0.
   1. 1. 0.
   1. 0. 1.
  /
END
```

The plane defines a block of x,y,z coordinates where the fluxes of all primary variables will be summed. Calculation of the largest tracer mass flow on the hillslope and low spot vs time will be done by either a post processing script which will look at multiple observation points to find the maximum flux or via code development to PFLOTRAN to add an option to output maximum flux within INTEGRAL_FLUX or another card.

Tracer inventory remaining in the repository with time will be calculated by using the TOTAL_MASS_REGIONS keyword within the MASS_BALANCE_FILE output in PFLOTRAN:

```
MASS_BALANCE_FILE
 PERIODIC TIMESTEP 1
```

```
 TOTAL_MASS_REGIONS
   repository
  /
END
```

A region is specified containing the repository and the total mass and the mass of each tracer in the repository with time is output.

References:

Bear J. 1993. *Flow and Contaminent Transport in Fractured Rocks,* Academic Press: 1-37.

Follin, S., L. Hartley, P. Jackson, S. Joyce, D. Roberts, and B. Swift 2007. *Hydrogeological characterization and modeling of deformation zones and fracture domains, Forsmark modelling stage 2.2*. SKB R-07-48. Svensk Kärnbränslehantering AB, Stockholm, Sweden.

Hammond, G.E., Lichtner, P.C. and Mills, R.T., 2014. Evaluating the performance of parallel subsurface simulators: An illustrative example with PFLOTRAN. Water Resources Research, 50(1), 208-228. doi: 10.1002/2012wr013483

Hyman, J. D., S. Karra, N. Makedonska, C. W. Gable, S. L. Painter, and H. S. Viswanathan 2015. "DFNWORKS: A discrete fracture network framework for modeling subsurface flow and transport". *Computers & Geosciences*, 84, 10-19. doi: 10.1016/j.cageo.2015.08.001

Stein, E. R., J. M. Frederick, G. E. Hammond, K. L. Kuhlmann, P. E. Mariner, and S. D. Sevougian 2017, April 9-13, 2017. *Modeling Coupled Reactive Flow Processes in Fractured Crystalline Rock*. Paper presented at the International High-Level Radioactive Waste Management Conference, Charlotte, NC.

Sweeney, M.R., Gable, C.W., Karra, S., Stauffer, P.H., Pawar, R.J., Hyman, J.D., 2020. Upscaled discrete fracture matrix model (UDFM): an octree-refined continuum representation of fractured porous media. Comput. Geosci. 24, 293–310. https://doi.org/10.1007/s10596-019-09921-9

Swiler, L. P., E. Basurto, D. M. Brooks, A.C. Eckert, P. E. Mariner, T. Portone, and E. R. Stein 2020. *Advances in Uncertainty Quantification and Sensitivity Analysis Methods and Applications in GDSA Framework*. SAND2020-10802 R. Sandia National Laboratories, Albuquerque, NM.

Appendix B

DOE Salt Reference Case

B-1. Numerical Approach

The simulator used for this task is PFLOTRAN (Hammond et al. 2014), an open source, state-of-the-art massively parallel subsurface flow and reactive transport code. The numerical approach taken here is to utilize a high-resolution, three-dimensional (3D) thermal-hydrological (TH) model to analyze the pressure and saturation evolution over time within the geologic repository. The finite-volume code PFLOTRAN is used to simulate mass and heat transport within the two-phase (air & water) system. Two different flow modes are utilized with PFLOTRAN, General and Richards mode. General mode involves two-phase liquid water-gas flow coupled to the reactive transport mode. Richards mode applies to single phase, variably saturated, isothermal systems. Two different modes are utilized because multiphase flow (General mode) is considerably more computationally demanding than single-phase, variably saturated flow (Richards) and a code comparison between the two will be beneficial for future PA tasks. An additional challenge added to this task is the geometric complexity of the Figure 4-1. The combination of the repository design and geologic cross-section make it difficult to create a hexahedral mesh with high enough resolution to simulate processes at the waste canister scale while keeping the number of elements at a reasonable amount to keep computational requirements at a minimum. While hexahedral meshes can be deformed to capture some of the configurational complexity, some grid cells may be badly scaled leading to non-orthogonality (i.e., element faces not perpendicular to the line connecting adjacent element centers) that can cause flux errors in finite volume meshes leading to mass no longer being conserved when fluid flows between elements. To avoid this potential numerical issue, here we use VoroCrust (Abdelkader et al., 2018; 2020), a fully automated Voronoi meshing software that has been adapted to create simulation grids for PFLOTRAN in complex geological systems.

B-2. Performance Assessment Case

B-2.1 Simulation Model Construction

This study combines Voronoi meshing of the Task F geologic repository and TH numerical modeling to investigate the pressure and saturation evolution of the repository within domal salt. The workflow used here to create a Voronoi mesh for PFLOTRAN uses two programs; LaGriT (LANL, 2017) and Vorocrust (Abdelkader et al., 2018; 2020). LaGriT is a library of mesh generation and optimization tools in two and three dimensions that was used to create borehole- and drift-bounding surfaces for input into Vorocrust. Figure 12-7 illustrates the surfaces created in LaGriT, which consists of half the repository and one shaft, the repository was designed to have half symmetry to reduce computational needs. The current model domain is 2000 m x 2000 m x 2000 m consisting of 431,072 grid cells. Vorocrust creates a 3D Voronoi mesh. Figure 12-8 shows a slice down the center of the model domain parallel to the repository at a depth of 795 m and illustrates how the mesh is highly refined around areas of interest and coarsens outward. Figure 12-9A and B are zoomed-in sections of the (A) repository and the (B) disposal drifts to illustrate the mesh refinement within and around the disposal drifts. Vorocrust can resolve the mesh around possibly curved areas of interest while coarsening rapidly away from the area of interest, to reduce the total number of elements and computational burden. Voronoi elements, by construction, are the optimal elements for finite volume simulators like PFLOTRAN. Unlike hexahedral meshes, Voronoi meshes do not have a fixed number of connections per element, which leads to a higher connectivity than structured

meshes, resulting in more poorly conditioned residual matrices. To address this issue, we used a constrained pressure residual pre-conditioner, which aids with the added numerical challenges associated with a Voronoi mesh (Park et al., 2021).

While steps were taken to reduce the complexity of the meshing and simulations described above, additional assumptions are made in order to help with convergence:

1. Currently only one geologic formation is accounted for, domal salt
2. Only one relative permeability model is used for all material types, Van Genuchten models from Stein et al (2021)
3. Shaft and drift seals are simplified into one homogeneous material
4. Liquid saturation is initially set to 20% within the repository, drifts, and shaft

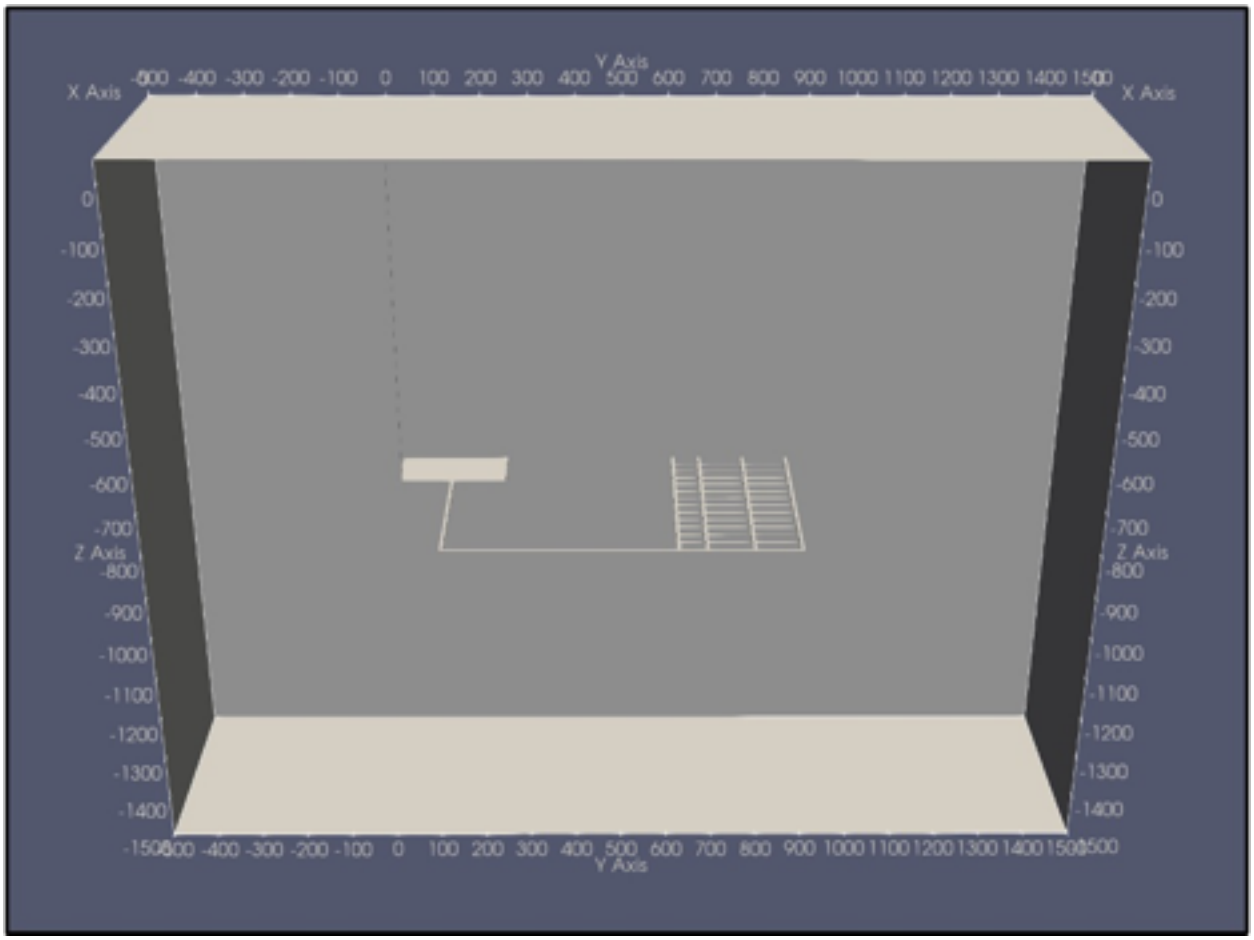

Figure 12-7. The geologic repository created with LaGrit. This surface object is used by Vorocrust to create the full meshes.

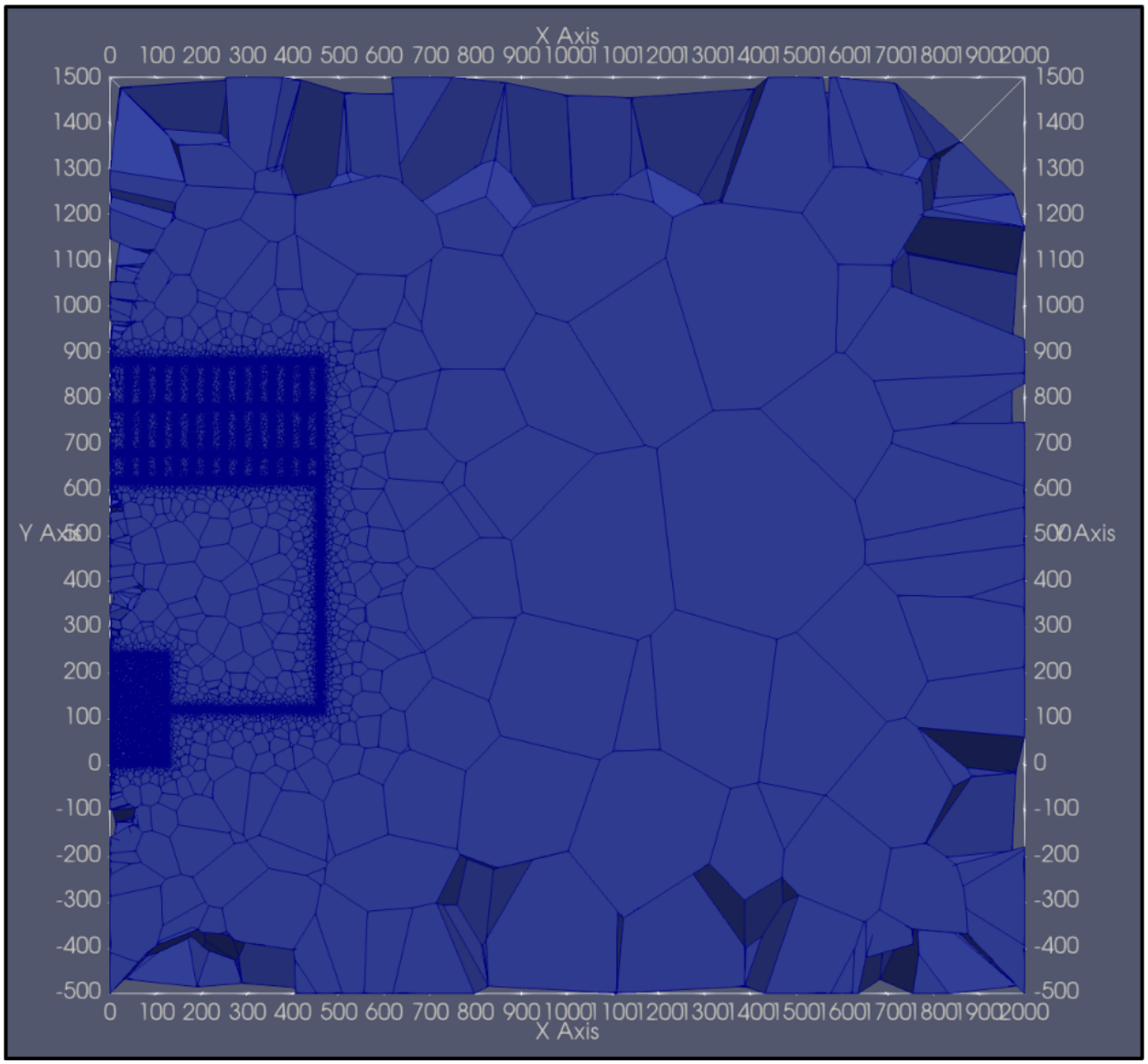

Figure 12-8. Mesh created by Vorocrust. This slice is parallel to the repository at a depth of 795m. Note the high resolution meshing near the repository and coarsening outwards.

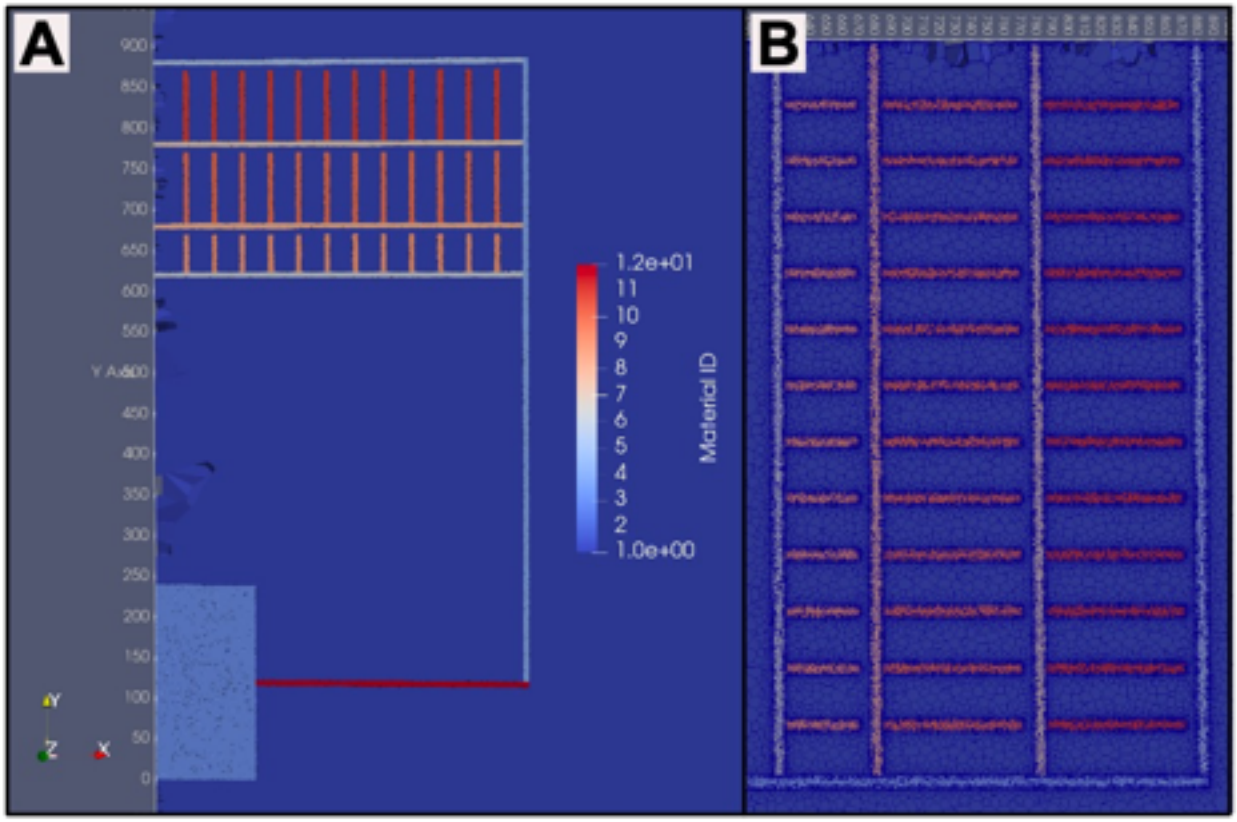

Figure 12-9. Zoomed in slices of the (A) repository and (B) disposal drifts.

B-2.2 Preliminary Results

The preliminary modeling of the Task F geologic repository using a 3D Voronoi mesh are illustrated by comparing the pressure and saturation evolution between two different flow modes within PFLOTRAN, General and Richards mode. Figure 12-10 and Figure 12-11 illustrate the wetting up of the repository at 10,000, 20,000, and 30,000 years for General and Richards mode, respectively. The differences between the two modes is fairly small, where at 10,000 years the repository has a slightly higher liquid saturation in General vs. Richards mode. The same observation can be seen at 20,000 and 30,000 years as well. By 40,000 years, the repository is fully liquid saturation in both cases. Additional simulations are required to compare and contrast the results between these two modes. The total simulation time differs; to simulate 100,000 years on 180 processors General mode takes 37.3 hours and Richards mode takes 25.5 hours. As more complexity is built into these models (heterogeneity, multiple relative permeability models, geologic layers, etc.), it is possible that the simulation time difference between the modes will increase. While these results are preliminary, they do provide confidence in the current workflow and model conceptualization presented here.

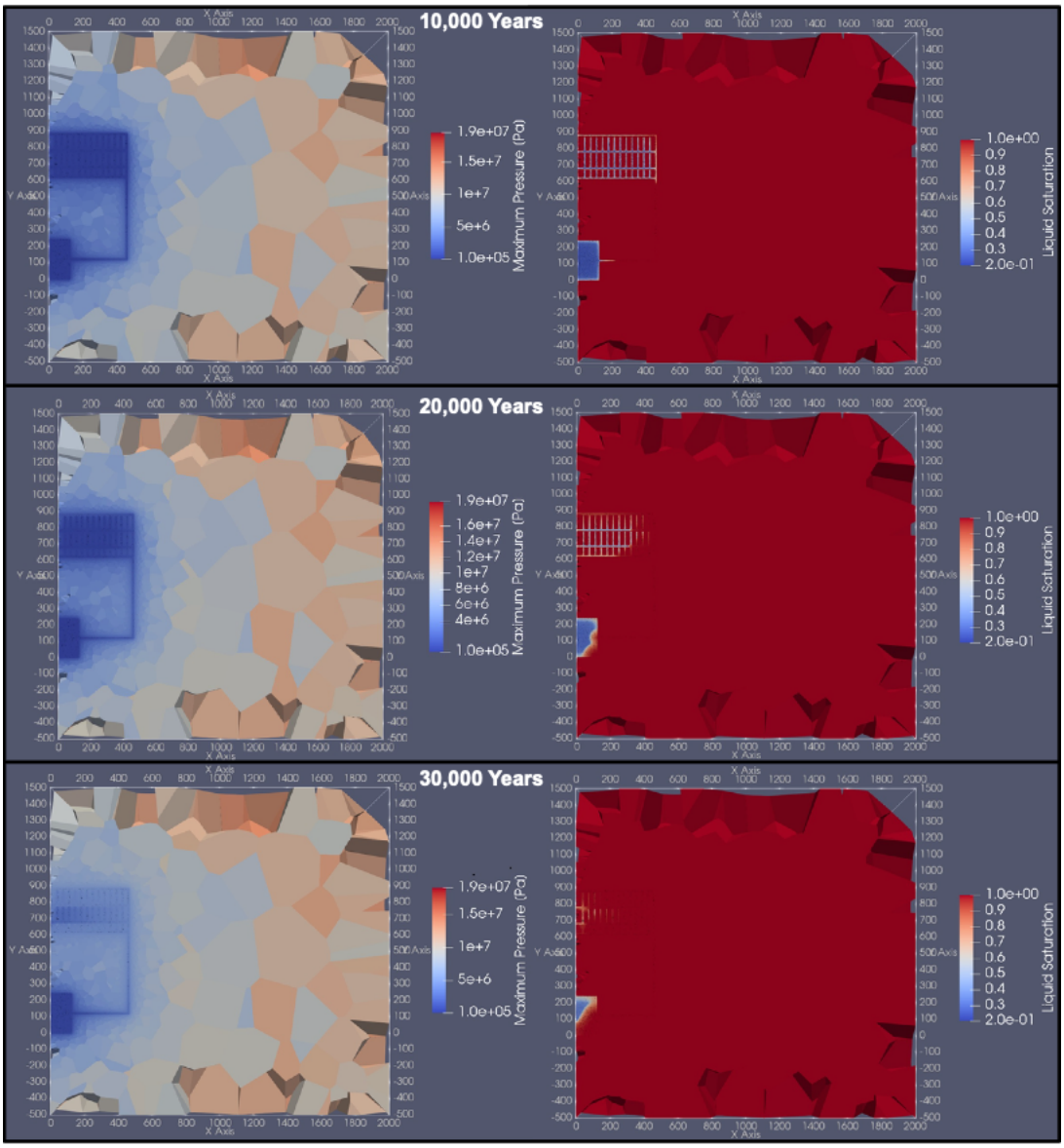

Figure 12-10. General mode results for pressure (left) and saturation (right) at 10,000, 20,000, and 30,000 years.

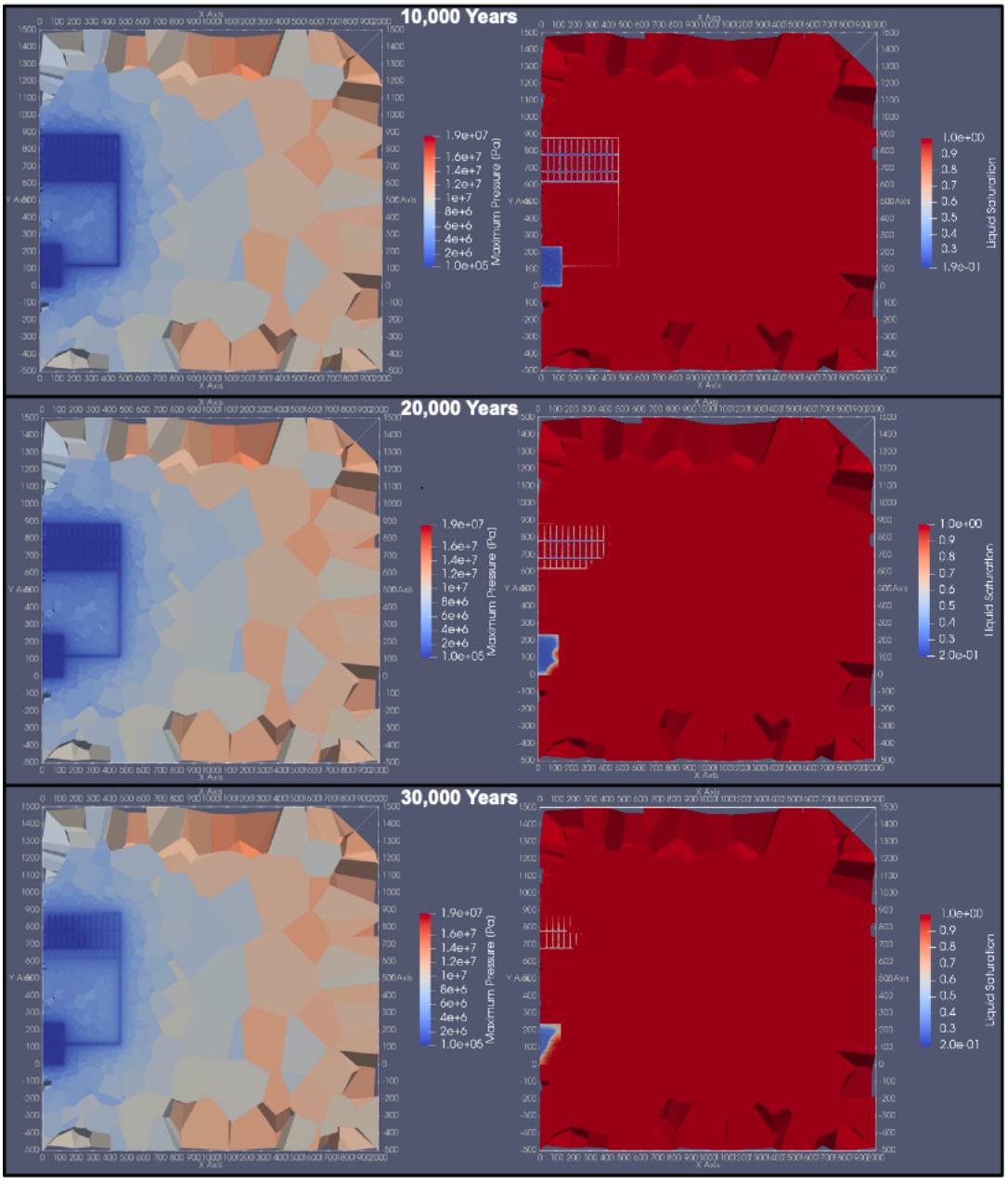

Figure 12-11. Richards mode results for pressure (left) and saturation (right) for 10,000, 20,000, and 30,000 years.

B-3. Lookaheads

The numerical methods and model conceptualization utilized here are a simplified version of the task specification. This was done in order to make trouble-shooting the workflow an easier process. As a result, there are a number of assumptions and simplifications that can be changed in order to match the current task specification. Some of these items include: using material properties specified for the disposal drifts, drift seals, and shaft seal; adding in geologic layers including the freshwater aquifer, increasing model domain size to incorporate all geologic layers; and possibly meshing up the drift and shaft seals explicitly to include all materials. Additionally, moving onto the next step in Task F will

require the addition of radionuclide mobilization and transport which will be done with both General and Richards mode of PFLOTRAN to continue model comparisons.

B-4. References

Abdelkader, A., Bajaj, C.L., Ebeida, M., Mahmoud, A.H., Mitchell, S.A., Owens, J.D., & Rushdi, A.A. 2018. Sampling conditions for conforming Voronoi meshing by the VoroCrust algorithm. Leibniz international proceedings in informatics 99.

Abdelkader, A., Bajaj, C.L., Ebeida, M.S., Mahmoud, A.H., Mitchell, S.A., Owens, J.D., & Rushdi, A.A. 2020. VoroCrust: Voronoi meshing without clipping. ACM Transactions on Graphics (TOG) 39(3):1–16.

Hammond, G.E., Lichtner, P.C., & Mills, R.T. 2014. Evaluating the performance of parallel subsurface simulators: An illustrative example with PFLOTRAN. Water Resources Research 50:208–228.

Los Alamos National Laboratory (2017) Los Alamos grid toolbox, LaGriT. http://lagrit.lanl.gov.

Park, H.D., Hammond, G.E., Valocchi, A.J., & LaForce, T. 2021. Linear and nonlinear solvers for simulation multiphase flow within large-scale engineered subsurface systems. Advances in Water Resources, 156.